Metals and Ceramics Division

Heavy Vehicle Propulsion Materials Program
Quarterly Progress Report for
January through March 2004

D. R. Johnson
Technical Project Manager

Prepared for
U.S. Department of Energy
Assistant Secretary for Energy Efficiency and Renewable Energy
Office of FreedomCAR and Vehicle Technologies Program
VT 05 01 020

Prepared by the
OAK RIDGE NATIONAL LABORATORY
Oak Ridge, Tennessee 37831-6066
Managed by
UT-Battelle, LLC
for the Department of Energy
Under contract DE-AC05-00OR22725

CONTENTS

Materials for Fuel Systems

Manufacturing Technology for Cermet Components (SIU-C)

High Toughness Materials (ORNL)

Materials for Exhaust Aftertreatment

Materials for Exhaust Aftertreatment (Caterpillar Inc.)

Development of NO_x Sensors for Heavy Vehicle Applications (ORNL and Ford Motor Company)

Ultra-High Resolution Electron Microscopy for Characterization of Catalyst Microstructures and De-activation Mechanisms (ORNL)

Microstructural Changes in NO_x Trap Materials under Lean and Rich Conditions at High Temperatures (ORNL)

Materials for Air Handling, Hot Section, and Structural Components

Lightweight Valve Train Materials (Caterpillar Inc.)

Engineered Surfaces for Diesel Engine Components (Caterpillar Inc.)

Nanoengineered Materials (North Carolina A&T State University)

NDE of Diesel Engine Components (Argonne National Laboratory)

Durability of Diesel Engine Component Materials (ORNL)

Life Prediction of Diesel Engine Components (ORNL and Caterpillar)

Advanced Machining and Sensor Concepts (University of Michigan)

Advanced Cast Austenitic Stainless Steels for High-Temperature Components (ORNL and Caterpillar Inc.)

TiAl Nanolaminate Composites (Lawrence Livermore National Laboratory)

Laser Surface Texturing of Lubricated Ceramics (ORNL)

High-Density Infrared Surface Treatment of Materials for Heavy-Duty Vehicles (ORNL)

Titanium Alloys for Heavy-Duty Vehicles (ORNL)

Mechanical Behavior of Ceramic Materials for Heavy Duty Diesel Engines (ORNL)

Deformation Processes for the Next Generation Ceramics (ORNL)

Synthesis of Nanocrystalline Ceramics (Pennsylvania State University)

Development of Titanium Components for a Heavy-Duty Diesel Engine Turbocharger (Caterpillar Inc.)

Test and Materials Standards

Surface Modification of Engineering Materials for Heavy Vehicle Applications (NIST)

IEA Implementing Agreement for a Programme of Research and Development on Advanced Materials for Transportation Applications (ORNL)

Testing Standards (NIST)

IEA – Rolling Contact Fatigue (ORNL)

Low-Cost Manufacturing Processes for Ceramic and Cermet Diesel Engine Components

D. E. Wittmer
Southern Illinois University

Objective/Scope

The purpose of this work is to investigate the potential of low-cost manufacturing processes for ceramic and cermet diesel engine components. The primary task is to develop cost effective processing, forming and sintering methodologies for cermet and ceramic formulations, used by industrial diesel engine manufacturers.

Technical Highlights

Task 1. Collaboration with industrial partner(s).

This task involves the collaboration with industrial partners to assist them in processing and sintering of their diesel engine components. Our goal is provide assistance in processing and sintering which may result in a reduction in surface reactions and part warping. Moreover, this may also provide an alternative sintering process that will allow improved throughput efficiency and manufacturing economy. Due to the proprietary nature of this task, any research data generated from this task is normally controlled by the terms of each specific confidentiality agreement. The reporting of this data and any results are the responsibility of the industrial partner(s).

During this reporting period several prototype plungers previously prepared by low-pressure injection molding were sintered. The cermet composition used was the reaction sintered Ni3Al-TiC (50/50) formulation which has been discussed in previous reports. Most of the plungers warped during sintering. This warpage is believed to be due to migration of the Ni3Al during sintering due to the high liquid volume. To test this theory, two prototype plungers we sintered with the long axis perpendicular to the direction of belt travel in the continuous furnace. The appeared to improve the warpage substantially. One of the plungers was sent off for surface machining, which should be completed during the next reporting period.

Task 2. Cost Effective Processing and Sintering

This task was completed and reported in previous quarterly report.

Task 3. Economic Comparison of Materials and Processing of Cermets for Use as Diesel Engine Components

This task was completed as reported previously.

Task 4. Effect of High Heating Rates on Sintering of Cermets

The goal of this is to evaluate the use of very high heating rates on the densification of selected intermetallic bonded-TiC cermets. If extremely high heating rates can be used to sinter these cermets, it offers the opportunity to even further reduce the manufacturing cost.

During this reporting period, several one inch diameter discs of Ni3Al-TiC (50/50) were dry pressed at 30 Ksi, using 3 wt % PVP as a binder. The binder was removed in Ar-4%H prior to continuous sintering at 1400°C. Belt speeds of 0.75, 1.5, 3.0 and 4.5 in/min were employed to give a wide range of heating rates. The plot of heating rate as a function of belt speed is given in Figure 1. In order to test the heating rate on the specimens, the belt was stopped when the specimens were in the center of the hot zone and held for the required time to give an effective sintering time of 30 min. During the first trial, several SiC belt pins failed and needed to be replaced. This is the first problem with the belt created by standard wear conditions in the 8 years the furnace has been used. This is a testament to the durability of the continuous furnace.

A total of 8 test runs were made during this reporting period. The densities were obtained by Archimedes method (shown in Figure 2) and the samples were then diamond polished for hardness testing and microstructural analysis. The samples are currently being evaluated by SEM. The results will be reported during the next reporting period.

Status of Milestones

1.	Collaboration with Industrial Partners	On Schedule
2.	Cost Effective Processing and Sintering of Diesel Engine Components	Completed
3.	Economic Comparison	Completed
4.	Effect of high heating rates	On Schedule

Communications/Visits/Travel

D. E. Wittmer spoke with Terry Tiegs about the technical progress.

D. E. Wittmer was visited by Jim Stephen from CoorsTek and he was given 4 test bars sintered at SIUC in the continuous furnace for evaluation.

Problems Encountered

Several link pins in the SiC belt on the continuous furnace failed due to wear which delayed sintering rate tests. Replacement pins were received and the belt was repaired.

Publications and Presentations

None

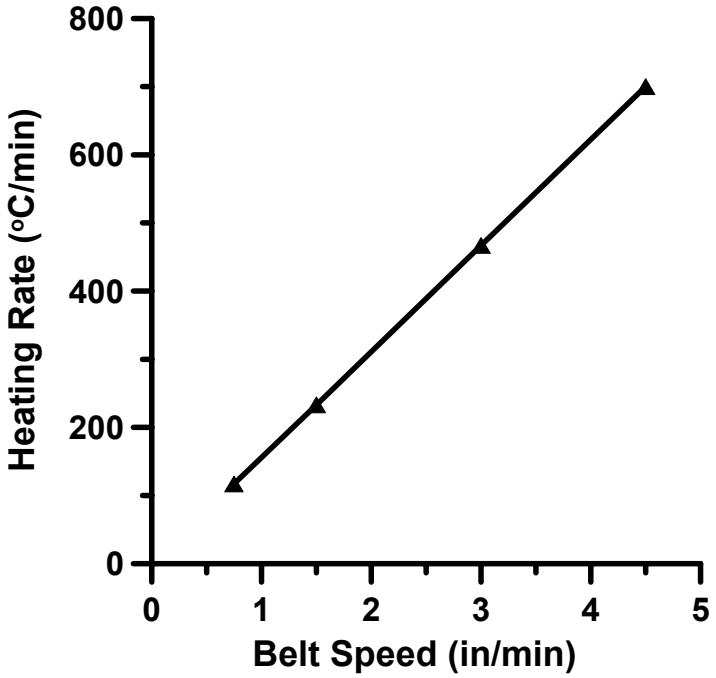

Figure 1. Heating rate as a function of belt speed.

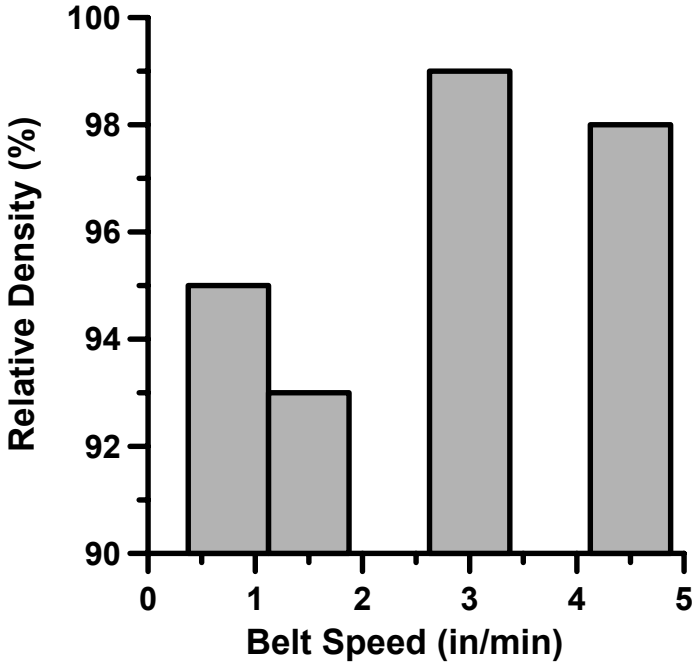

Figure 2. Relative density as a function of belt speed.

Low Cost-High Toughness Ceramics

T. N. Tiegs, F. C. Montgomery, and P. A. Menchhofer
Oak Ridge National Laboratory

Objective/Scope

Significant improvement in the reliability of structural ceramics for advanced diesel engine applications could be attained if the critical fracture toughness (K_{Ic}) were increased without strength degradation. Currently, the project is examining toughening of ceramics by incorporation of ductile intermetallic phases.

Technical Highlights

Previous studies have shown that the properties of the aluminide-bonded ceramics are attractive for diesel engine applications and consequently, development of these materials was started. At the present time, TiC-based composites with 40-60 vol % Ni_3Al are being developed because they have expansion characteristics very close to those for steel. Previously, the general property envelope has been studied and the compositions refined. Further processing studies are needed to examine lot-to-lot variation using statistically designed experiments, determine compaction behavior, assess dimensional control during sintering, identify suitable binders which will not add carbon ash during sintering, and develop a viable and cost-effective source of NiAl powder. The development effort is being done in collaboration with CoorsTek, Inc.

Alternate Precursors for Ni_3Al Formation - All previous work used a combination of Ni and NiAl for an in-situ reaction to form the Ni_3Al. Because the costs of the starting raw materials can be a significant fraction of the total cost of a component, alternative materials for fabricating the cermets are of interest. Several new batches are awaiting the repair of the sintering furnace, which has been out of service for 5 months.

Another Al-Ni precursor that is also used as a catalyst has been obtained from a commercial vendor. The powder has been processed into a blended mixture with TiC and is awaiting sintering.

Status of Milestones

On schedule.

Communications/Visits/Travel

Travel by T. N. Tiegs to Cocoa Beach, FL, Jan. 25-28 to attend American Ceramic Society Conference on Ceramics and Composites and present paper. .

Problems Encountered

The sintering furnace used for processing studies has been out of service for five months because of a bad controller.

Publications

T. N. Tiegs, F. C. Montgomery, and P. A. Menchhofer, "Effect of Ni-Al Precursor Type on Fabrication and properties of TiC-Ni_3Al Composites," to be published in Ceram. Eng. Sci. Proc. (2004).

Advanced Diesel Aftertreatment Program

Paul W. Park, Alexander G. Panov, Svetlana Zemskova, and Craig F. Habeger
Caterpillar Inc.

Objective/Scope

The objective of the effort is to develop and evaluate materials that will be utilized in aftertreatment systems for diesel engine applications. These materials include catalysts for NO_x abatement, filtration media for particulate abatement, and materials to improve NO_x sensing capabilities in the exhaust system. This project is part of a Caterpillar strategy to meet EPA requirements for regulated emissions in 2007 and beyond.

This year's focus is on the development of a reformer assisted Lean- NO_x technology to demonstrate >50% NO_x reduction with 5% fuel penalty, identification of the critical parameters for soot oxidation in a catalyzed particulate filter, and evaluation of the current state of art NO_x sensor technologies as well as development of materials to improve sensing capabilities.

Technical Highlights

Lean-NO_x. A synergy effect was identified when alumina and zeolite based materials was combined. The combination catalyst significantly improves Lean- NO_x performance with selected liquid hydrocarbon reductants. The concept of "Reformer Assisted Lean- NO_x Catalysis" has been assessed with various catalyst materials and reformer technologies. Engine tests using a 275 hp diesel engine equipped with a prototype Lean- NO_x system consisted of catalysts and a reformer technology demonstrated 45% NO_x reduction with 9% fuel penalty (13 OICA mode steady state test). The 2nd engine test is scheduled to improve NO_x reduction as well as optimize fuel penalty.

Diesel Particulate Filter (DPF). An improved DPF test protocol was developed and better control of soot loading was achieved on DPF samples. The development of test protocols to obtain kinetics data for DPF modeling applied for a real engine exhaust is underway. Invention disclosure regarding a new method of cleaning DPF (soot and ash regeneration) has been filed. Proof of concept tests demonstrated the efficiency of the developed method.

NOx Sensor. The NO_x sensor test bench has been re-calibrated after it underwent major service maintenance. The dip-coating method was used to prepare organic thin films on substrates for NO_x sensor development. Preliminary data was collected at room temperature using an organic material on a substrate using an electromagnetic technique (measuring energy loss caused by NO_x interaction with the targeted sites). As low as 10ppm NO_x was detected by the selected organic molecule. The results are being analyzed.

Future Plans

1) Compete engine test to assess feasibility of "Reformer Assisted Lean- NO_x Catalysis".
2) Identify a potential application of the developed Lean- NO_x system.
3) Complete evaluation of oxygen pumping electrodes for amperometric NO_x sensors.
4) Continue to collaborate with Ceramatec Inc. to develop a sensor for diesel applications
5) Complete the catalyzed filters study.
6) Develop a model for simulation of DPF regeneration in the engine exhaust.

Travel

Paul Park to ArvinMeritor at Columbus Indiana to evaluate the feasibility of ArvinMeritor's reformer for the Lean- NO_x catalyst system.

Craig Habeger and Svetlana Zemskova to Cocoa Beach, FL, to make presentations. The 28th International Conference & Exposition on Advanced Ceramics & Composites, Cocoa Beach, FL, USA, January 25-30, 2004.

Status of FY 2004 Milestones

1) Down select combination catalyst materials: *completed*
2) Assess reformer technologies: *completed*
3) Scale-up catalyst preparation: *completed*
4) Evaluate the performance (lean/rich cycles, water presence) of current NOx sensor technologies to meet diesel emission regulations: *in progress*
5) Development of test protocol for evaluation of catalyzed DPFs: *completed*

Publications

Effect of SO_2 on the Activity over Ag/γ-Al_2O_3 Catalysts for the Reduction of NO_x in Lean Conditions, Carrie L. Boyer, Paul W. Park *submitted to Appl. Catal. B.*

United States Patent No. 6,706,660, entitled METAL/METAL OXIDE DOPED OXIDE CATALYSTS HAVING HIGH $DENO_X$ SELECTIVITY FOR LEAN NO_X EXHAUST AFTERTREATMENT SYSTEMS, issued on March 16, 2004.

United States Patent No. 6,703,343, entitled METHOD OF PREPARING DOPED OXIDE CATALYSTS FOR LEAN NO_X EXHAUST, issued on March 9, 2004.

Conferences/Seminars/Presentations

Svetlana Zemskova, P.W. Park, J.S. Lin (Oak Ridge National Laboratory), J. Wen, I. Petrov (University of Illinois at Urbana- Champaign), "STUDY OF HIGH SURFACE AREA ALUMINA AND GA-ALUMINA MATERIALS FOR $DENO_X$ CATALYST APPLICATIONS," The 28th International Conference & Exposition on Advanced Ceramics & Composites, Cocoa Beach, FL, USA, January 25-30, 2004.

Craig Habeger, "REQUIREMENTS FOR NO_X SENSORS IN HEAVY DUTY DIESEL EXHAUST ENVIRONMENTS," The 28th International Conference & Exposition on Advanced Ceramics & Composites, Cocoa Beach, FL, USA, January 25-30, 2004.

Development of NO_x Sensors for Heavy Vehicle Applications

Timothy R. Armstrong, David L. West, Fred C. Montgomery
Oak Ridge National Laboratory

CRADA No. ORNL 01-0627
with Ford Motor Company

Objective

The proposed project seeks to develop technologies and materials that will facilitate the development of NO_x and ammonia sensors. The development of low-cost, simple NO_x will facilitate the development of ultra-low NO_x emission engines, directly supporting the OHVT goals.

Technical Highlights

Single material sensor configuration

1. Total NO_x sensor behavior improved by altering electrode geometry and catalyst composition. Current design and materials offers wide operational current biasing range from 500-600°C. (Figures 1 &2)

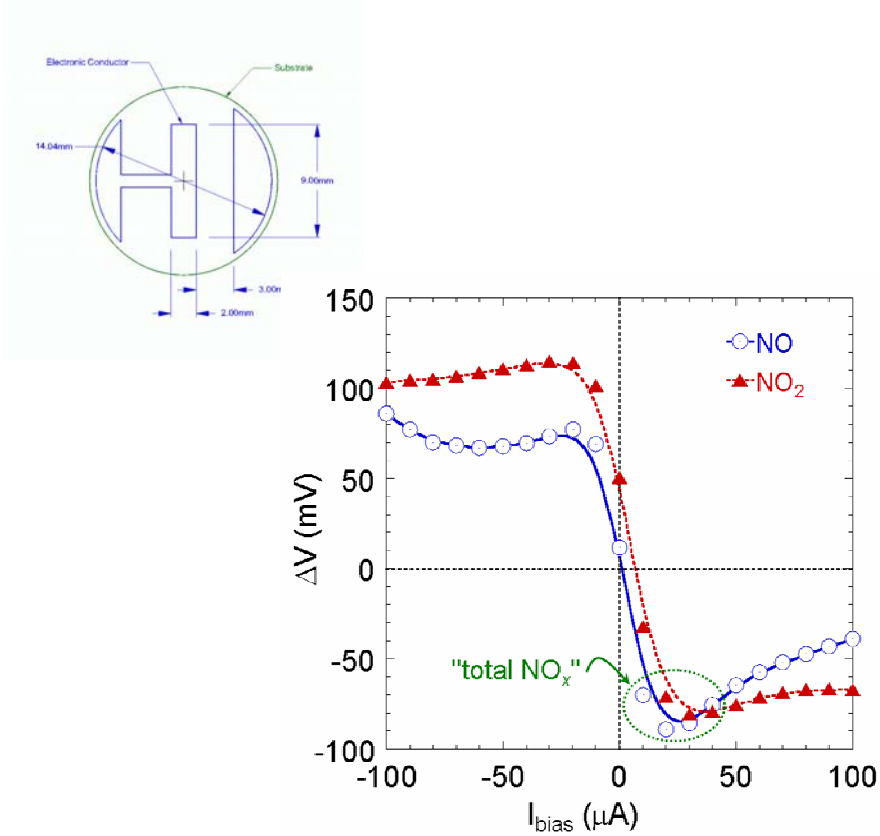

Figure 1. Sensor geometry (standard) and performance using standard 2 pad design at 600°C.

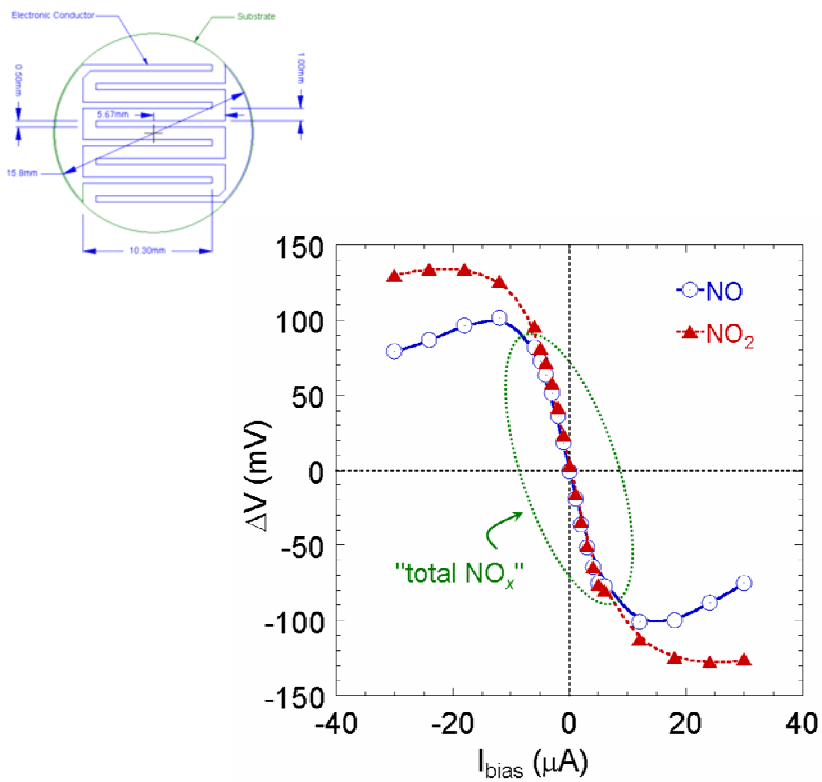

Figure 2. Sensor geometry and performance using interdigited electrode design at 600°C. This use of this design broadens the operating range (current range) that can be used to obtain a total NO_x sensor.

<u>Two material sensor configuration (oxide on Pt only)</u>

2. New electrode geometries investigated this quarter (use two materials, same number as "original" design).
3. NO response (w/o bias) tends to be stronger than "original design", although still much less than NO_2 response.
4. Semicircular and interdigitated geometries appear to offer enhanced recovery time (in mixed-potential mode) when compared to original design (operating without bias).
5. Response/recovery time not a strong function of geometry for semicircular and interdigitated geometries.
6. New element geometries (semicircular and interdigitated) exhibited "NO-selective" behavior when current biased.

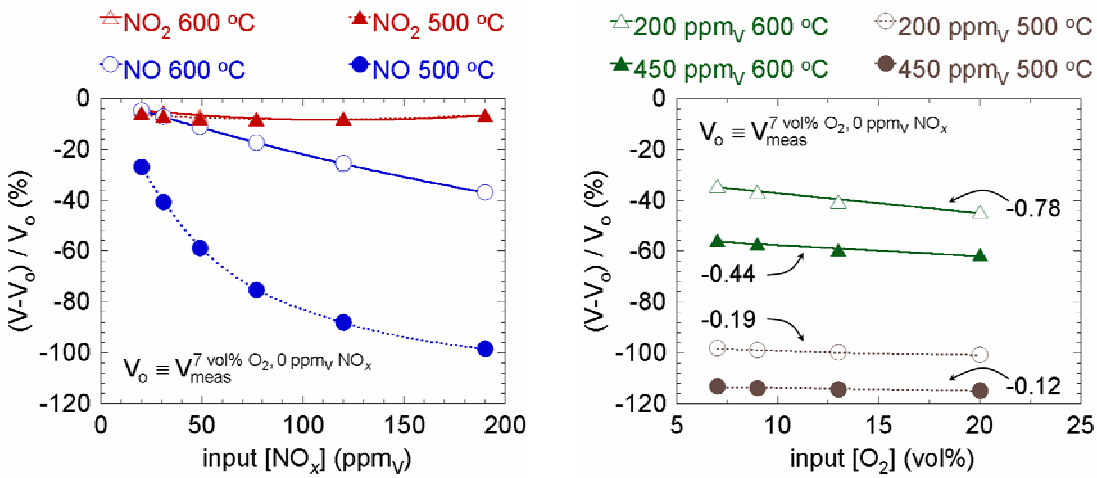

Figure 3. NO_x sensing performance of the semicircular element with current bias. For the graph on the right, the input NO_x was NO and the numbers are the slope of a linear fit to $(V-V_o) / V_o$ vs. $[O_2]$.

Status of FY 2003 Milestones

Although this project had a late kick-off, we are ahead of schedule of most of the milestones:

1. Modify current sensor test stand for operation at 800°C (delayed at request of Ford)
2. Test NGK sensor in modified test stand (delayed at request of Ford)
3. Deliver NO_x catalyst assessment and program plan to Ford (completed 6/2002)
4. Construct NO_x electrode test stand. (Completed 12/2003)
5. Deliver report on initial rest results (Completed 2/2003)
6. Design and procure screens for simplified NO_x sensor design. (Completed 12/2003)
7. Produce first simplified NO_x sensors for testing (Completed September 2003).

FY 2004 Milestones on target

Communications/Visits/Travel

1. A quarterly was sent to Ford in March 2004
2. A meeting was held in Washington DC with DOE (R. Sullivan, LLNL (R. Glass, P. Martin, Ford (J. Visser, R. Soltis) and me to discuss an expanded collaborative sensor development effort in February 2004.

Problems Encountered

None to date.

Publications

1. High Temperature NO_x Sensing Elements Using Conductive Oxides and Pt, submitted to Proceedings of the ICEF, Long Beach, CA Oct. 2004.

Intellectual Property Filed

None this quarter.

Ultra-High Resolution Electron Microscopy for Characterization of Catalyst Microstructures and De-activation Mechanisms

L. F. Allard, D. A. Blom, K. K. Lester, C.K. Narula and M. A. O'Keefe
Oak Ridge National Laboratory

Objective/Scope

The objective of the research is to characterize the microstructures of catalyst materials of interest for the treatment of NO_x emissions in diesel and lean-burn gasoline engine exhaust systems. The research heavily utilizes new capabilities and techniques for ultra-high resolution transmission electron microscopy (UHR-TEM). The research is focused on understanding the effects of reaction conditions on the changes in morphology of heavy metal species on "real" catalyst support materials (typically oxides). These changes are being studied utilizing samples treated in both steady-state bench reactors and a special *ex-situ* catalyst reactor system especially constructed to allow appropriate control of the reaction.

Technical Progress

ACEM tested in Japan and cleared for shipping, first experimental catalyst images obtained.

ORNL's new aberration-corrected electron microscope (ACEM), funded by EERE Office of Freedom Car and Vehicle Technologies primarily for studies of automotive catalytic materials at the atomic level, was tested at the JEOL Co. factory in Japan and authorized for shipping. Performance tests were conducted over a 2-1/2 day period in late February, with shipping occurring in mid-March. Delivery was projected for May 3 at ORNL, where the instrument was to be installed in the new Advanced Microscopy Laboratory, constructed specially to house the ACEM and several other advanced aberration-corrected electron microscopes, which require an ultra-quiet environment in order to routinely achieve their design specifications (e.g., sub-Ångstrom image resolution and single atomic-column energy-loss spectroscopy for chemical species identification). Figure 1 shows the electron-optical column of the instrument at the factory. This instrument is one of two nearly identical machines that will be installed in the US; the second one will be delivered to Lehigh University at the same time as the ACEM is delivered to ORNL. Thus the EERE research programs supported by electron microscopy at the HTML will have access to world-class imaging capabilities of the highest order, when the instrument is finally accepted for beneficial operation later this year.

The ACEM incorporates a corrector for electron optical aberrations designed by CEOS Co. of Heidelberg, Germany. The corrector is placed in the illumination system of the microscope (above the specimen plane), in order to allow an ultra-fine diameter electron probe to be generated so that the technique of high-angle annular dark-field imaging (HA-ADF) can be used to give images at a resolution limit of 0.7Å. Suitable test specimens have been designed to allow the point-to-point resolution of this new generation of electron microscope to be unambiguously determined, but at the JEOL factory, the environment was not adequate to allow the ultimate resolution to be determined. However, a test was conducted to show clearly that the electron

Fig. 1 JEOL 2200FS-AC "ACEM" at JEOL factory, during February 2004 performance test-out, showing corrector element. Larry Allard is the "magnification marker" at 173cm.

probe diameter was reduced from a standard level of 1.4Å down to approximately the projected level of 0.7Å. As an example of the improvement in image resolution permitted by aberration-correction, even in the detrimental environment of the JEOL factory, Fig. 2 shows an HA-AD image of a silicon single crystal along with a computed diffractogram of the image, indicating a periodicity out to 0.95Å resolution (our first image containing "sub-Ångstrom" information!). Figure 3a shows a different orientation of the silicon single crystal, taken using the JEOL 2010F instrument in the HTML, compared to the same orientation taken using the ACEM. While both images show the 1.36Å separation of the "<110> dumbbells" (see computed structure inset), it is clear that the aberration-corrected image is much higher contrast, and shows better resolution. Finally, a short time was spent at the end of the factory test looking at one of our experimental catalysts (see Quarterly report Oct-Dec 2003). The first aberration-corrected image of a Fresh sample of 2% by weight Pt on a mixed CeO_2-ZrO_2-La_2O_3-BaO-Al_2O_3 support material, which has ultra-fine clusters essentially down to monoatomic dispersions, is shown in Fig. 4. It is

expected that, at 0.7Å resolution, catalysts comprising heavy metal species (such as Pt or Pd) on light oxide substrates (such as Al_2O_3 or TiO_2) will be able to be imaged to show not only single atoms, but also to allow the determination of the location of the single atoms relative to the top or bottom of the support particle, and, ultimately, to identify chemical species at the single atom level using the in-column energy filter for electron energy loss spectroscopy.

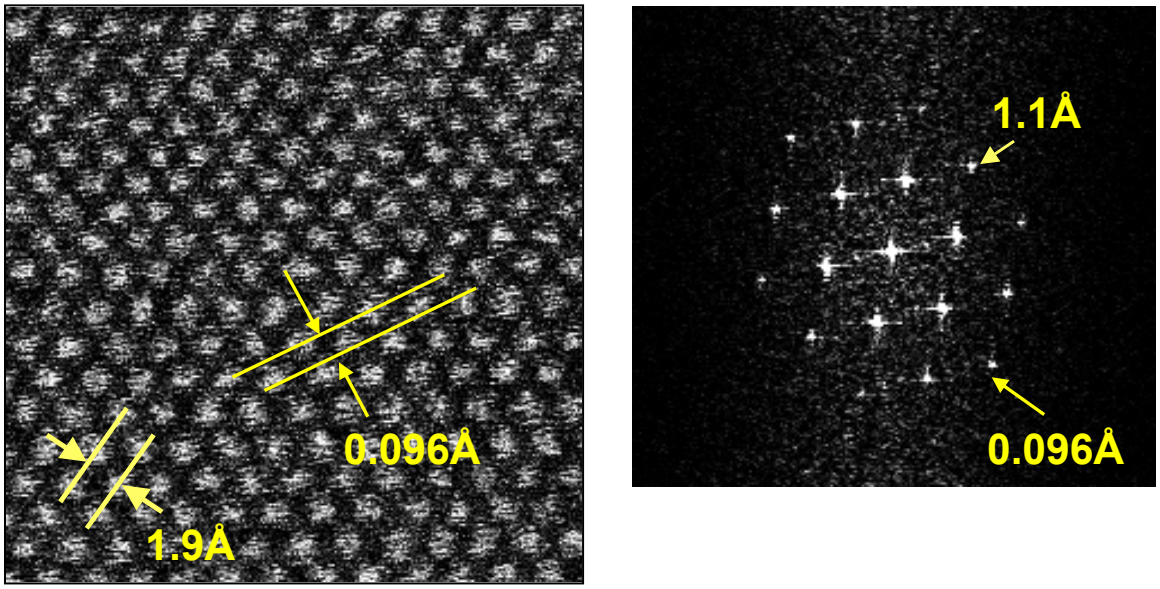

Fig. 2a) HA-ADF image of silicon single crystal in <111> orientation, taken with aberration corrector *on*. b) Fourier transform of the single crystal image, showing information transfer to 0.096Å [silicon lattice planes with this spacing labeled in (a)].

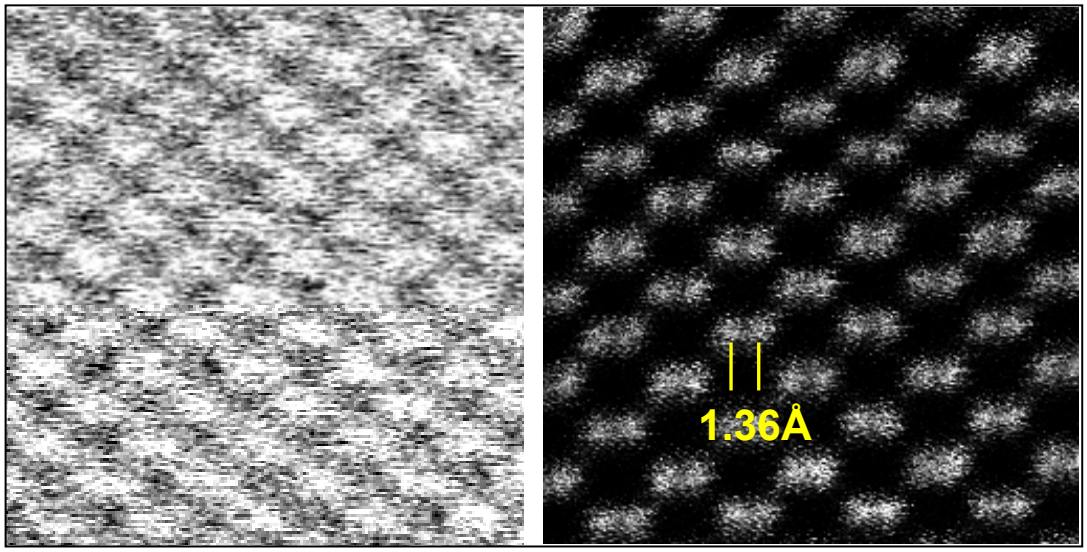

Fig. 3a) HA-ADF image of silicon single crystal in <110> orientation, with *no* aberration correction; b) similar image taken with aberration corrector turned *on*.

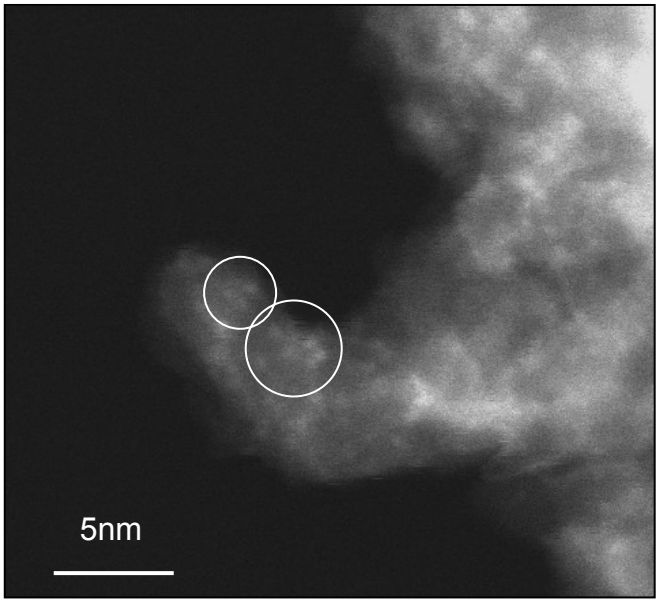

Fig. 4 Fresh Pt/mixed oxide catalyst, imaged with the ACEM in annular dark-field mode, with aberration correction turned on, showing clusters less than 5Å in size (e.g., circled). Clear identification of single atoms in an aberration-corrected image is expected when the instrument is installed in the new Advanced Microscopy Laboratory, with a suitable quiet environment (as compared to the factory conditions under which this image was obtained).

Microstructural Changes in NO_x Trap Materials under Lean and Rich Conditions at High Temperatures

C.K. Narula, K. K. Lester, and L.F. Allard
Oak Ridge National Laboratory

Objective/Scope

The introduction of diesel-engine-based heavy-duty trucks and passenger vehicles depends on the successful development of a strategy to treat nitrogen oxides (NO_x) emissions. A catalyst or a combination of catalysts that can convert NO_x into inert gases under oxidizing conditions over a complete range of exhaust temperatures does not presently exist. Among NO_x treatment strategies, lean NO_x traps (LNT) are the most likely candidates for early deployment because they are consumer transparent (no action needed on the part of consumers) and can be system-integrated into current vehicle control strategies [1].

NO_x traps collect engine out NO_x during lean operation and treat it during short rich operation cycles [2]. The NO_x traps can be considered to be derived from commercial three-way catalysts (TWC) installed to treat stoichiometric emissions from engines operating at air-fuel ratios of ~14. As such, the basic components of NO_x traps are identical to three-way catalysts. The advance version of three-way catalyst is a two layer system on a honeycomb substrate with the inner layer based on platinum-alumina and the outer layer on rhodium-ceria-zirconia. The NO_x traps derived from advanced three-way catalysts are identical to these with the exception of high baria content (the upper limit being close to 20%) in the alumina layer.

Fresh NO_x traps work very well but cannot sustain their high efficiency over the life-time of vehicles. The gradual and persistent deterioration in the performance of commercial TWC is quite well known [3]. The performance deterioration in NO_x traps is believed to be caused by aging due to high-temperature operation and sulfation-desulfation cycles necessitated by the sulfur oxides in the emissions from the oxidation of sulfur in fuel. The formation of barium aluminate is also considered to be a cause of performance deterioration since barium aluminate forms on thermal aging and is an inefficient NO_x adsorber. Until last year, the aging related microstructural changes in precious metals component were not available in open literature. In our previous reports, we summarized our studies of fresh and aged supplier samples that clearly show changes that occur on aging under various operating conditions. The prominent changes are sintering and migration of precious metals and migration of barium leading to reduced precious metal-adsorber surface area available for NO_x adsorption in lean cycles.

In order to design a thermally durable NO_x trap, there is a need to understand the changes in the microstructure of materials that occur during various modes of operation (lean, rich, and lean-rich cycles). This information can form the basis for selection and design of new NO_x trap materials that can resist the deterioration under normal operation. The first goal of the project is to determine if one or all of the microstructural changes take place during lean, rich, or lean-rich cycles.

The tasks to achieve this goal are as follows:

- Complete microstructural characterization of fresh and thermally aged NO_x trap materials to determine the species formed as a result of aging.
- Complete microstructural characterization of fresh NO_x trap materials after exposure to lean conditions to determine the species formed during lean cycles.
- Complete microstructural characterization of fresh NO_x trap materials after exposure to rich conditions to determine the species formed during rich cycles.

The second goal of the project is to investigate and design new materials that can withstand NO_x trap operating conditions without undergoing detrimental structural changes. The results from first goal will provide insights into changes that occur in NO_x trap materials at a microstructural level upon extended exposure to NO_x trap operating conditions enabling selection and design of materials for the second goal.

In order to carry out a detailed study of role of operating condition in inducing these changes, we synthesized a model NO_x trap catalyst 2%Pt-98%[10%CeO_2-ZrO_2-90%(2%La_2O_3-98%BaO.6Al_2O_3)]. The structural characterization of this catalyst was also summarized in the previous reports. The TEM studies of the freshly prepared model catalyst 2%Pt-98%[10%CeO_2-ZrO_2-90%(2%La_2O_3-98%BaO.6Al_2O_3)] show the substrate to be primarily amorphous. The precious metal particles (Pt particles) are generally ~1nm in diameter.

We completed the thermal aging and microstructural characterization of the model NO_x trap catalyst 2%Pt-98%[10%CeO_2-ZrO_2-90%(2%La_2O_3-98%BaO.6Al_2O_3)]. We carried out the thermal aging of the 2%Pt-98%[10%CeO_2-ZrO_2-90%(2%La_2O_3-98%BaO.6Al_2O_3)] at 500, 600, 700, 800, and 900°C for 4 hours in air. The substrate does not show significant difference except the XRD peaks for the barium aluminate component gradually increases with increased sintering temperature (previous report). The TEMs of fresh and thermally aged samples at 500ºC (previous report) showed that sintering of Pt occurs even at 500ºC with an increase in particle size to ~30-40nm. Sintering of Pt increases with an increase in the thermal aging temperature. After aging at 900ºC, the Pt particle size increases to 70-80nm (with an occasional very large particle ~150nm).

Previous report also summarized our preliminary study of aging of 2%Pt-98%[10%CeO_2-ZrO_2-90%(2%La_2O_3-98%BaO.6Al_2O_3)] under lean or rich NO_x conditions carried out in the updated ex-situ reactor (described previously). In the following sections, we describe our results on the aging of the NO_x trap materials.

<u>Aging of Model Catalyst under Simulated Lean Diesel Exhaust:</u> The TEM of a fresh sample of model catalyst, 2%Pt-98%[10%CeO_2-ZrO_2-90%(2%La_2O_3-98% BaO.6Al_2O_3)], and Pt particle size distribution, centered at 1.4 nm, is shown in Figure 1.

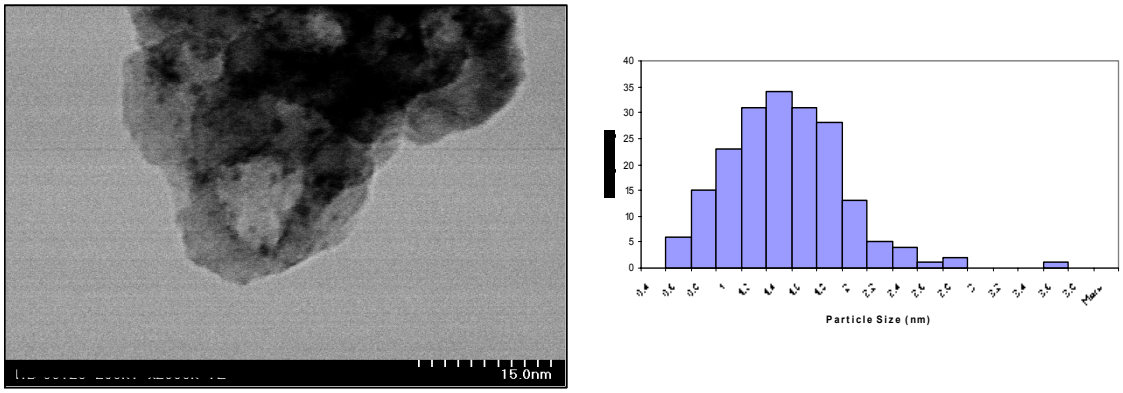

Fig. 1: Transmission electron image and Pt particle size distribution of fresh Pt/[10%CeO_2-ZrO_2-90%(3% La_2O_3-97%BaO.6Al_2O_3)].

We placed a fresh sample of the model catalyst in the ex-situ reactor system (described previously) and exposed it to lean or rich diesel exhaust conditions at 500°C for 4 hours [CO, CO_2, H_2, HC, NO_x, H_2O, flow rate 100cc/min]. Some sintering of Pt particles is observed under these conditions and the size grows to ~2.5nm, see Figure 2, 3. However, the sintering is significantly less than that observed on thermal aging (~30-40nm) at 500°C in air.

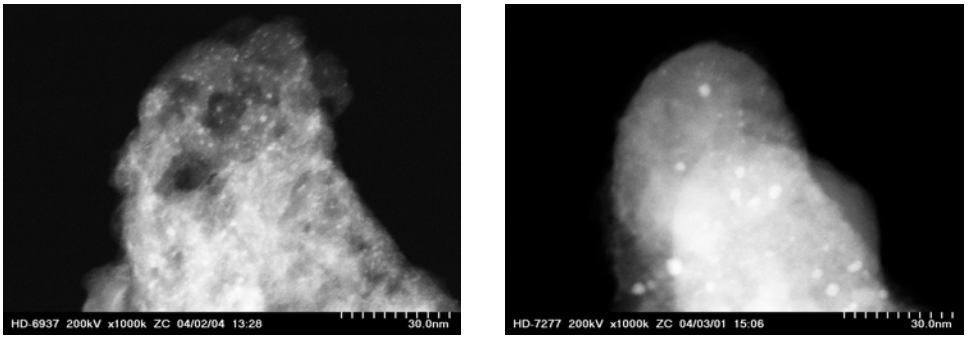

Fig. 2: Transmission electron image of fresh Pt/[10%CeO_2-ZrO_2-90%(3% La_2O_3-97%BaO.6Al_2O_3)] and after 4 h exposure to simulated lean exhaust at 500ºC in ex-situ reactor.

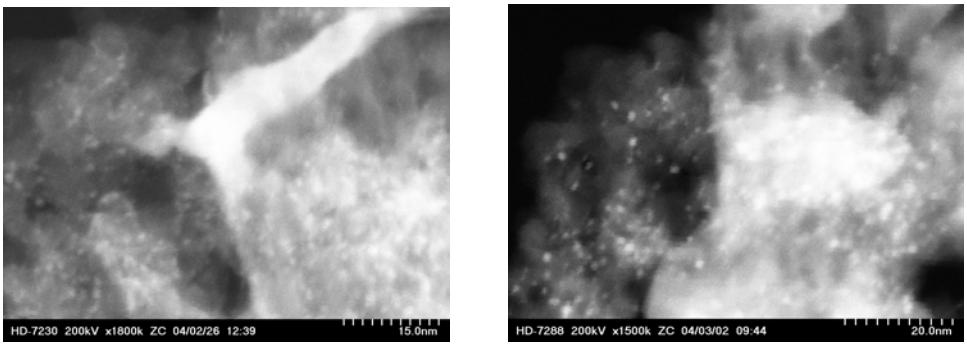

Fig. 3: Transmission electron image of fresh Pt/[10%CeO_2-ZrO_2-90%(3% La_2O_3-97%BaO.6Al_2O_3)] and after 4 h exposure to simulated rich exhaust at 500ºC in ex-situ reactor.

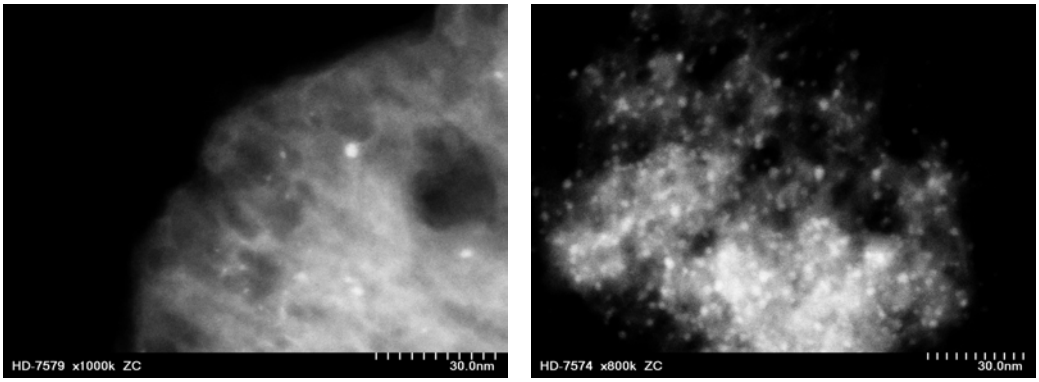

Fig. 4: Transmission electron image of fresh Pt/[10%CeO_2-ZrO_2-90%(3% La_2O_3-97%BaO.6Al_2O_3)] and after 4 h exposure to simulated lean (left) or rich (right) exhaust at 500ºC in bench top reactor.

In the previous report, we reported a surprising observation of re-dispersion of Pt in model catalyst, 2%Pt-98%[10%CeO_2-ZrO_2-90%(2%La_2O_3-98%BaO.6Al_2O_3)], when thermally aged the sample exposed to lean diesel exhaust conditions at 500°C. We repeated this experiment on a 1.0g batch of sample a bench-flow reactor and found that some re-dispersion does occur. However, no re-dispersion was observed if thermally ages sample was exposed to rich diesel exhaust conditions at 500C for 4 h either in the ex-situ reactor or bench flow-reactor.

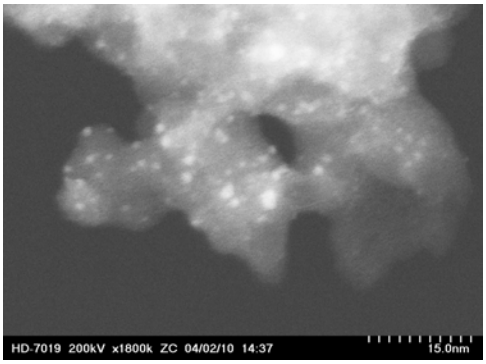

Fig. 5: Dark-field Z-contrast image of thermally aged Pt/[10%CeO_2-ZrO_2-90%(3%La_2O_3-97%BaO.6Al_2O_3)] after exposure to lean simulated exhaust in a bench flow reactor. Pt particles are ~3-4 nm in diameter.

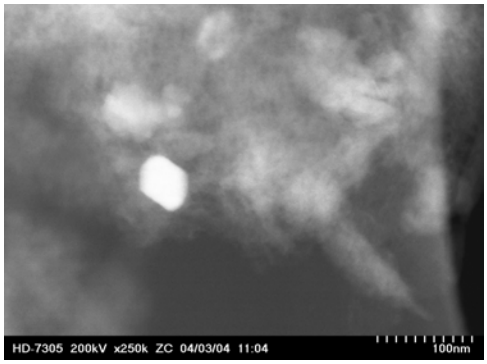

Fig. 6: Dark-field Z-contrast image of thermally aged Pt/[10%CeO_2-ZrO_2-90%(3%La_2O_3-97%BaO.6Al_2O_3)] after exposure torichsimulated exhaust in a bench flow reactor. Pt particles are ~20-40 nm in diameter.

In general, the particle size of precious metal component of the catalysts increases upon extended exposure to automotive operating conditions [3]. <u>The redispersion of Pt particles under simulated diesel exhaust is quite unexpected because these conditions do not match the conditions under which redispersion has previously been observed.</u> Chu and Ruckenstein found that after a number of heating cycles, in H_2 or O_2, Pt particles redisperse upon a final heating in O_2 and sinter upon a final heating in H_2 [4]. Johnson and Keith found that thermal aging of Pt/alumina under oxidizing conditions and subsequent heat treatment in H_2 leads to Pt redispersion [5].

Weller and Montagna also found the redipersion of Pt in Pt-Al_2O_3 on cyclic exposure to O_2 and H_2 during reduction step [6] They also noted that the redispersed Pt is resistant to sintering [6]. The redispersion is not limited to Pt-Al_2O_3 systems but has also been observed in Ni-Al_2O_3 and Ni-SiO_2 systems when oxidation was carried out at 600ºC and reduction at 400ºC [7]. In our system, the samples were thermally aged in air, then exposed to lean exhaust conditions, and finally cooled under lean conditions. The results have been found to be reproducible.

It is important to note that the experiments in the ex-situ reactor system do not precisely duplicate the aging of NO_x traps during normal operation. The alternating lean/rich conditions are not present in our experiments; instead, our samples are exposed to lean conditions, and lack of control on space velocity due to very small amount of catalyst leads to NO_x absorber saturation conditions. The saturation condition persists throughout our treatment.

Although the mechanism of redispersion under simulated lean NO_x diesel conditions remains to be determined, these results seem to suggest that the Pt particles only grow to 5-10 nm in size after sintering in a lean diesel exhaust at 500ºC (as opposed to 30-40nm after exposure to air at 500ºC) because the concurrent redispersion prevents further increase in particle size.

Our studies in the next quarter will be focus on following experiments:

- The studies of micro-structural changes at 900C under lean or rich conditions.
- The time needed to achieve redispersion.

Other activities

We are updating ex-situ reactor to build a lean-rich cycling capabilities. Gas flow controllers, water pump, and gas analyzers have been received and we initiate assembly of a bench-top flow reactor in a laboratory at National Transportation Research Center (NTRC). Other items will be added to the flow reactor upon receipt.

Communications/Visitors/Travel

CKN traveled to Purdue University to give a seminar on NOx trap catalysis.

References

1. Miyoshi, N.; Matsumoto, S.; Katoh, K.; Tanaka, T.; Harada, J.; Takahashi, N.; Yokota, K.; Sigiura M., and Kasahra, K.; "Development of New Concept Three-Way Catalyst for Automotive Lena-Burn Engines", SAE paper 95-0809.
2. Takahashi, N.; Shinjoh, H.; Iijima, T.; Suzuki, T.; Yamazaki, K.; Yokota, K.; Suzuki, H.; Miyoshi, N.; Matsumoto, S.; Tanizawa, T.; Tateishi, S.; and Kasahara, K.; "The New Concept 3-Way Catalyst for Automotive Lean-Burn Engine: NO_x Storage and Reduction Catalyst", Catalysis Today, 1996, **27**, 63-69.
3. Gandhi, H.S., Graham, G.W., and McCabe, R.W., "Automotive Exhaust Catalysis", J. Cat., 2003, **216**, 433-442.
4. Chu, Y.F.; Ruckenstein, E.; "On the Sintering of Platinum on Alumina Model Catalyst", Journal of Catalysis, 1978, 55, 281-298.
5. Johnson, M.F.L.; Keith, C.D.; "The State of Platinum in Re-Forming Catalysis", 1963, **67**, 201.

6. Weller, S.W., Montagna, A.A.; "O_2 Chemisorption at High Temperatures on Platinum-Alumina and Platinum-Zeolite", J. Catal., 1971, **20**, 394.
7. Nakayama, T.; Arai, M.; Nishiyama, Y.; "Dispersion of Nickel Particles Supported on Alumina and Silica in Oxygen and Hydrogen", J. Cat., 1984, **87**, 108.

Lightweight Valve Train Materials

Mark J. Andrews
Caterpillar Inc.

Introduction

Valve train components in heavy-duty engines operate under high stresses and temperatures, and in severe corrosive environments. In contrast, the valve train components in the light-duty engine market require cost-effective reliable materials that are wear resistant and lightweight in order to achieve high power density. For both engine classes, better valve train materials need to be identified to meet market demand for high reliability and improved performance while providing the consumer lower operating costs.

Advanced ceramics and emerging intermetallic materials are highly corrosion and oxidation resistant, and possess high strength and hardness at elevated temperatures. These properties are expected to allow higher engine operating temperatures, lower wear, and enhanced reliability. In addition, the lighter weight of these materials (about 1/3 of production alloys) will lead to lower reciprocating valve train mass that could improve fuel efficiency. This research and development program is an in-depth investigation of the potential for use of these materials in heavy-duty engine environments.

The overall valve train effort will provide the materials, design, manufacturing, and economic information necessary to bring these new materials and technologies to commercial realization. With this information, component designs will be optimized using computer-based lifetime prediction models, and validated in rig bench tests and short-and long-term engine tests.

Program Overview

Information presented in this report is based on previous proprietary research conducted under Cooperative Agreement DE-FC05-97OR22579.

Ceramic Materials

Silicon nitride materials have been targeted for valve train materials in automotive and diesel industries since early 1980's. Some silicon nitride material grades have reached a mature level of materials processing, capable of implementing into production. Commercial realizations have been reported in both automotive and diesel valve trains, with large-scale production underway. The silicon nitride valve train components in production are used in high rolling contact stress applications and have exhibited superior wear resistance, and longevity.

Intermetallic Materials

Titanium aluminide based intermetallics retain their strength to elevated temperature and are highly corrosion-resistant. They are lightweight, and posses high fracture toughness. These alloys are actively being investigated for several aerospace and automotive applications.

Current Quarter Summary

Valve Test Rig

The valve bench rig continues to extend the impact and wear study for the NT551 silicon nitride engine valves. Tables 1 summarizes the impact and wear test parameters for the valves that are

accumulating 1000 hours of test time. No NT551 valves have failed during these rig tests but additional polishing type wear has been observed on the contact region of the valves. In addition, an unknown deposition has been observed on the valve contact region and in the fillet radius region (see figure 1). These tested valves will be examined by ANL using optical and NDE techniques to assess the accumulation of cyclic damage and then destructively tested to determine the retained strength of the valves.

Advanced Materials Technology is acquiring a second valve test rig presently located in TC-L at the Tech Center. This test rig can accommodate 3400 and 3500 series engine valves and uses standard Caterpillar seat insert components. The rig applies a hydraulic load to the valve face cyclically, simulating the combustion pressure load of the engine. The rig can also apply a cyclic thermal load through induction heating. Relocation of the test rig is anticipated in the next reporting period.

Machining Study

The SN235P cylindrical test specimens that were subject to three different super-finishing machining processes were strength tested in four-point flexure. The tests were conducted at the Oak Ridge National Laboratory through a Facility User agreement. A specialized four-point test fixture was designed and built for the cylindrical test specimens by A. Wereszczak of ORNL. All tests were conducted at ambient temperature conditions and at the displacement rate of 0.5 mm/minute, as specified in the ASTM C-1161 standard.

Figures 2 and 3 show the uncensored Weibull moduli and characteristic strength of twelve different surface finish conditions. Some of the finishing processes improve the data variance as indicated by the high Weibull modulus value. The characteristic strength shown in Figure 3 suggests that the inherent strength of the SN235P material is met regardless of machining condition. Plausible explanations for the increase in the Weibull modulus values could be related to the residual stress that is a result of the finishing processes. ORNL staff members are examining some of the test specimens using x-ray diffraction to assess the presence of residual stress and these results are anticipated in the next quarterly report.

Silicon Nitride Valve Blanks

Forty-eight silicon nitride engine valve blanks fabricated from SN235P silicon nitride were finished machined at Junker Machining in Norarch, Germany. An error by Junker was made in reading the valve print specifications, resulting in the absence of a specialized grinding wheel. The surface Ra in the fillet radius region is approximately three times rougher than specified by the prints (see Figure 4).

Requests for quotes have been sent out to determine the most cost effective manner to finish machine the SN235P valves in the rough machined region, and results from these inquiries are anticipated in the next reporting period.

Engine Tests for Advanced Materials Valves

Upon completion of bench test results, the SN235P valves are scheduled for engine tests later in 2004. These tests will be conducted at the National Transportation Research Center (NTRC)

located near the ORNL. Arrangements are underway to instrument an engine head for obtaining relevant performance metrics for engine valves.

Intermetallic Materials Research

Ten γ-TiAl valve head blanks were received from Junker Machining in Norarch Germany after completing rough machining the heads. The prototype components have undergone friction welding, attaching a Ti-6V-4Al stem to the valve head. The prototype valve blanks are scheduled for final machining to Junker in Germany and completed valves are anticipated in the next reporting period.

ANL

Shipments of cylindrical test specimens and NT551 ceramic valves were made to ANL for NDE assessment. A specific set of rough machined cylindrical test specimens will be examined as a means to identify the failure site on the test specimen before strength testing. Results of the strength testing and NDE predictive behavior are anticipated in the next reporting period.

Presentations

None

Future Work

SN235P prototype engine valves will begin impact and wear bench tests and will be subject to cyclic simulated combustion loads when the second test rig is relocated to AMT. The 1000 hour impact and wear NT551 valves will be strength tested at ORNL to assess their retained strength. An investigation into the unknown deposition observed on the NT551 valves will begin. RFQs for finish machining the SN235P valves will be received and a decision will be made as to the most cost effective manner to finish the valves. Completed γ-TiAl attached to Ti-6V-4Al valves will be bench tested after final machining at Junker. Efforts will continue collaborating with ANL assessing the subsurface damage from machining processes and preparations will continue for engine tests at the NTRC.

Table I. Bench test matrix for NT551 valves for completing 1000 hours on valve rig.

Valve Number	100-hr valve-**seat**	400-hr valve- **seat**	500-hr valve- **seat**	Total hours
CV04, CV12	30-**30**	30-**30**	30-**30**	1000
CV19, CV20	45-**45**	45-**45**	45-**45**	1000
CV18, CV25	45-**30**	30-**30**	45-**30**	1000
CV08, CV15	30-**45**	30-**ECC**	30- **ECC**	1000
CV14, CV16	30- **ECC**	30- **ECC**	30- **ECC**	in process

Notes: **bold** number and letters indicate the contact angle of the seat insert while nonbold numbers indicate the valve contact angle. ECC = eccentric seat insert, specifically machined to have two high contact points

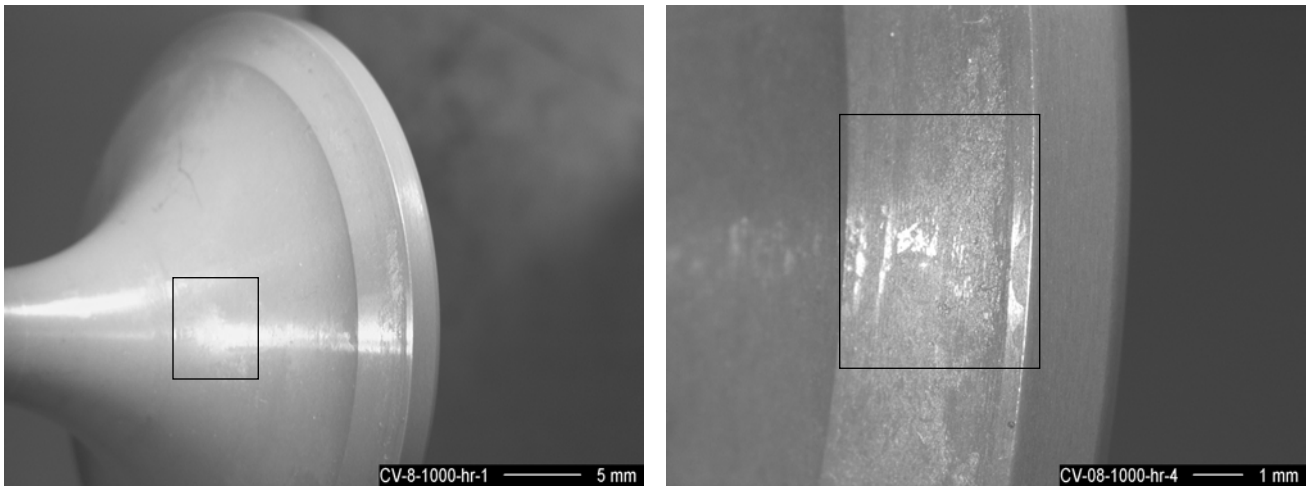

Figure 1. NT551 engine valves subject to 1000 hours of impact / wear tests. Note the deposition in the fillet radius and the contact regions (boxed regions).

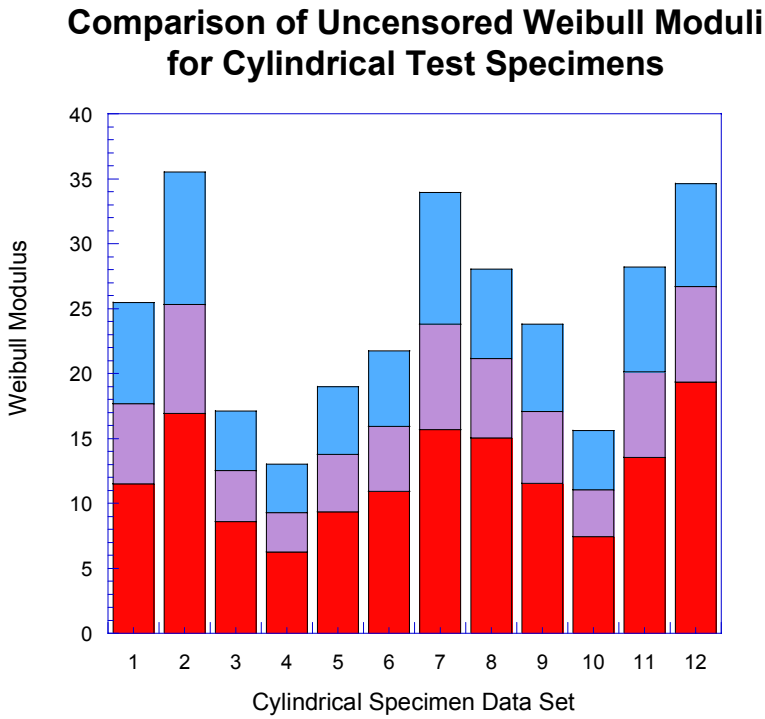

Figure 2. Uncensored Weibull moduli from SN235P cylindrical test specimens tested in four-point flexure for various finish machining conditions. Regions at the top of each column represent the 95% confidence interval of the data

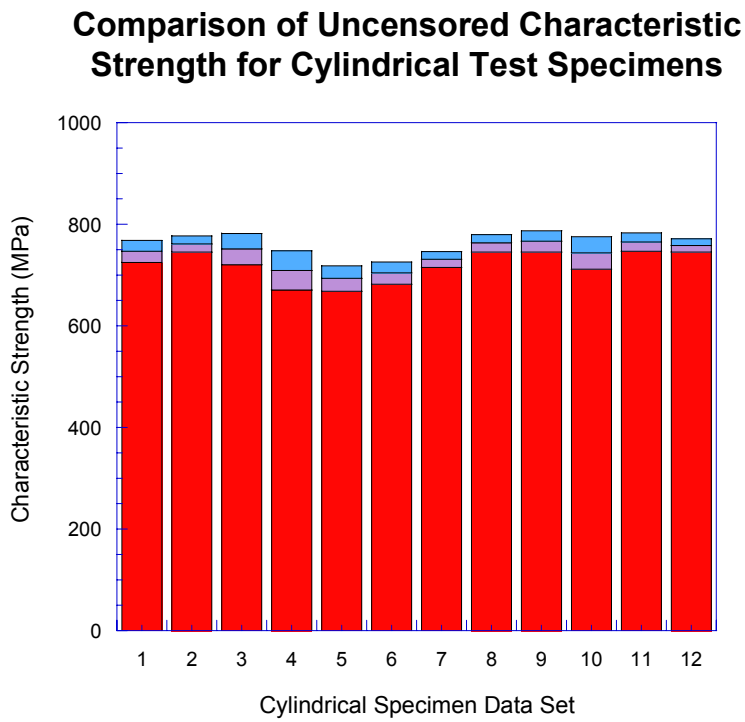

Figure 3. Uncensored Weibull characteristic strength of cylindrical SN235P test specimens tested in four-point flexure. Regions at the top of each column represent the 95% confidence interval of the data

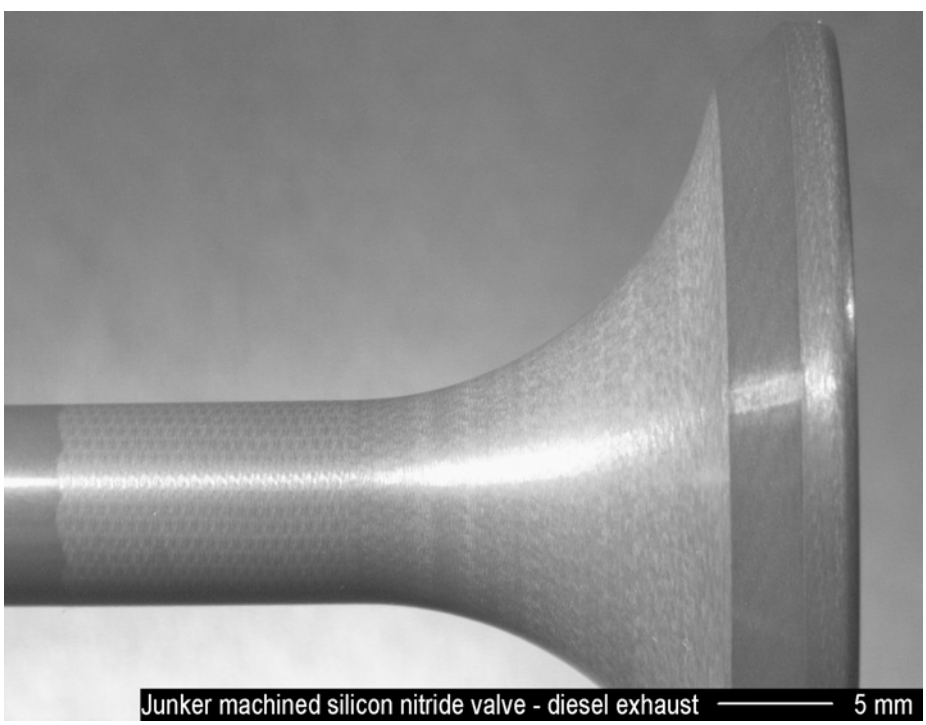

Figure 4. Illustration of the rough machining region on the SN235P engine valves.

Engineered Surfaces for Diesel Engine Components

M. Brad Beardsley and Jesus G. Chapa-Cabrera
Caterpillar Inc.

Objective/Scope

Engine testing of thermal sprayed coatings has demonstrated their use as thermal barriers and wear coatings can reduce fuel consumption, reduce wear and reduce component temperatures. The durability of thermal sprayed coatings, particularly thermal barrier coatings, remains as the major technical challenge to their implementation in new engine designs. New approaches to coating design and fabrication will be developed to aid in overcoming this technical hurdle. New laser technology of surface dimpling, cleaning and laser assisted spraying will be applied to enhance adherence and increase coating strength. Refinements of current seal coating technologies will be developed to further enhance the durability of the coating structure. New quasicrystalline materials will be evaluated as thermal barrier coatings as well as wear coatings for ring and liner applications and as low friction coatings for camshafts and crankshafts. Plasma spraying, D-Gun and HVOF processing will be used to develop these new coatings.

Technical Highlights

Laser Tacking - Laser tacked TBC specimens for tensile adhesion testing have been processed. Investigation of the tacked areas by metallography has shown that the "key-hole" tacking was only partial successful at the lower power levels and at the higher power levels, the ceramic TBC material cracked and delaminated from the substrate, Figures 1-2. The cracking and delamination of the ceramic indicates that the laser tacking will not be a viable method to pursue. However, the melting of the surface at low power (Figure 1) and the good microstructure of the bond coating laser tacked at medium laser power, Figure 3, indicates promise for the coupling of the laser and plasma spray processes in the laser-assisted plasma process.

Laser Assisted Thermal Spraying – A visit to the Fraunhofer Dresden, Germany, facility has been scheduled for June. The process should be nearly ready for demonstration at this time and discussions will take place in regard to the setup of the process at Caterpillar's Technical Center. A 4 kW YAG laser has been identified within Cat's surplus inventory that can be utilized. The laser will become available in July.

Laser Dimpling for Adherence – A visit to the IREPA and ISPE institutes in France is planned for June to hold discussion in regard to licensing their patent PROTAL process. A demonstration of the process is planned and specimens will be done for Caterpillar's evaluation.

Quasicrystals – Diffusion couples of the $Al_{71}Co_{13}Fe_8Cr_8$ quasicrystal have been run at Iowa State University. The couples included a 4140 steel substrate, two NiCrAlY bond coatings with different chrome and aluminum contents and a FeCrAlY bond coating. Micrographs of the initial diffusion zones show high reaction at the quasicrystal and bond coating or substrate interfaces, Figure 4. Microprobe analysis will be done to determine the diffusion specie.

Future Plans
Full microprobe analysis of the quasicrystal diffusion couple samples will be completed and oxidation test specimens will be sprayed. Trips to Fraunhofer in Dresden, Germany and France to discuss the laser-assisted plasma and PROTAL processes will be in June.

Travel
None this quarter; two trips to Europe are planned for next quarter.

Status of FY 2003 Milestones
321. Determine the effect on TTBC bond strength due to laser micro-dimpling of the substrate surface prior to coating. (July 31, 2003)

Q-switched laser technology identified as a path to achieve surface topography required for bonding without the need for grit blasting.

322. Determine the effect on TTBC coating strength and permeability due to laser shock peening after coating application. (July 31, 2003)

The Q-switched laser technology will be investigated for this effect. April 2004.

323. Determine the effect on the hardness and microstructure of the TTBC due to laser assisted plasma deposition. (July 1, 2003)

No progress to report.

324. Incorporate torsional fatigue testing results into life models. (Completed May 29, 2002)

The final report of this work has been received from the University of Illinois.

325. Develop FEA models to aid in the design of life prediction tools for the TTBC system. (December 1, 2003)

No progress to report.

325. Evaluate the microstructure of the ceramic TTBC material using varying laser power.

No progress to report.

Publications
None this period.

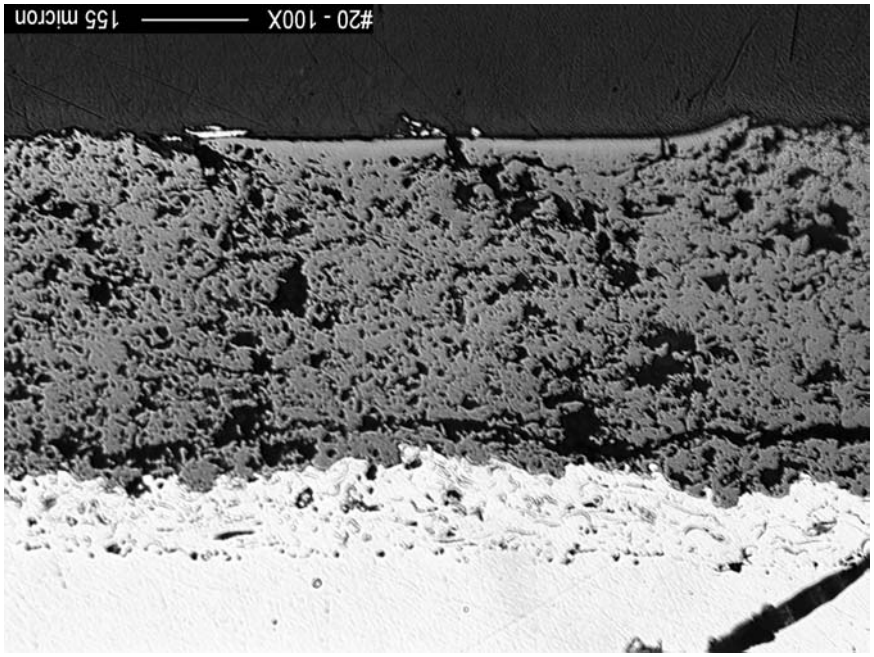

Figure 1. Ceramic TBC laser tacked at low laser power showing only small level of melting at the surface of the coating.

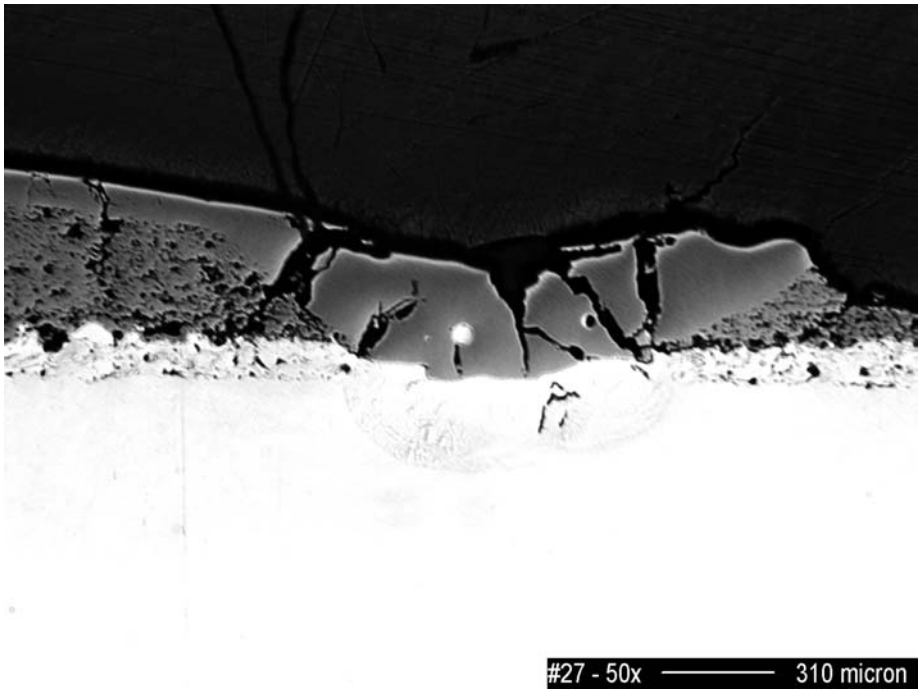

Figure 2. Ceramic TBC laser tacked at high laser power showing only complete melting of the ceramic with cracking and delamination.

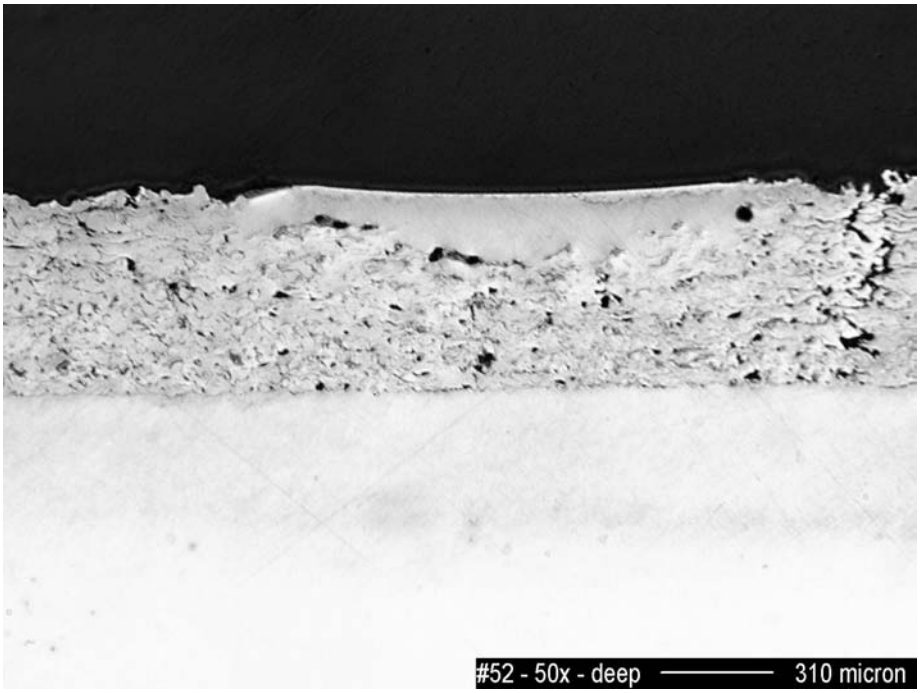

Figure 3. Laser tacked bond coating specimen showing melting and cracking of the coating.

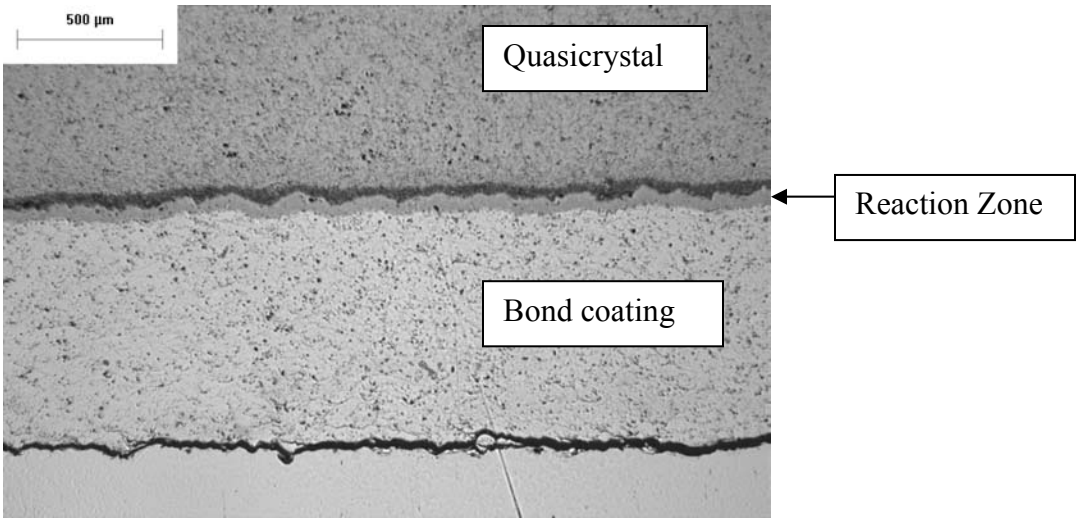

Figure 4. Diffusion couple run at 700ºC for 500 hours shown large reaction zone.

Processing and Characterization of Structural and Functional Materials for Heavy Vehicle Applications

J. Sankar, Z. Xu, and S. Yarmolenko
North Carolina A & T State University

Objective/Scope

Study and develop a slurry casting technique to fabricate planar cathodes for solid oxide fuel cells (SOFCs).

Task

Investigate the effect of the processing parameters of slurry casting technique on the microstructure of the cathodes.

Technical Highlights

Slurry casting is a very suitable method to prepare green form of ceramic tiles. It can be a very low-cost way to prepare porous cathode and anode components for the application of SOFCs.

The general procedures involves mixing powders with binder and solvent, preparing slurry with ball milling, casting and drying to obtain green forms and sintering to obtain the final products. The purpose of this research is to study how to mix the source powders, how to grind the power mixture using ball milling to obtain the desired microstructural properties of the sintered cathodes. This technique can also be applied to the fabrication of the anode of SOFCs. The results of this research can lead to low cost production of the electrodes of SOFCs and thin film SOFCs by combining our thin film electrolyte coating techniques.

For slurry casting, commercial strontium doped lanthanum manganite (LSM) and yttria stabilized zirconia (YSZ) powders were used for the structural materials of the sintered cathodes. Carbon black powder was used as filler in the green forms. Pre-formulated water-based polymeric binger solution (WB4101, Polymer innovations, Inc.) was used to facilitate casting properties of the slurry. Certain amount of ethanol was added to reduce the viscosity of the slurry. Cast was dried at room temperature in open atmosphere. The final cathodes were obtained by high temperatures sintering.

Results and Discussion

Preparation of the slurry (Ball Mill)

Mixture of powder, binder and solvent was ball milled for different times. The jar of size 000 (US Stoneware) and ~190 rpm were used for ball milling. The samples were taken from the milled mixture and observed with SEM. Their micrographs are shown in Figure 1. The purpose of this procedure was to reduce the particle size and prepare stable homogeneous slurry for tape casting.

One hour ball milling was only for an initial blending of the mixture. The slurry was inhomogeneous and the particle size ranged from 100 nm to 800 nm which were almost the same sizes as the source powders. After 56 h milling, the particle size was greatly reduced and the

homogeneity of the slurry was remarkably improved. 20 more h milling further improved the properties of the slurry. However, the slurry after 104 h milling did not show noticeable difference from that after 80 h milling. It seems that 80h can be used as a standard milling time with the present system.

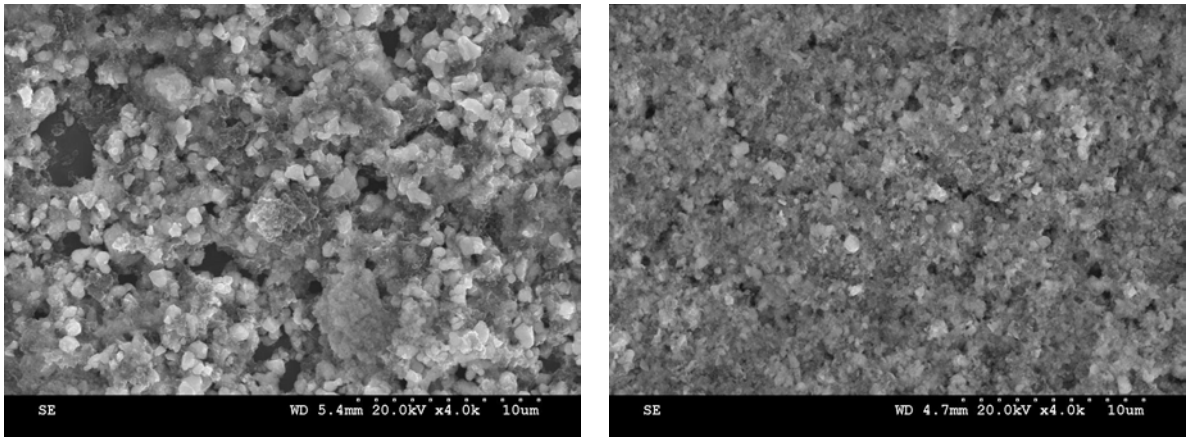

(a) Milled 1 h (b) Milled 56 h

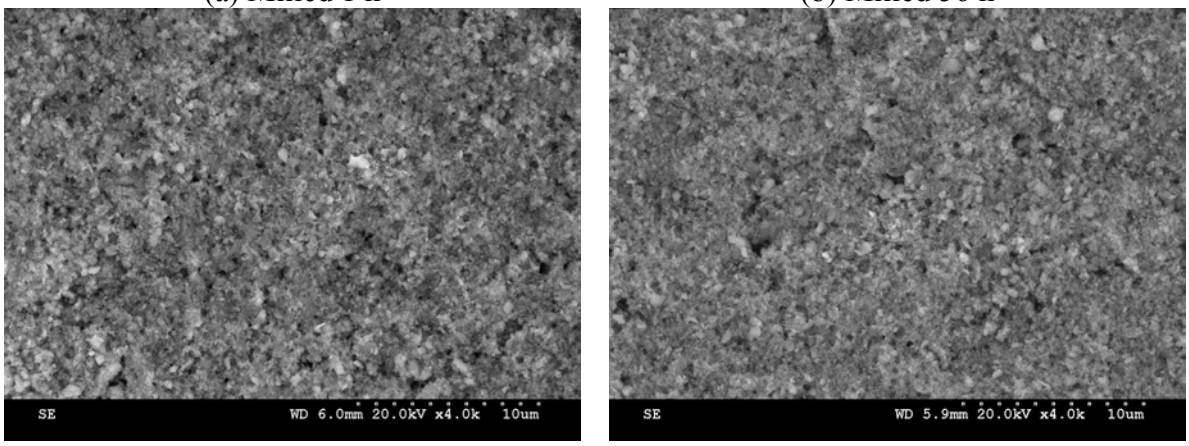

(c) Milled 80 h (d) Milled 104 h

Figure 1. Change in particle size and homogeneity of the mixture with the time of ball milling.

Tape Casting

Tape casting was implemented on a glass plate. Four pieces of aluminum stripes were used to form a mold on the plate. A blade was used to make the surface of the cast. The cast was dried at room temperature for 48 h to form the green form and was cut into desired sizes.

Figure 2 shows the micrographs of the cross-sections of the green forms. It can be seen that the microstructure in the green form is acceptably homogeneous.

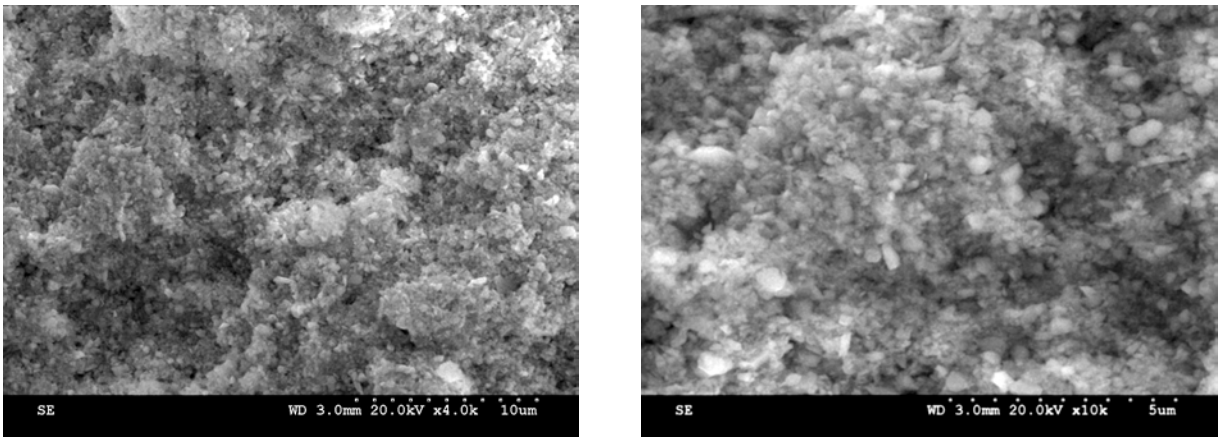

(a) (b)

Figure 2. Cross-section views of a dried green form at two magnifications: a) at x4.0k, b) x10k.

Sintering of the Green Form

Sintering temperature:Sintering was used to remove the organic phase and carbon inclusion, and to sinter the ceramic particles. The green forms were sintered at different temperatures. The one-step sintering was initially used. The heating rate was 20ºC/min. Three maximum sintering temperatures were 950ºC, 1100ºC and 1250ºC, respectively. The soaking time at the maximum temperatures was 30 min. Figure 3 shows the micrographs of the cross-sections of the sintered samples. Temperature of 950ºC did not turn out satisfactory sintering and particle growth was not appreciable. The sample was easy to be crushed into powder. Sintering was able to be seen in the 1100ºC treated sample since particle growth and necking between particles can be observed. Porosity was also apparent. The sample processed at 1250ºC seems to be over sintered. The particle size was greatly increased and most pores were sealed, which is not acceptable for cathode of SOFCs.

Sintering profile: A multi-stepped sintering profile shown in Figure 4 was employed later. The first step was set at 600ºC below which all the organic phases could be burned out. A soaking time of 2 h was designed for complete removal of the organic phase. The second step was set at 1000ºC with a one-hour soaking, below which the carbon could be oxidized and removed. According the previous sintering experiments at different temperatures, temperature of 1100ºC was used as the maximum temperature of sintering. A rate of 5ºC/min was utilized for the heating and cooling ramps.

Figure 5 shows the difference between the samples sintered by a simple one-step cycle and a multi-step cycle. It is evident that multi-stepped sintering produces better defined pore shape and microstructure uniformity.

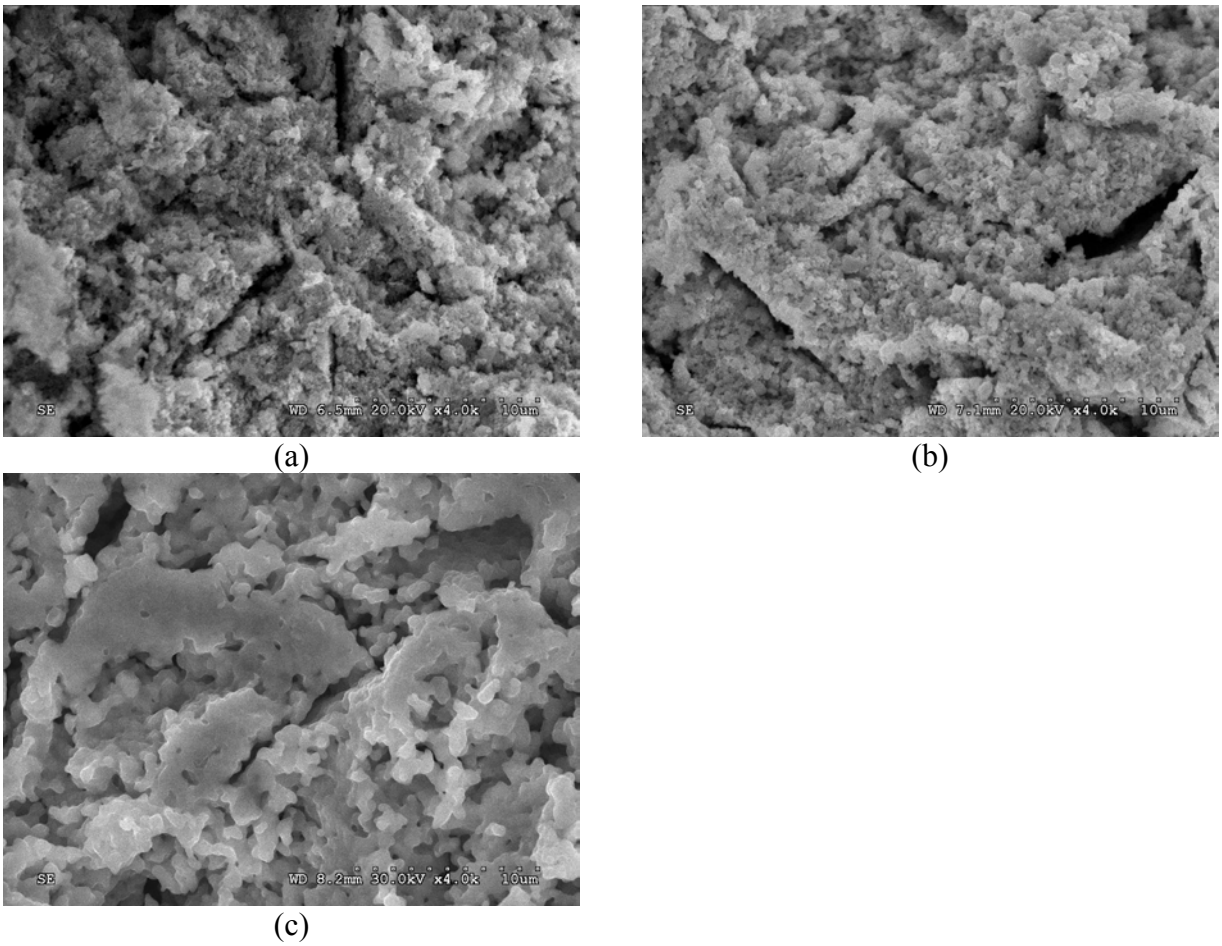

Figure 3. Microstructures of the samples sintered at different maximum temperatures: a) 950ºC, b) 1100ºC, and c) 1250ºC with a soaking time of 30 min.

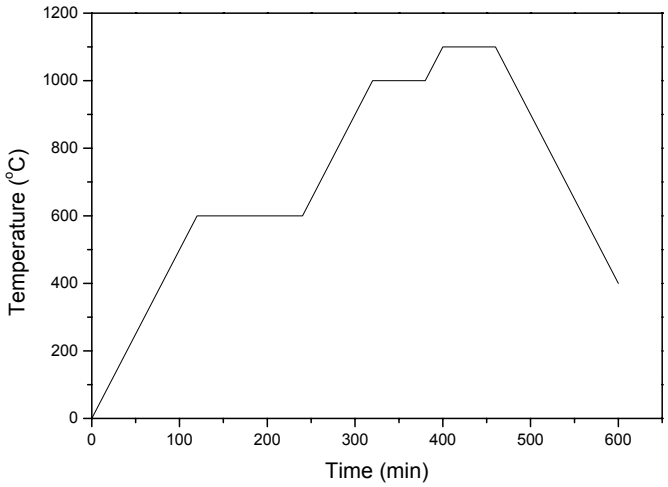

Figure 4. A multi-stepped profile of thermal annealing.

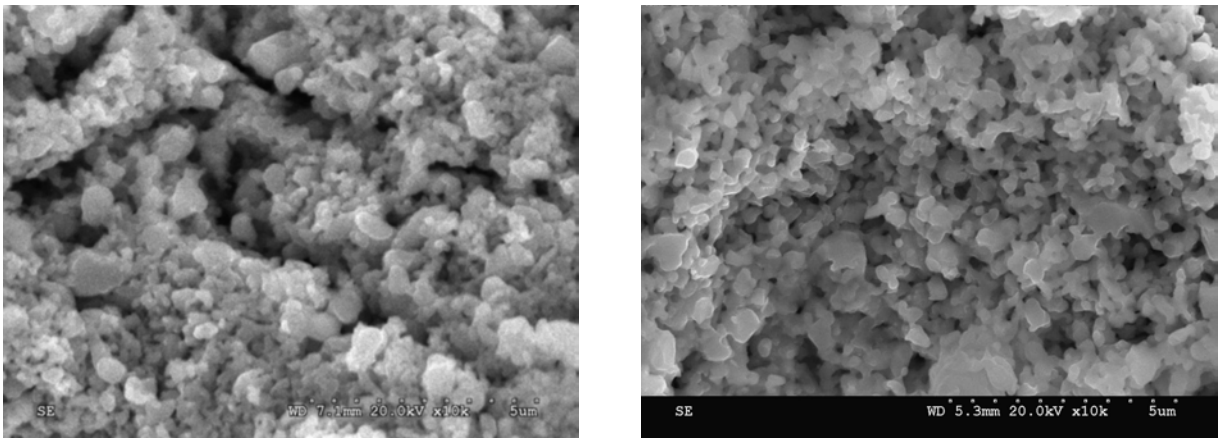

(a) (b)

Figure 5. Micrographs of the samples sintered with a) one-step cycle and b) multi-step cycle.

The effect of graphite amount on porosity

Two different amount of graphite were used to study its effect on porosity of the final products. The amount of the graphite, R_g, is defined as follows,

$$R_g = \frac{V_g}{V_{LSM} + V_{YSZ}}$$

where, V_g is volume of graphite, V_{LSM} is that of LSM powder, and V_{YSZ} is that of YSZ powder. In this experiment, R_g = 10 and 30% were used.

Figure 6 shows the microstructures of the samples with different graphite amounts after the above-mentioned multi-stepped sintering.

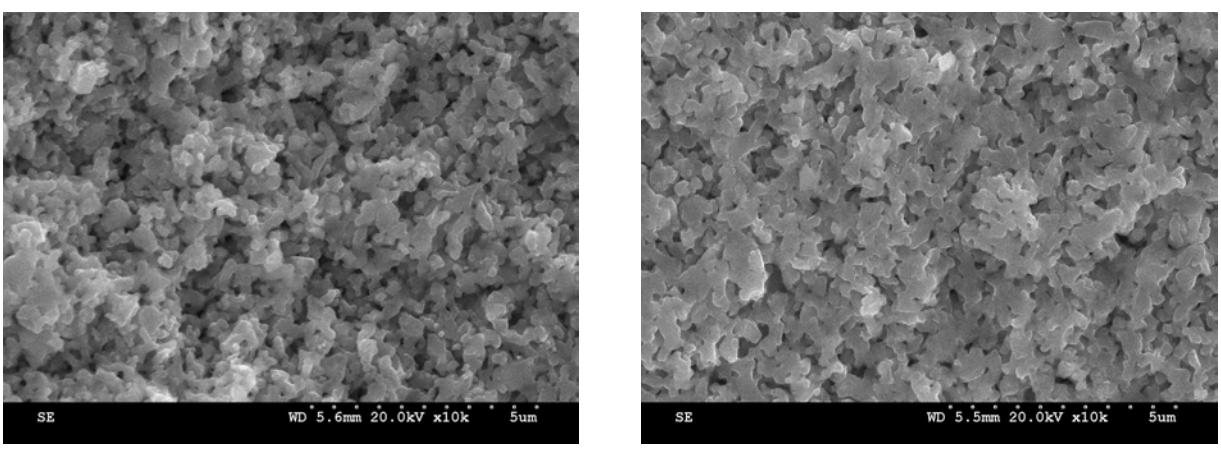

(a) (b)

Figure 6. Microstructures of sintered samples with different amounts of graphite, a) 30 vol % and b) 10 vol %.

The micrographs indicate that with more graphite in the powder mixture, the final products will be more porous and less sintered.

When we have proper equipment to measure the porosity of the products, it is possible to optimize the amount of graphite added in the mixture.

Conclusions

Ball milling of 80 h is sufficient to reduce the particle size of the powders. The water-based binder is effective to produce structural strength and plasticity to handle the green forms. Multiple-stepped sintering cycle provides satisfactory microstructures of the products. Sintering at the maximum temperature of 1100ºC is successful to produce adequate extent of sintering among the ceramic particle. Carbon black as fill is useful to leave pores in the final products after sintering. The porosity is also related to the amount of the carbon addition.

Communications/Visitors/Travel

None

Problems Encountered

None

NDE Development for Ceramic Valves for Diesel Engines

J. G. Sun, J. M. Zhang,
Argonne National Laboratory
and M. J. Andrews
Caterpillar, Inc.

Objective/Scope

Emission reduction in diesel engines that are designated to burn several types of fuels has lead to assessing ceramic engine valves to mitigate valve corrosion and extend service lifetimes. The objective of this work is to evaluate several nondestructive evaluation (NDE) methods to detect defect/damage in structural ceramic valves for diesel engines. The primary NDE to be utilized is the elastic optical scattering or laser scattering method. The goal is to demonstrate that investigations using this method can identify defects/damage that can be used for predicting material microstructural and mechanical properties. There are two tasks to be completed: (1) Characterize surface/subsurface defects and machining damage and correlate NDE data with mechanical properties for rectangular and cylindrical flexure test specimens of candidate silicon nitrides selected for fabricating into prototype valves. Laser-scattering studies will be conducted at various wavelengths using a He-Ne laser and a tunable-wavelength solid-state laser to optimize detection sensitivity. NDE studies will be coupled with examination of surface and subsurface microstructure and fracture surface to determine defect/damage depth and fracture origin. NDE data will also be correlated with mechanical properties. (2) Assess and evaluate accumulated damage in full-size ceramic valves due to rig or engine tests. All prototype silicon nitride valves will be examined at ANL prior to bench tests, after accumulating a specified number of test hours, and at the end of the planned test runs.

Technical Highlights

Work during this period (January-March 2004) focused on acquiring and analyzing laser-scattering NDE data to determine machining-induced subsurface damage in SN235P Si_3N_4 ceramic rods that were machined from two sources: Junker and Supfina.

1. Elastic Optical Scattering NDE for Subsurface Defect/Damage

During the previous and the present periods we received from Caterpillar three sets of cylindrical SN235P Si_3N_4 specimens that are (1) as-processed, (2) machined by Junker, and (3) machined by Supfina. All cylindrical rods are 75-mm long, and they are shown in Fig. 1. Detailed conditions of the rods are listed in Table 1.

All SN235P rods are scanned at 5-micron spatial resolution using laser-scattering NDE method. Figure 2 shows the laser-scattering image of the central 30-mm-long surface of the as-processed SN235P rod #5. It is clear that the subsurface microstructure of this rod is not uniform. As shown in Fig. 2, large (~100 microns), high scatter-intensity spots are detected in the top enlarged image while smaller, low scatter-intensity spots are seen in the lower enlarged image. Higher optical-scatter intensity indicates increased subsurface porosity in the material.

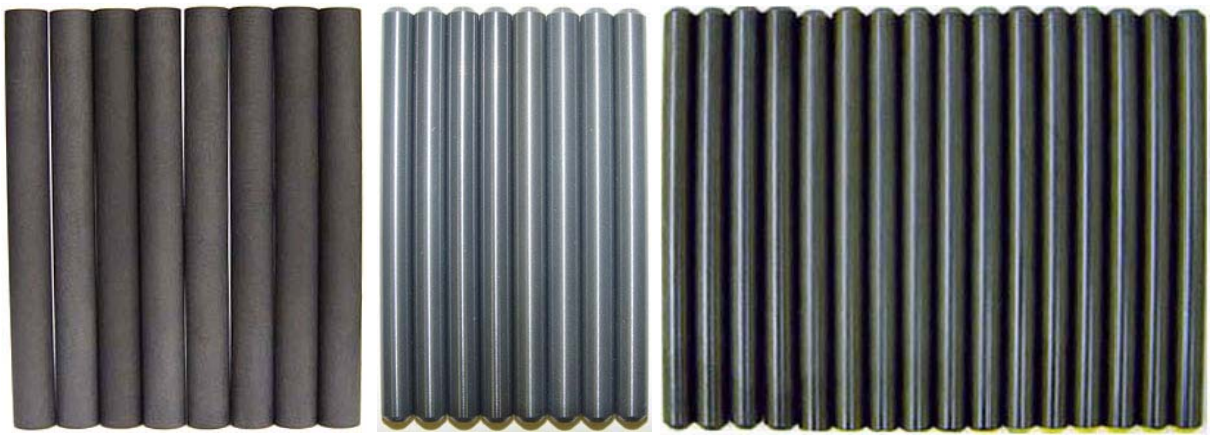

(a) (b (c)

Fig. 1. Photographs of SN235P Si_3N_4 rods: (a) as-processed, and machined by (b) Junker and (c) Supfina.

Table 1. Detailed information of scanned rods.

Rods	Machining conditions			Diameter(mm)
As-processed	Rods 1-8, no machining			8.000
Machined rods by Junker	Finish ground rods 1-4	Rods 1 & 2	Wheel speed: 100 m/s; traverse speed: 50 mm/min	6.000
		Rods 3 & 4	Wheel speed: 125 m/s; traverse speed: 100 mm/min	6.000
	Rough ground rods 5-8	Rods 5 & 6	Wheel speed: 100 m/s; traverse speed: 75 mm/min	6.125
		Rods 7 & 8	Wheel speed: 125 m/s; traverse speed: 150 mm/min	6.125
Machined rods by Supfina	Rough machined rods 1-4	Rods 1 & 2	Wheel speed: 125 m/s; traverse speed: 150 mm/min	6.015
		Rods 3 & 4	Wheel speed: 100 m/s; traverse speed: 75 mm/min	6.015
	Finish machined rods 5-16	Rods 5-12	Finish condition/Belt	6.000
		Rods 13-16	Finish condition/Stone	6.000

Figure 3 shows a comparison of laser-scatter NDE images and photomicrographs of typical finish-ground and rough-ground rods by Junker. For the finish-ground rod, Fig. 3a, the scatter image shows not only porosity spots (high-scatter-intensity spots), but also some indications of subsurface grinding damage (horizontal higher-scatter-intensity lines) although they are few and very faint. For the rough-ground rod, Fig. 3b, grinding damages of various severities are clearly observed. The difference between the finish and rough ground rods is, however, not apparent from the surface photomicrographs as shown in Fig. 3.

Figure 4 shows a comparison of laser-scatter image and photomicrograph of typical fine and rough machined rods by Supfina. Machining damage is clearly detected in the rough-ground rod but not observed in the fine-machined rod. All surfaces of fine-machined rods from Supfina show a distinct grainy appearance (in Fig. 4a) that does not resemble to a typical ground surface as shown in the photomicrograph in Fig. 4b.

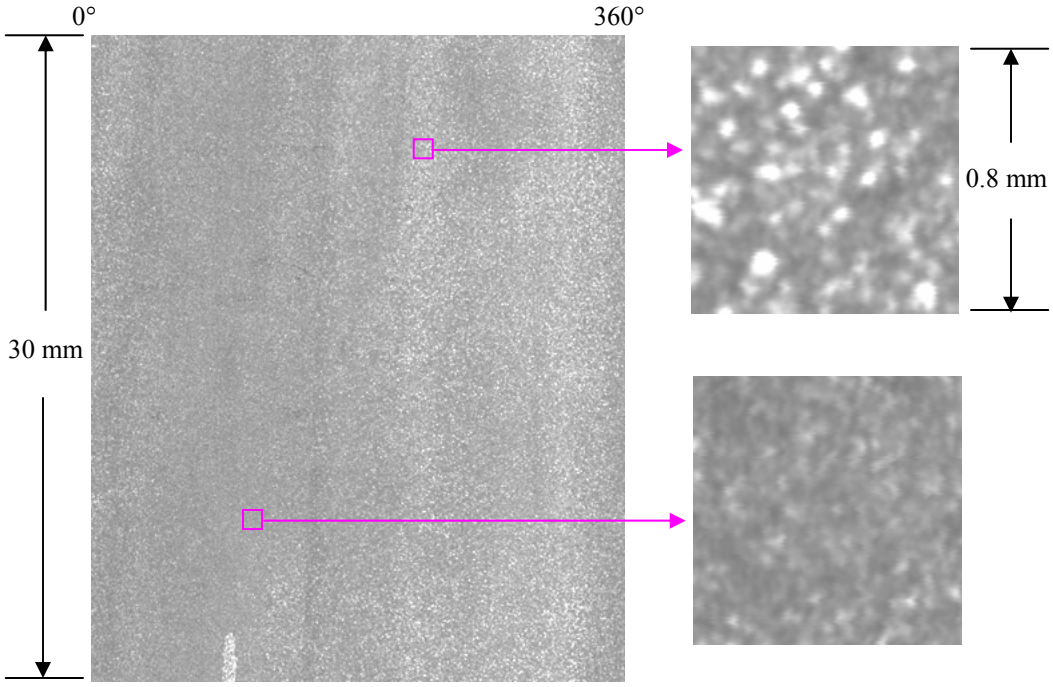

Fig. 2. Laser-scatter image of the central 30-mm-length area of the as-processed SN235P rod #5.

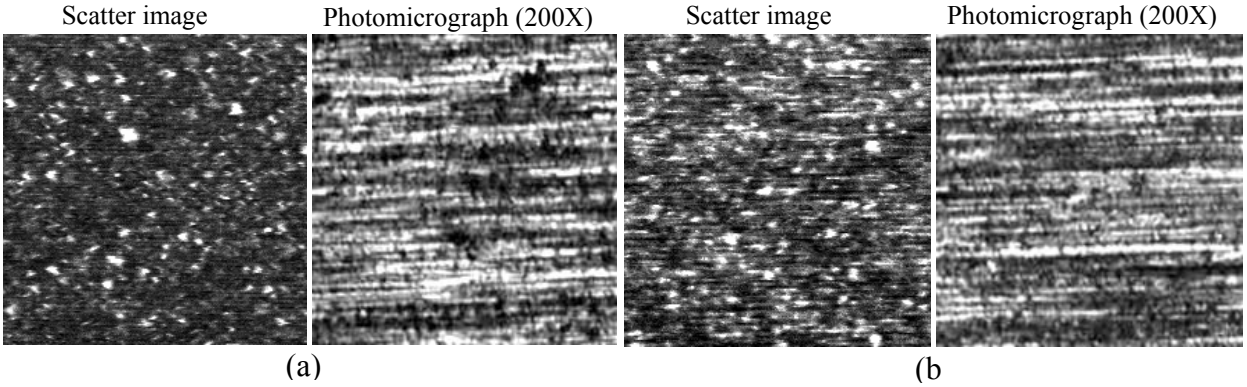

Fig. 3. Laser-scatter image and photomicrograph of typical (a) finish and (b) rough ground rods by Junker.

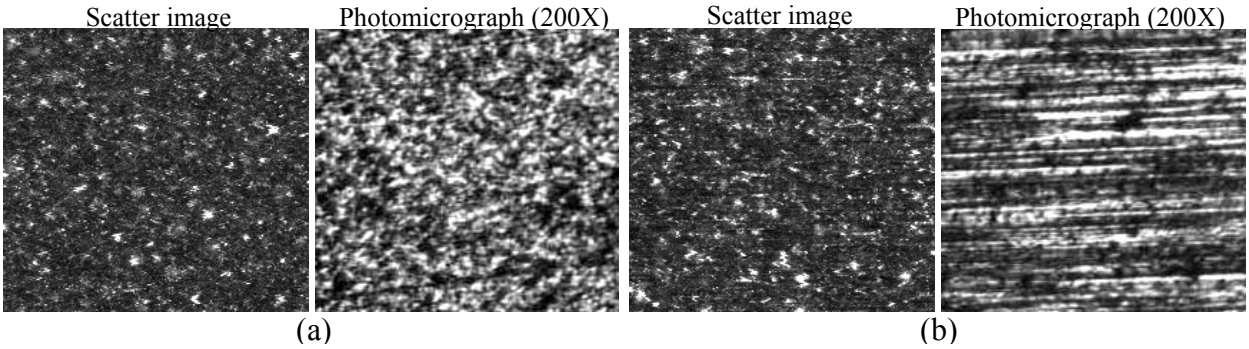

Fig. 4. Laser-scatter image and photomicrograph of typical (a) finish and (b) rough machined rods by Supfina.

Figure 5 shows comparisons of laser-scatter NDE data for rough-ground rods by Junker and by Supfina with same machining conditions (wheel speed and traverse speed). For wheel speed of 100 m/s and traverse speed of 75 mm/min, a comparison of the scatter images in Figs. 4a and 4b seems to indicate that there is more machining damage in the Junker-ground rod than in the Supfina-ground rod. The same is true for the rods machined with wheel speed of 125 m/s and traverse speed of 150 mm/min, as shown in Figs. 4c and 4d. Quantitative comparison based on statistical data analysis of the NDE data will be attempted and reported in the next period.

Besides the machining damage, color variation on the rod surface, which is very faint to eyes, can be detected clearly from the scatter images. Figure 6 shows the color variation observed on Supfina rough-ground rod #1, which has the clearest indication among all the rods. This coloration change is probably due to non-uniform mixing of second phase materials in Si_3N_4 during material processing, so it may have some effect on the mechanical property of the rods.

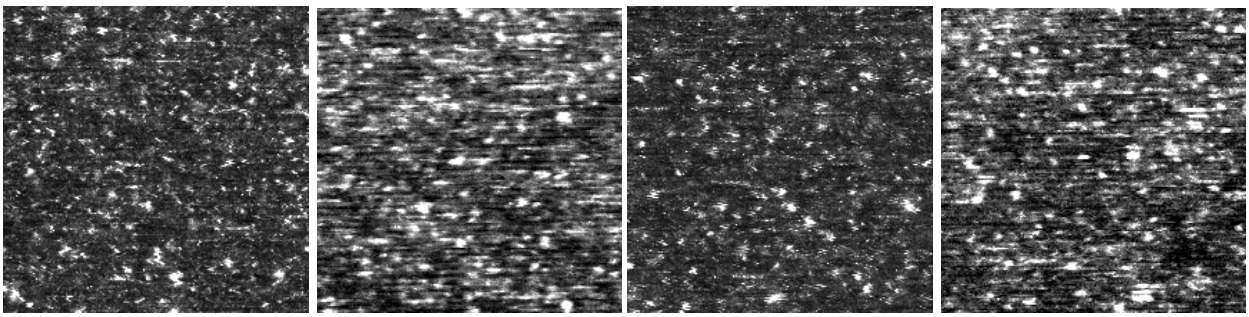

(a) (b) (c) (d)

Fig. 5. NDE data of rough-machined rods by (a) Supfina and (b) Junker at wheel speed of 100 m/s and traverse speed of 75 mm/min, and by (c) Supfina and (d) Junker at wheel speed of 125 m/s and traverse speed of 150 mm/min.

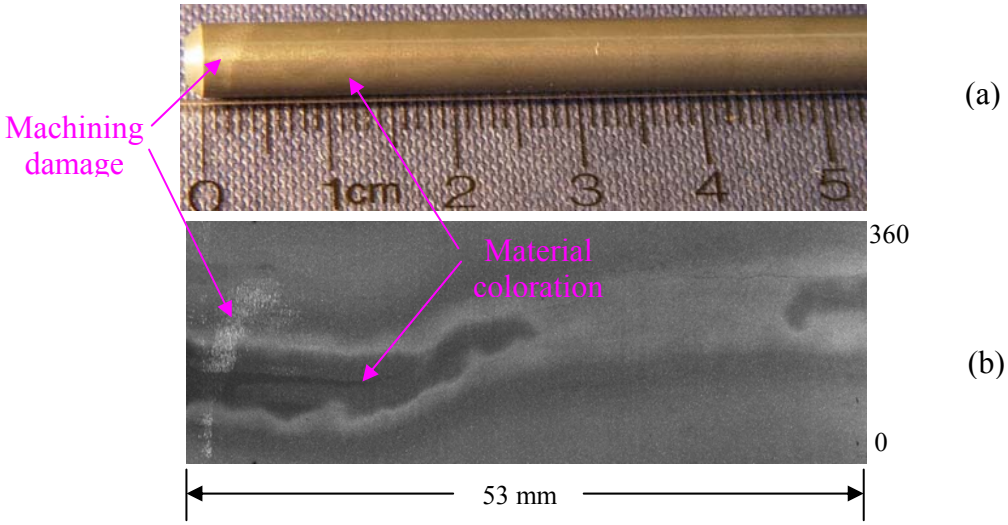

Fig. 6. Color variation shown in (a) photograph and (b) scatter image of Supfina machined rod 1.

2. Laser-Scattering Characterization of Si_3N_4 Valves

During this period we received 48 as-processed (machined) SN235P Si_3N_4 valves. Eight valves have been NDE scanned and were returned to Caterpillar. The remaining 40 valves are shown in Fig. 7 and they are currently being scanned. Scanning of each valve takes about 7 hours. The scan speed is limited by the semiconductor optical detector which has a maximum speed of ~3 kHz. By replacing the semiconductor detector by a photomultiply tube (PMT) which can be operated at much higher speed, the scan time for each valve can be significantly reduced. A PMT will be purchased and implemented in the valve-scan system in the next period.

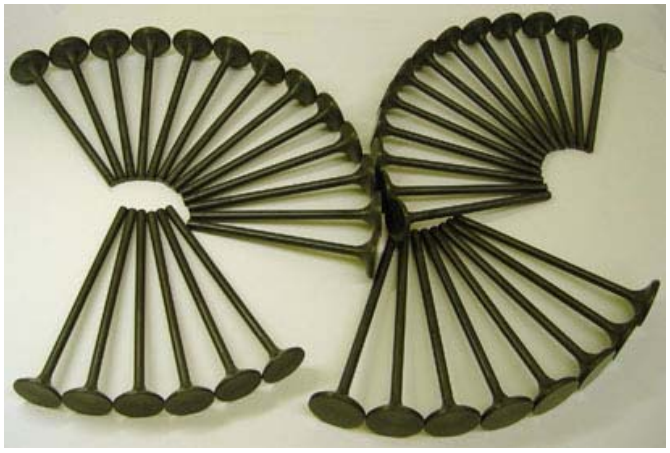

Fig. 7. Photograph of 40 as-processed SN235P Si_3N_4 valves.

Status of Milestones

Current ANL milestones are on schedule.

Communications/Visits/Travel

Dr. M. J. Andrews and Dr. D. M. Longanbach of Caterpillar Inc. visited ANL on Jan. 16, 2004 to discuss project issues.

J. G. Sun attended the American Ceramic Society's annual Cocoa Beach Conference, Cocoa Beach, FL, Jan. 25-30, 2004.

J. G. Sun visited Caterpillar Inc. on March 4, 2004 to discuss project issues.

Problems Encountered

None in this period.

Publications

A paper entitled "Laser Scattering Characterization of Subsurface Defect/Damage in Silicon Nitride Ceramic Valves" by J. G. Sun, J. Zhang, and M. J. Andrews has been accepted for publication in the Proceedings of the American Ceramic Society's annual Cocoa Beach Conference, Cocoa Beach, FL, Jan. 25-30, 2004.

Durability of Diesel Engine Component Materials

Peter J. Blau
Oak Ridge National Laboratory

John Truhan
University of Tennessee, Knoxville, TN

Jun Qu
ORISE Post-Doctoral Fellow

Objective/Scope

The objective of this effort is to enable the development of more durable, low-friction moving parts in diesel engines for heavy vehicle propulsion systems by conducting friction, lubrication, and wear analyses of advanced materials, surface treatments, and coatings. The scope of materials and coatings broadly includes metallic alloys, intermetallic compounds, ceramics, or composite materials depending on which is likely to be best-suited for the given application. Parts of current interest include scuffing-critical components, like fuel injector plungers and EGR waste gate components. Bench-scale simulations of the rubbing conditions in diesel engine environments are used to study the accumulation of surface damage, and to correlate this behavior with the properties and compositions of the surface species. The effects of mechanical, thermal, and chemical factors on scuffing and reciprocating sliding wear are being determined. Results are used to develop graphical methods for scuffing performance mapping and to select materials for durability-critical engine components.

Technical Highlights

Work on the development of a method to display the initiation and propagation of scuffing damage, especially on cylindrical pins such as fuel injector plungers, has been described in a milestone report (see below). The portrayal of scuffing characteristics of materials for engine components is not straightforward because:

- Scuffing damage is localized and generally non-uniform across the affected surface.
- Unlike other types of wear, scuffing may not generate a net loss of material and therefore cannot be measured simply by using mass loss.
- Developing quantitative criteria for whether a material has or has not scuffed is not trivial. Visual inspection is often used in practice but that does not lend itself to quantification.
- Scuffing is a function of the lubrication regime, surface finish, and material characteristics; thus, displaying all the key variables as graphical axes versus scuffing performance (as in a "scuffing map") is not straightforward.

Commonly, scuffing tests measure wear rate, establish the critical load for scuffing, or describe the extent of scuffing. However, in the case of fuel injectors, it is much more important to detect and predict the onset of scuffing because the onset of scuffing can quickly lead to catastrophic failure within the tight tolerances between plungers and bores. In earlier tests of annealed 52100 steel, the change in the average friction coefficient per stroke was used as a scuffing indicator [1]; however, later studies showed that this approach was not sensitive enough to detect scuffing

of hardened steel, zirconia, or cermet materials [2-3]. An improved method was subsequently developed. It uses a series of friction traces of individual stroke cycles. The new method was further enhanced by plotting the change in the friction coefficient in space and time domains, enabling one to visualize aspects of both initiation and propagation stages. For example, a 3-D dynamic friction map is shown in Fig. 1. The test used to construct it was conducted on self-mated 52100 steel with a surface roughness R_q of 0.267 μm in Jet A fuel. The sampling rate was 1000 readings/cycle, or 100 readings/stroke. The stroke length was 10 mm. One second of friction data was sampled every 10 seconds to plot the map shown in Fig 1.

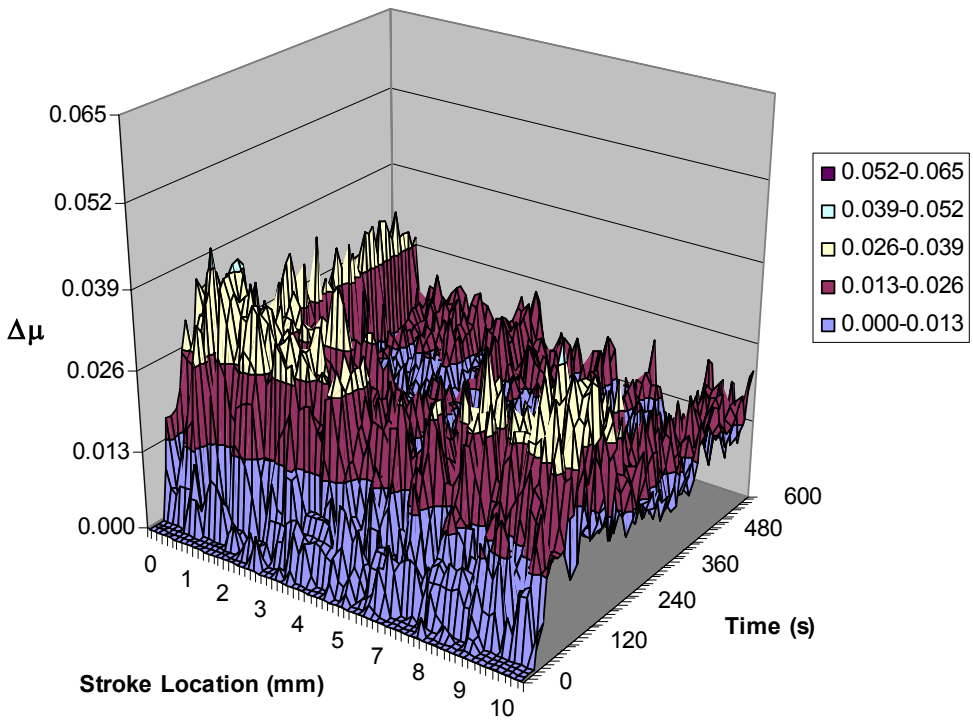

Figure 1. Scuffing map depicting the change in friction coefficient as a function of time at different locations on the surface of twin cylindrical specimens in the 'pin-on-twin/ test.

By defining a critical change in friction coefficient to signal the initiation of scuffing (say, an increase of 10% over the initial friction coefficient), it is possible to use maps such as Fig. 1 to indicate the location and progression of scuffing damage. One of the interesting features of this representation is how scuffing can begin at the ends of a specimen and proceed toward the center. It is also interesting to observe how, in some material combinations, damage can 'heal.' That is, the surface can first roughen, raising the friction, and then become smoother, lowering it again.

3-D scuffing maps, like that in Figure 1, can be subsequently used to develop scuffing transitions diagrams, as are described in considerably more detail in the recent milestone report, cited below. These transition diagrams plot the time to initiate scuffing damage versus the velocity along the length of the sliding stroke. Thus, the local velocity, which affects the regime of lubrication, is related to a material's ability to resist scuffing at a given surface location.

Visualization of the scuffing history, such as that in Fig. 1, will be helpful in developing models for plunger scuffing.

Future Plans

1. Continue to develop dynamic friction maps and scuffing transition diagrams for materials of current interest as fuel injector plungers and bores.

2. Begin the development of a lubricant and material-based model for the scuffing process.

Travel

None.

Status of Milestones

1) Report on the effects of sulfur in the fuel on the scuffing behavior of current and future candidate fuel injection system materials (September 30, 2003 - completed).

2) Prepare transition diagrams for current and promising, new fuel system materials that exemplify the relationship between real contact pressure, surface finish, and the onset of scuffing in diesel fuel environments. (March 31, 2004 - completed)

3) Develop a model for selecting materials and their optimal surface finishes for scuffing applications in diesel engines. (September 30, 2004**)**

Publications

P. J. Blau, J. J. Truhan, Jr., and J. Qu, "Scuffing Transition Diagrams for Fuel Injection System Materials," Project milestone report, March 31, 2004, 19 pp.

Numbered References

1. Qu, J., Truhan, J., Blau, P.J., Ott, R.,"The development of a pin-on-twin scuffing test to evaluate materials for heavy duty diesel fuel injectors," submitted to *Tribology Transactions*, 2003.

2. Qu, J., Truhan, J., Blau, P.J., "Detecting the Onset of Localized Scuffing with the Pin-on-Twin Fuel-Lubricated Test for Heavy Duty Diesel Fuel Injectors," Presented at *Boundary Lubrication for Transportation*, Copper Mountain, Colorado, Aug. 3-8, 2003. Submitted to the *International Journal of Engine Research,* 2004.

3. Qu, J., Truhan, J., Blau, P.J., "Evaluating Candidate Materials for Heavy Duty Diesel Fuel Injectors Using a "Pin-on-Twin" Scuffing Test," submitted to *Tribology International,* 2004.

Life Prediction of Diesel Engine Components

H. T. Lin, T. P. Kirkland, A. A. Wereszczak, M. K. Ferber
Oak Ridge National Laboratory
and M. J. Andrews
Caterpillar

Objective/Scope

The valid prediction of mechanical reliability and service life is a prerequisite for the successful implementation of structural ceramics and advanced intermetallic alloys as internal combustion engine components. There are three primary goals of this research project which contribute toward that implementation: the generation of mechanical engineering data from ambient to high temperatures of candidate structural ceramics and intermetallic alloys; the microstructural characterization of failure phenomena in these ceramics and alloys and components fabricated from them; and the application and verification of probabilistic life prediction methods using diesel engine components as test cases. For all three stages, results are provided to both the material suppliers and component end-users.

The systematic study of candidate structural ceramics (primarily silicon nitride) for internal combustion engine components is undertaken as a function of temperature (<1200°C), environment, time, and machining conditions. Properties such as strength and fatigue will be characterized via flexure and rotary bend testing.

The second goal of the program is to characterize the evolution and role of damage mechanisms, and changes in microstructure linked to the ceramic's mechanical performance, at representative engine component service conditions. These will be examined using several analytical techniques including optical and scanning electron microscopy. Specifically, several microstructural aspects of failure will be characterized:

(1) strength-limiting flaw-type identification;
(2) edge, surface, and volume effects on strength and fatigue size-scaling
(3) changes in failure mechanism as a function of temperature;
(4) the nature of slow crack growth; and
(5) what role residual stresses may have in these processes.

Lastly, numerical probabilistic models (i.e., life prediction codes) will be used in conjunction with the generated strength and fatigue data to predict the failure probability and reliability of complex-shaped components subjected to mechanical loading, such as a silicon nitride diesel engine valve. The predicted results will then be compared to actual component performance measured experimentally or from field service data. As a consequence of these efforts, the data generated in this program will not only provide a critically needed base for component utilization in internal combustion engines, but will also facilitate the maturation of candidate ceramic materials and a design algorithm for ceramic components subjected to mechanical loading in general.

Technical Highlights

Silicon Nitride Exhaust Valves

Studies of dynamic fatigue behavior in four-point bending for Kyocera SN235P silicon nitride after 1000h exposure to an exhaust gas environment were completed during this reporting period. The SN235P silicon nitride billets were manufactured with the same powder batch employed to process the SN235P exhaust valve blanks. The current study was carried out to verify the mechanical reliability of co-processed valve materials after long-term exposure to a simulated diesel engine environment. The co-processed SN235P silicon nitride bend bars were longitudinally machined based per the revised ASTM C116 standard with 600 grit surface finish. The 1000h exhaust gas exposure was carried oust at Caterpillar. Test results previously generated and reported for the as-machined SN235P samples, which was also co-processed with the exhaust valve blanks, showed a very high fatigue exponent (N ~ 93) at 850°C, indicative of no susceptibility to SCG process. Therefore, the dynamic fatigue tests for exposed SN235P samples were only carried out at 850°C and 0.003 MPa/s in air per ASTM C1465 due to the limited number of specimens available.

Results of dynamic fatigue tests at 850°C and 0.003 MPa/s showed that the exposed SN235P silicon nitride exhibited a very comparable inert characteristic strength to those obtained from the as-machined samples tested under the same condition (Table 1, and Fig. 1). Also, there is no difference in characteristic strength values between oil-ash exposed and exhaust gas exposed samples. In addition, the exhaust gas exposed samples exhibited a higher Weibull modulus, similar to the value obtained for the samples exposed to oil ash environment, as compared with the value obtained for the as-machined samples,. The higher Weibull modulus of exposed samples may arise from the surface sealing effect due to the formation of oxide scale after exposure. A detailed analysis of fractography and SEM examination will be carried out to identify the critical strength limiting flaws as well as the extent of oxidation/corrosion zone in selected test samples. The dynamic fatigue results suggest that the SN235P-CP exhibits excellent corrosion resistance to diesel engine environments and would meet the application criteria for exhaust valve components of diesel engines.

Studies of dynamic fatigue properties of a commercial grade silicon nitride, i.e., SN147-31E, manufactured by Ceradyne Advanced Ceramic, Inc., CA, were also continued during this reporting period. The SN147-31E was processed with similar sintering additives to those employed for SN147-31N evaluated previously. However, the SN147-31E contains a crystalline secondary phase achieved by a post heat treatment. Thus, it is anticipated that SN147-31E would exhibit a higher temperature mechanical reliability than SN147-31N due to the presence of crystalline secondary phase.

Dynamic fatigue results at 850°C showed that the longitudinally machined SN147-13E exhibited a characteristic strength that is 10% lower than that obtained at room temperature, similar to the trend obtained for SN147-31N. Also, the SN147-31E samples exhibited a 20% lower strength value than those obtained for SN147-31N samples, which were machined and tested under the same conditions (Table 2 and Fig. 2 and 3). The difference in measured strengths could result from the change in residual stress arising from the post heat treatment. On the other hand, the SN147-31E samples, in general, exhibited lower Weibull moduli than those obtained for SN147-31N samples, independent of the test conditions. Fractography and SEM analysis will be carried

out to provide an insight into the strength limiting flaws and change in Weibull modulus. Dynamic fatigue results showed the SN147-31E exhibited a relative low fatigue exponent of 56 with respect to SN147-31N (N ~ 131), indicative a susceptibility to SCG process at temperatures. The low fatigue exponent obtained for SN147-31E suggests an incomplete crystallization of glassy phase during the post heat treatment. The presence of these residual glassy phase(s) could play an important role in the high-temperature mechanical performance and susceptibility to SCG.

Diesel Particulate Filters

This study, part of a CRADA between Cummins and ORNL, is carried out to characterize the mechanical properties of DPF substrate and develop analytical tools for long-term reliability and durability prediction. Miniature test samples have been successfully machine from the substrates of diesel particulate filter (DPF) acquired from Corning (Fig. 4) during this reporting period. The samples have nominal dimensions of 0.20mm x 0.90mm x 15 mm. A miniature test fixture has also been designed and machined (Fig. 5). The alumina test fixture has inner and outer spans of 1mm and 2mm, respectively. Mechanical tests will be carried out using a micro test system to characterize the flexural strength of DPF substrate under a specified condition, and test results will be discussed in the next quarterly report.

Status of Milestones

Milestone: "Complete testing and analysis of prototype silicon nitride valves after bench rig testing" was on schedule.

Communications / Visitors / Travel

- Communication with M. J. Andrews at Caterpillar on the update of the dynamic fatigue test results of Kyocera SN235P silicon nitride after 10000h exhaust gas test.
- Communication with M. J. Andrews at Caterpillar on the on the update of the dynamic fatigue test results of Ceradyne SN147-31E silicon nitride
- Communication with M. J. Andrews at Caterpillar on the machining status of the MOR bend bars from SN235P valve blanks.
- Communication with Edgar Lara-Curzio at ORNL on the update of the mechanical results for diesel particulate filter materials.

Problems Encountered

None.

Publications

None.

References

[1] H. T. Lin, T. P. Kirkland, M. K. Ferber, and M. J. Andrews, "Life Prediction of Diesel Engine Components," Heavy Vehicle Propulsion System Materials Program Quarterly Technical Progress Report to DOE Office of Transportation Technologies, Oct. – Dec., 2002.
[2] H. T. Lin, T. P. Kirkland, M. K. Ferber, and M. J. Andrews, "Life Prediction of Diesel Engine Components," Heavy Vehicle Propulsion System Materials Program Quarterly Technical Progress Report to DOE Office of Transportation Technologies, Oct. – Dec., 2003.

Table 1. Summary of uncensored Weibull and strength distributions for Kyocera SN235P silicon nitride specimens longitudinally machined per ASTM C1161. Data of Kyocera SN235/SN235P, also machined longitudinally, generated previously are used for comparison.

Material	# of Spmns. Tested	Stressing Rate (MPa/s)	Temp. (°C)	Uncens. Weibull Modulus	± 95% Uncens. Weibull Modulus	Uncens. Chrctstic Strength (MPa)	± 95% Uncens. Chrctstic Strength (MPa)
SN235P-CP*	30	30	20	11.94	8.58. 15.94	820	794, 847
SN235P-CP*	30	0.003	20	14.56	10.93, 18.64	741	721, 761
SN235P-CP*	30	30	850	20.56	15.16, 26.87	684	671, 697
SN235P-CP*	30	0.003	850	19.44	14.49, 25.01	621	608, 633
SN235P-CP**	15	0.003	850	30.40	19.47, 44.19	660	647, 672
SN235P-CP***	12	0.003	850	25.07	15.55, 36.81	677	659, 694

* Specimens were machined from co-processed billets of exhaust valve blanks.
** Specimens were exposed to an oil ash environment at 850°C for 1000 h in air.
*** Specimens were exposed to an exhaust gas environment at 850°C for 1000 h.

Table 2. Summary of uncensored Weibull and strength distributions for Ceradyne SN147-31E silicon nitride specimens transversely machined per ASTM C1161. Data of SN147-31N machined longitudinally as well as transversely is used for reference.

Material	# of Spmns. Tested	Stressing Rate (MPa/s)	Temp. (°C)	Uncens. Weibull Modulus	± 95% Uncens. Weibull Modulus	Uncens. Chrctstic Strength (MPa)	± 95% Uncens. Chrctstic Strength (MPa)
SN147-31N*	15	30	20	21.73	14.07. 31.09	836	814, 858
SN147-31N**	15	30	20	13.76	8.96, 19.59	677	649, 705
SN147-31N*	15	30	850	20.35	13.58, 28.20	777	755, 799
SN147-31N*	15	0.003	850	16.19	10.57, 23.02	732	706, 757
SN147-31E*	15	30	20	17.30	10.86, 25.58	668	645, 690
SN147-31E**	15	30	20	7.44	4.89, 10.58	623	575, 671
SN147-31E*	15	30	850	9.36	6.01, 13.62	604	567, 641
SN147-31E*	15	0.003	850	12.06	7.70, 17.52	509	485, 533

* Specimens were longitudinally machined.
** Specimens were transversely machined.

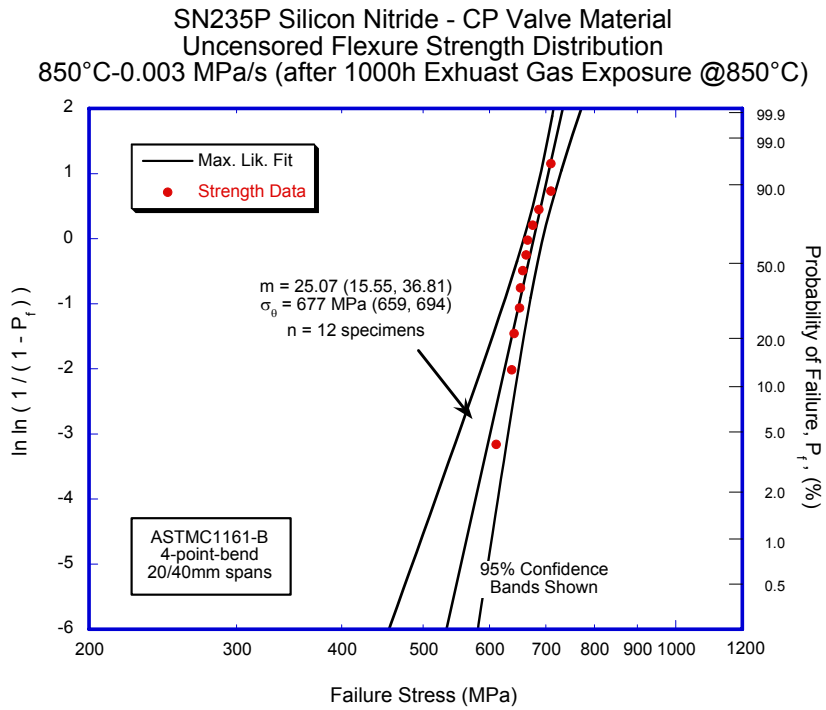

Figure 1. Strength distribution of Kyocera SN235P-CP longitudinally machined and tested at 850°C and at 30 MPa/s after 1000 h exposure in exhaust gas environment at 850°C in air.

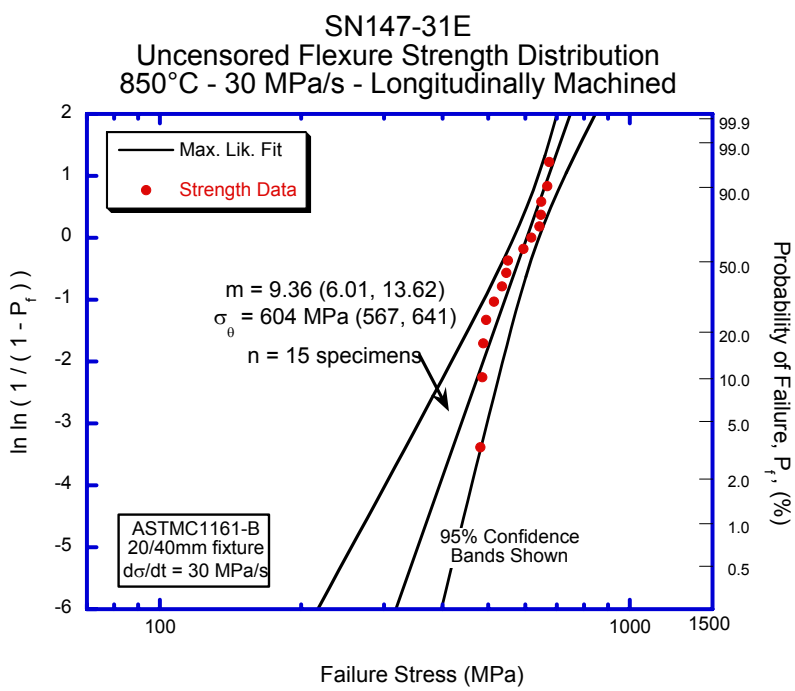

Figure 2. Strength distribution of Ceradyne SN147-31E longitudinally machined and tested at 850°C and at 30 MPa/s.

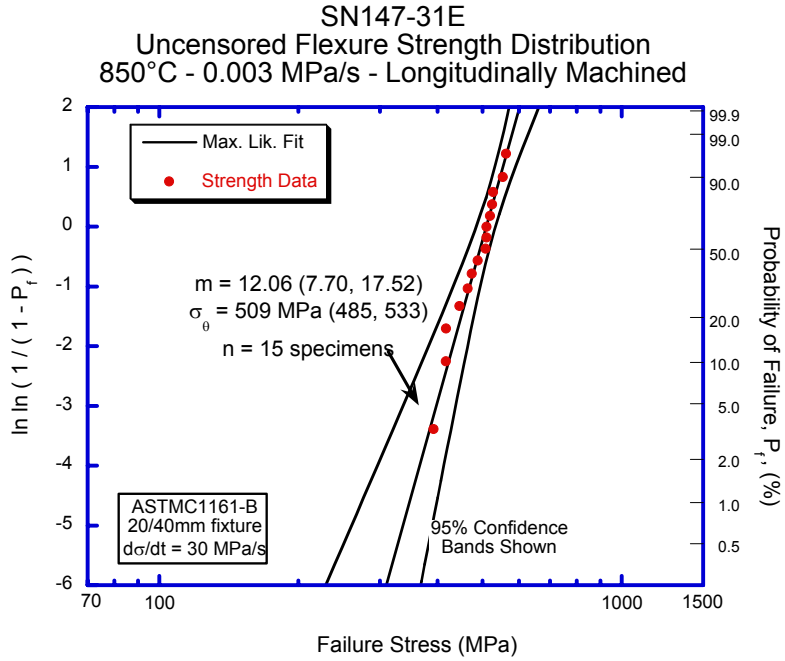

Figure 3. Strength distribution of Ceradyne SN147-31E longitudinally machined and tested at 850°C and at 0.003 MPa/s.

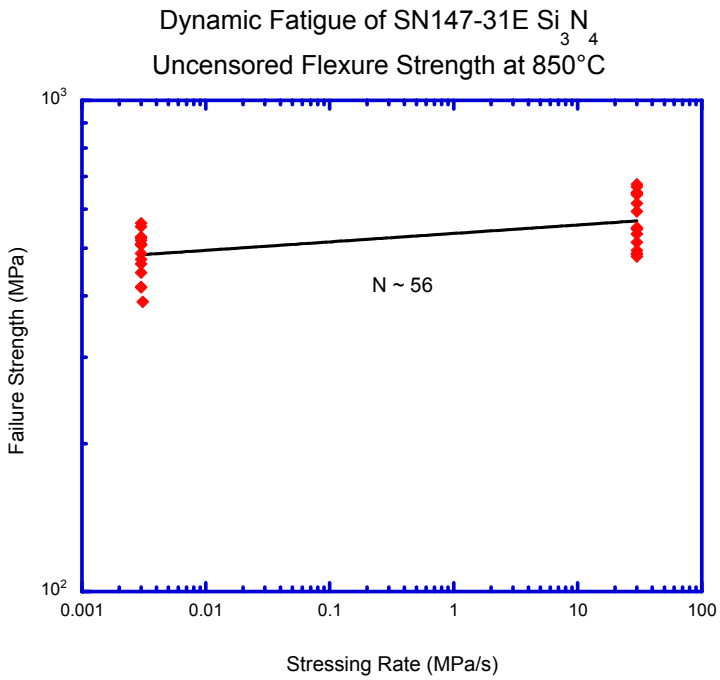

Figure 4. Failure strength versus stressing rate curve of SN147-31E tested at 850°C in air.

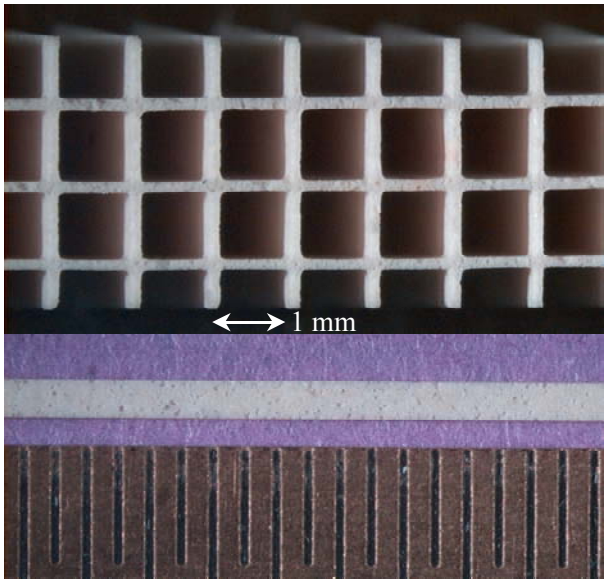

Figure 5. Photos show a section of diesel particulate filter, and sample machined from its substrate

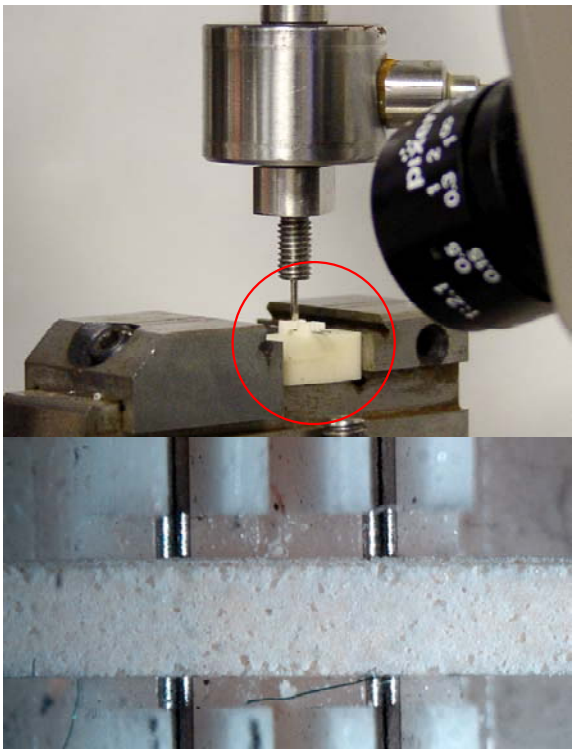

Figure 6. Photos show the micro test system and miniature test fixture.

Diesel Exhaust Filter Temperature Measurement and Cost-Effective Machining of Titanium Alloys

Albert Shih
University of Michigan

Objective

The objective of this research is to investigate new technologies for cost-effective machining of Ti alloys. New tool materials and comprehensive finite element modeling of the machining process are applied to gain better understanding of effects of machining process parameters and the deformation, stress and temperature in the tool and Ti workpiece.

Technical Highlights

In this quarter, experiments and 3D finite element modeling of Ti machining have been conducted. Compared to the 2D finite element modeling, 3D simulation can provide more detailed results of stress, strain and temperature distributions in the tool and workpiece. Ti machining experiments have been setup and measured cutting forces are compared with finite element simulation results. The feasibility of using the TiC-Ni_3Al metal matrix ceramic (MMC) as tool material for the Ti machining has been explored in this study.

1. Ti machining experimental setup

The Ti machining experiment was conducted on a Lodge and Shipley 30 HP CNC lathe, as shown in Fig. 1(a). A Kistler 9257A piezoelectric dynamometer was used to measure the cutting forces in three directions. The force signal was processed using the charge amplifiers and recorded by a PC-based data-acquisition system with the National Instruments PCI-MIO-16E-1 card and LabVIEW software. The grade 2 commercially pure Ti rod, 1.25 inch in diameter, was the workpiece. As shown in Fig. 1(b), a tool holder, Kennametal CTAPL-163D, was fixed on the dynamometer. Kennametal, the collaborator of this project, provided both the tool holder and triangular shape tool inserts. Fig. 1(c) shows the closed-up view of the tool clamping and the cutting of Ti rod workpiece.

As shown in Fig. 2, the side rake, back rake, and lead angles [1], set by the tool holder, are 5°, 0°, and 0°, respectively, for the machining experiment. The uncoated WC-Co tool, Kennametal TPG322 with 0.8 mm corner radius and K313 carbide grade (fine grain size WC in 6% Co matrix), was used in this study. Several other tool materials and coatings have been tested and the machining test is still on-going. A TiC-based tool with the material made at ORNL and finish machined at University of Michigan was also tested. All tests were conducted dry without using coolant.

Figure 2 shows the three measured cutting forces, marked as radial, axial and tangential forces on the triangular-shape tool. These measured force components will be compared to the finite element modeling results. Figure 2 also illustrates the 0° lead and back rake angle, 5° side rake angle (α) and 6° relief angle (β) and the XYZ coordinate system used in 3D finite element modeling.

(a)

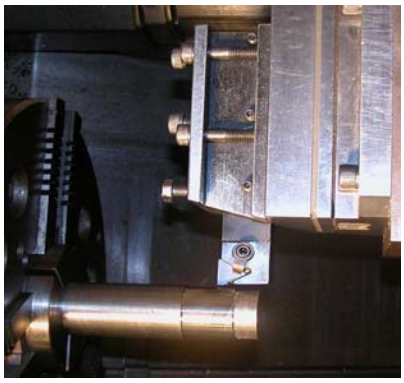

(b)

(c)

Fig. 1. Ti machining experiment setup: (a) the Lodge and Shipley lathe (b) the setup with dynamometer, cutting tool and workpiece (c) the closed-up view of tool and workpiece.

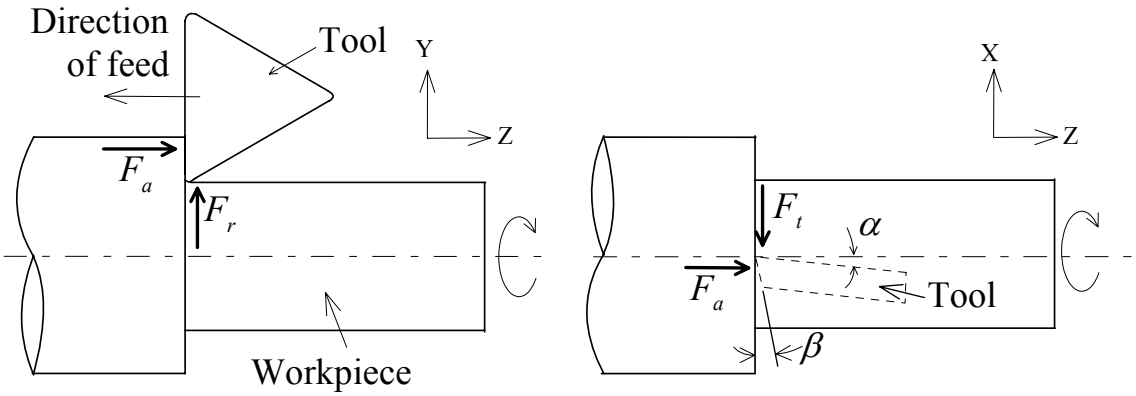

(a) Top view (b) Front view

Fig. 2. Schematic of the lathe cutting setup with side rake angle α, relief angle β, tangential force F_t, radial force F_r, and axial force F_a: (a) top view and (b) side view.

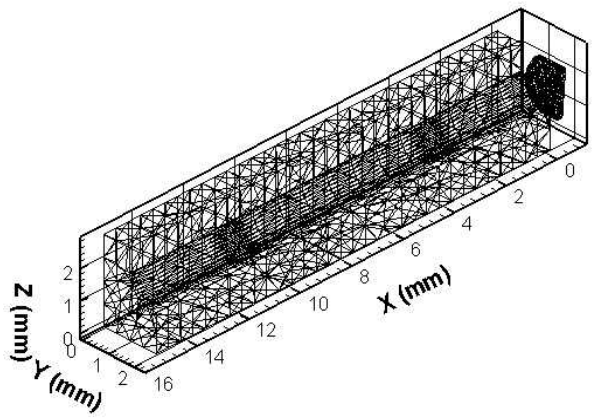

Fig. 3. The initial 3D finite element mesh of the workpiece and tool.

2. 3D modeling of Ti machining process

The AdvantEdge™ 3D machining simulation software (Third Wave Systems at Minneapolis, MN) was used to model the Ti machining process. The updated-Lagrangian finite element method with continuous remeshing and adaptive meshing techniques was applied [3]. The model incorporates the explicit dynamic, heat conduction, mesh-on-mesh contact with friction, and thermo-mechanically coupling effects.

Figure 3 shows the initial finite element mesh for 3D turning using the tool with corner radius. An XYZ coordinate is defined. The −X, Y, and Z directions correspond to the positive direction of tangential, radial, and axial forces measured in the cutting tests, respectively. The 3D 4-node, 12 degree-of-freedom tetrahedral finite element was used. The tool has the top and back surfaces fixed in all directions [4]. The workpiece is constrained in Z and Y directions on the bottom surface and moves at the cutting speed in the –X direction towards the stationary tool.

Figure 4(a) shows an example of chip curl and temperature distribution for cutting with 0.254 mm feed, 195 m/min cutting speed, 1.02 mm depth of cut, and 0.8 mm corner radius. The tool orientation is setup as in the turning test, 0° lead and back rake angle, 5° side rake angle, and 6° relief angle. The total tool travel distance is about 10 mm. It takes about 72 hours computational time in a 2.8 GHz, 1 GB RAM PC-based workstation.

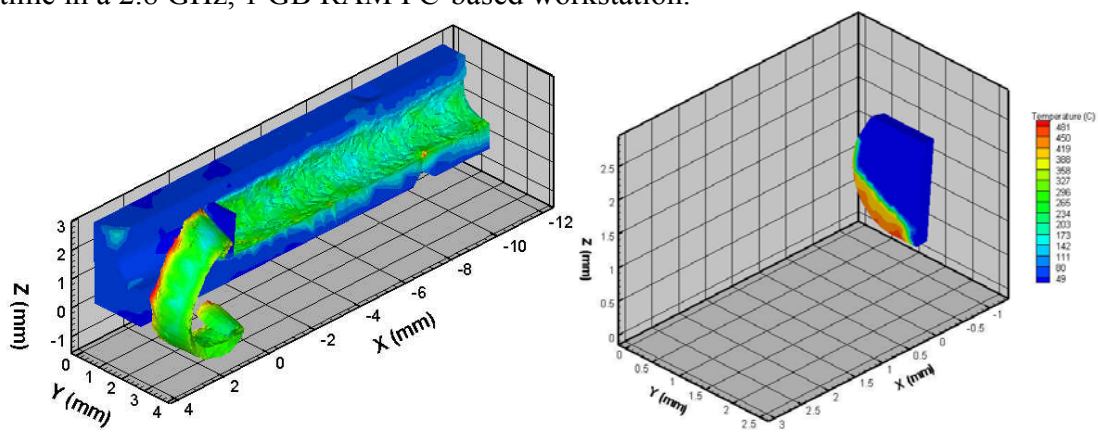

(a) (b)

Fig. 4. Simulation results: (a) chip curl and temperature and (b) tool temperature.

The highest temperature in machining the commercial pure Ti workpiece is about 480°C, as shown in the chip in Fig. 4(a) and tool in Fig. 4(b). This, compared to the more than 750°C peak tool temperature in machining Ti-6Al-4V, reported in previous quarterly report, is significantly lower. Future tests are planned on the Ti-6Al-4V workpiece.

The finite element method can predict cutting forces. As shown in Table 1, the three components of calculated and measured cutting forces are compared with reasonable agreement within 25%. This comparison provides the initial indication on the accuracy of the 3D finite element modeling of Ti machining process.

There are many input parameters that influence the finite element modeling results and a set of parametric study is undergoing to understand the effect of these parameters, which include mesh size, tool thickness, and workpiece size. A tool edge radius, which greatly influences the cutting forces, needs to be selected in finite element modeling. The precise measurement of tool edge radius is difficult. The influence of tool edge radius, as well as cutting speed and feed rate, on cutting forces is currently under investigation. Results will be presented in the next quarterly report.

Table 1. Comparison of cutting forces.

	Tangential force, F_t	Radial force, F_r	Axial force, F_a
FEM predicted (N)	305.1	62.79	32.71
Experimental measured (N)	347.5	51.89	40.64

3. Turning test with TiC-based tool material

An exploratory study of new TiC-based tool materials for machining of Ti, was conducted. Compared with conventional WC-Co, the TiC-based tool material has the following advantages in machining of Ti:

- Less susceptibility to diffusion wear because of the stable Ti content at high temperature [1]
- More favorable frictional characteristics and less susceptibility to abrasion wear [1]
- Applicability to be used in high cutting speeds at moderate chip cross-sections [2]
- Capability to produce high surface quality of the machined workpiece [2]
- High temperature cutting capability by using the high temperature $NiAl_3$ bond

However, TiC-based materials have lower resistance to fracture and higher thermal expansion coefficient than that of WC. The physical and mechanical properties of TiC-based materials can be tailored within certain limits to meet the requirements for cutting tool. For instance, the hardness can be increased by increasing the TiC content.

A sample TiC MMC with 20 vol % IC50 Ni_3Al bond, hot pressed at 1375°C for 15 min was used in the initial research about the feasibility of cutting Ti using TiC-based cutting tools. As shown in Fig. 5(a), two 3 mm thick triangular shape inserts, with the same geometry as the Kennametal TPG320 and TPG322 tool inserts were cut by the wire EDM from the 37.7 mm diameter blank.

Two inserts cut in Fig. 5(a) have different corner radius, one 0.1 and another 0.8 mm. Fig. 5(b) shows the closed-up view of the EDM machined insert with 0.8 mm corner radius.

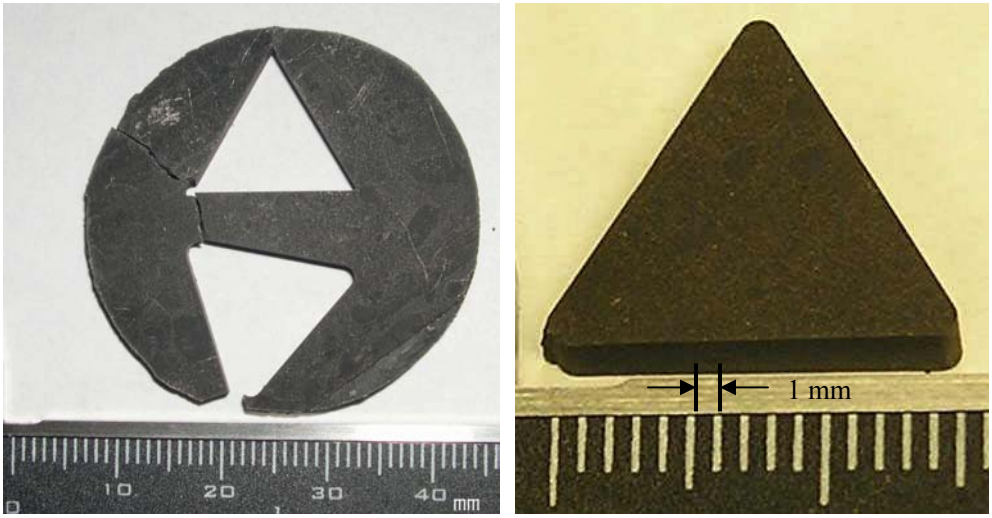

(a) (b)

Fig. 5. TiC-$NiAl_3$ tool insert: (a) the disk after wire EDM of two triangular tool inserts and (b) the machined triangular tool insert with 0.8 mm corner radius.

A turning test with 0.254 mm feed, 46.8 m/min cutting speed, 1.02 mm depth of cut, and 0.1 mm corner radius was conducted. The tool setup was 0° lead and back rake angle, 5° side rake angle, and −5° relief angle. At the start of cutting the Grade 2 Ti, the tool tip was fractured. The fractured tool tip is indicated in Fig. 6(a). The other two tool tips were damaged during machining due to the vibration of the tool and tool holder. Obvious build up edge was observed on the fractured tool tip. The chips were entangled around the workpiece, as shown in Fig. 6(b).

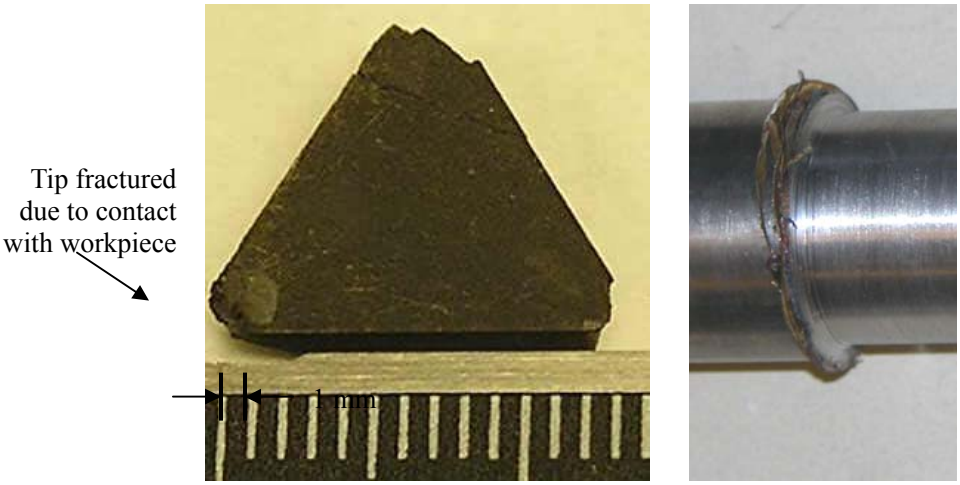

(a) (b)

Fig. 6. TiC tool machining of Ti (a) fractured tool insert and (a) workpiece with entangled chip.

The likely cause of the fractured TiC tool is the −5° relief angle, which causes the cutting edge not engaged at the start of the cutting process. The solution for this is to use negative rake angle cutting configuration or to manufacture the tool insert with the positive relief angle. The low

fracture toughness and high thermal expansion coefficient of the TiC MMC may also contribute to the tool fracture. This TiC MMC was tailored for diesel injector plunger, not cutting tool, application. This exploratory study shows the feasibility to produce TiC MMC cutting insert and test it for Ti machining. More study will be conducted to prove this concept.

Future Work

This research will continue in both 3D finite element modeling and experimental machining test of new tool materials and coatings. Parametric studies of the effects of various cutting conditions and tool geometries on the temperature, stress, strain distribution and cutting forces will be conducted in the following research. The machining of Ti with new tool materials and tool coatings are ongoing.

For the new TiC MMC, the next step is to acquire a new tool holder from Kennametal with negative side rake angle.

Status of Milestones

Milestone 1: 2D finite element modeling of titanium machining process.
Status: Effects of cutting speed, feed, and coating effects have been investigated using the Third Wave AdvantEdge software for machining of Ti-6Al-4V.

Milestone 2: 3D finite element modeling of titanium machining process.
Status: Extensive study of 3D machining of Grade 2 commercially pure Ti has been conducted and parametric investigation work is on-going.

Milestone 3: Investigation of TiC-based cutting tool material.
Status: Exploratory tests have been conducted.

Milestone 4: Titanium turning tests.
Status: Experiments have been set up at Univ. of Michigan for lathe turning of Ti alloys.

Milestone 5: Titanium drilling tests
Status: Nothing to report.

Communications/Visit/Travel

Albert Shih visited ORNL on Jan. 16th and Paul Becker visited University of Michigan at Ann Arbor on March 11th to review the progress of the project.

Publications

R. Li, A.J. Shih, "Finite Element Modeling of 3D Titanium Turning," *2004 ASME IMECE* at Anaheim, CA (abstract accepted).

References

[1] D.A. Stephenson, J.S. Agapiou, Metal Cutting Theory and Practice, Marcel Dekker, Inc., 1996.
[2] P. Ettmayer, H. Kolaska, W. Lengauer, K. Dryer, "Ti(C,N) Cermets-Metallurgy and Properties," Int. J. of Refractory Metals and Hard Materials, 13 (1995) 343-351.

[3] T.D. Marusich, M. Ortiz, “Modeling and Simulations of High-Speed Machining,” Int. J. Num. Meth. Eng, 38(21) (1995) 3675-3694.
[4] Third Wave AdvantEdge User’s Manual Version 4.4., Third Wave Systems, Inc., 2003.

Advanced Cast Austenitic Stainless Steels For High Temperature Components

P. J. Maziasz, J. P. Shingledecker, N. D. Evans
Oak Ridge National Laboratory
and M. J. Pollard
Caterpillar, Inc.

Objective/Scope

The objective of this follow-on CRADA project is commercial scale up of the new modified cast austenitic stainless steels developed in the first CRADA. These were developed by Caterpillar and ORNL as cost-effective high-performance upgrades to the standard SiMo ductile cast iron used for most diesel engine exhaust manifold and turbocharger housing components. Cast austenitic stainless steels can withstand prolonged exposure at temperatures of 750°C or above, and are much stronger than SiMo cast iron above 550-600°C. Two new modified stainless steels, CF8C-Plus and CN12-Plus, have better aging resistance and ductility after creep than standard commercial grades of the same steels. This project provides the more comprehensive properties data, particularly fatigue, thermal fatigue and creep, needed by designers to qualify these new alloys for component applications, and optimize component designs. This new advanced diesel engine CRADA (Cooperative Research and Development Agreement) project (ORNL02-0658) began on July 21,2002, and will last at least three years. More detailed information on this project must be requested directly from Caterpillar, Inc.

Technical Highlights

Background

Advanced large diesel engines must have higher fuel efficiency as well as reduced exhaust emissions, without sacrificing component durability and reliability. They require exhaust manifolds and turbocharger housings made from materials that can withstand temperatures ranging from 70 to 750°C or higher in a normal duty cycle. Such materials must withstand both prolonged, steady high-temperature exposure as well as more rapid and severe thermal cycling. New technology to reduce emissions and heavier duty cycles will both push temperatures of these critical components even higher.

Current diesel exhaust components are made from SiMo ductile cast iron, and higher engine temperatures push such materials well beyond their current strength and corrosion limits. The previous CRADA produced systematic data comparing cast CN12 stainless steel and SiMo cast iron for such diesel exhaust component applications. That data demonstrated a clear tensile strength advantage of standard CN12 steel above 550-600°C, and even larger advantages in creep strength and fatigue life above 700°C. The previous CRADA project also developed new CN12-Plus and CF8C-Plus modified cast austenitic stainless steels with better creep strength, and significantly better aging resistance and thermal fatigue resistance than standard CN12. The purpose of this follow-on CRADA project is commercial scale up and testing of these new modified cast stainless steel heats. This project develops the systematic and thorough data base required by designers to optimize component design, and to qualify them for trial component production.

Approach

Prior work on lab-scale (15 lb induction melts with argon cover gas) heats of CN12 - Plus and CF8C – Plus and screening tests (aging, tensile, creep) at 800-850°C at ORNL provided a best composition of each alloy for commercial scale up. High-temperature fatigue testing at Caterpillar Technical Center has identified significant advantages of the CN12-Plus steel over SiMo cast iron. Two commercial stainless steel foundries have produced 500 lb heats of the new CN12-Plus and CF8C-Plus stainless steels for testing and evaluation. One of those commercial foundries has been chosen to produce an additional static cast and a new centrifugally cast heat of the CF8C-Plus steel. ORNL is also producing additional laboratory heats to establish the effects of other minor additions on the high temperature strength of the new modified CF8C steel.

Technical Progress

Tensile and fatigue testing were completed previously, and initial thermal-mechanical fatigue (TMF) testing of as-cast material was completed previously at Caterpillar. Tensile data on the new commercial scale-up heats of the standard and modified cast stainless steels show that the CF8C Plus is about as strong as the standard and modified CN12 steels, but still has the same high ductility as the standard CF8C steel. This combination of good strength and ductility gives the new CF8C-Plus excellent fatigue and thermal fatigue resistance at high temperatures, as shown for TMF testing at 300-760°C in Fig. 1. More comprehensive fatigue and TMF testing to evaluate these new steels is ongoing, but the emphasis is now on the new CF8C-Plus steel, which won a 2003 R&D 100 Award.

An "engineered microstructure" alloy design approach gave the new CF8C -Plus steel a very stable austenite parent matrix phase that is free of the δ-ferrite typically found in standard CF8C steel in the as-cast condition. Creep strength of CF8C-Plus at high temperatures comes from nano-scale dispersions of NbC precipitates that form and remain stable, and are much finer than found in standard CF8C steel. Because CF8C-Plus has no δ-ferrite, it is also free of σ-phase after long term aging at 650-850°C relative to standard CF8C.

CF8C-Plus was deliberately designed to have the combination of good strength and ductility at both higher and lower temperatures, in order to achieve the best thermal fatigue resistance. Aging of tensile/fatigue specimens of the initial sand castings of CF8C-Plus and CN-12-Plus for 10, 000 h at 700-850°C at ORNL were completed this quarter, and sent to Caterpillar for testing and evaluation. Aging of a new sand-cast heat of CF8C-Plus at 700-850°C for1000 h was also completed was this quarter, and specimens were also sent to Caterpillar.

Additional lab-heats of CF8C-Plus were cast at ORNL previously, and creep testing was completed at 750 and 850°C this quarter. The alloys with Cu and W added show a clear creep-strength advantage, and will also be evaluated for commercial scale-up.

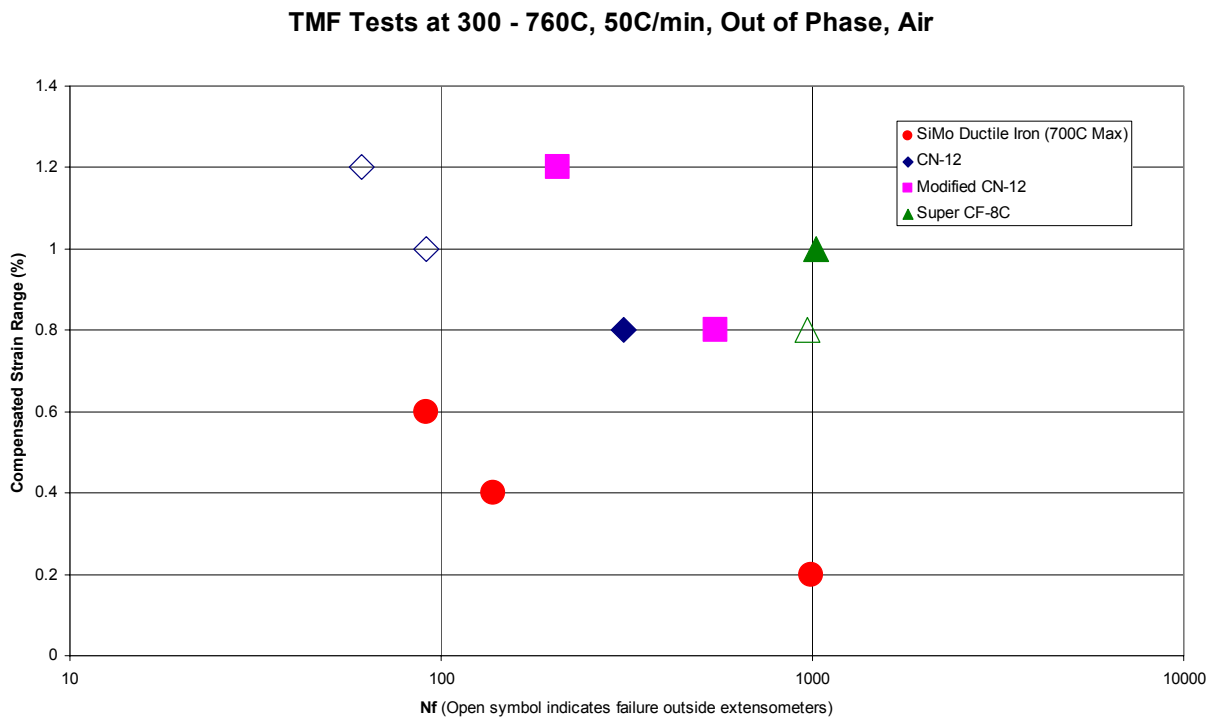

Figure 1 – Preliminay thermal-mechanical fatigue (TMF, out of phase, compression/hot and tension/cold) properties measured for the strain range indicated over the temperature cycle of 300-760°C at Caterpillar. Data include the commercial scale-up heats of standard CN12, new CF8C-Plus and CN-12-Plus stainless steels, and standard, commercial SiMo cast iron, all tested in air.

Caterpillar has chosen a commercial foundry to also produce centrifugally-cast heats of CF8C-Plus to evaluate the advantages of the new steel relative to the standard CF8C grade. Material was received at ORNL and Caterpillar for creep, tensile and fatigue testing that began this quarter. Standard CF8C steel is generally given a solution-annealing heat treatment at 1050°C (HT), but the new CF8C-Plus steel has generally be tested as-cast with no additional heat-treatment, so commercial heats were obtained with and without the heat-treatment. Creep-rupture testing at 140 MPa (a relatively high stress for shorter creep tests) at 750°C shows both rupture life and ductility advantages of CF8C-Plus relative to standard CF8C, and a clear benefit of the as-cast material with no additional heat-treatment for the CF8C-Plus steel (Fig. 2). Further testing, aging (1000 h and 10,000 h) and microstructural analysis will be done next quarter.

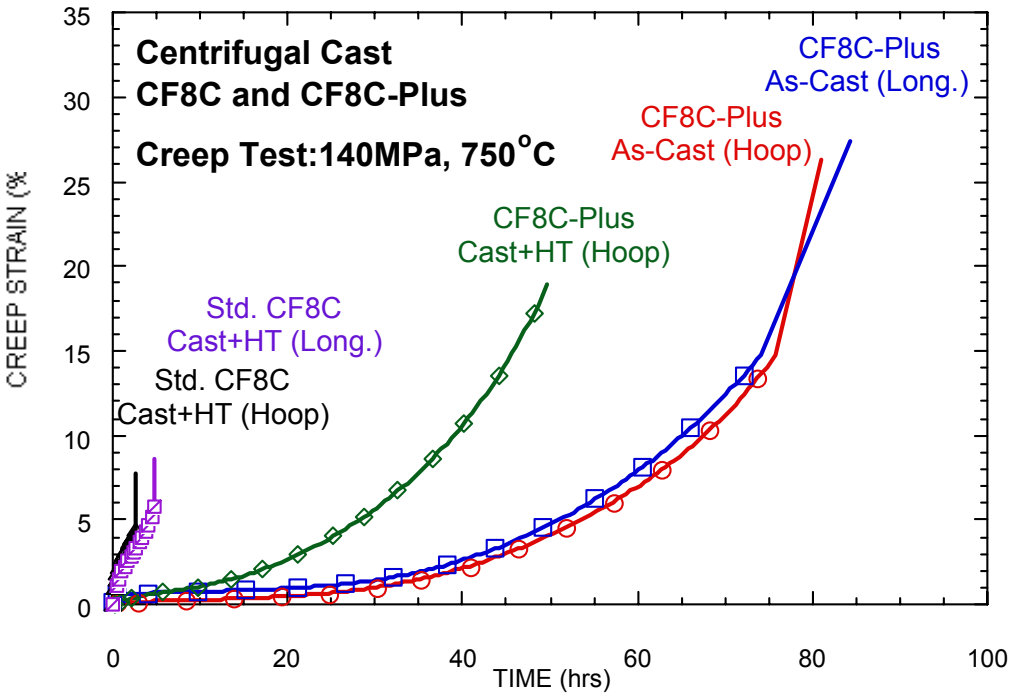

Figure 2 – Creep-rupture testing (at ORNL) at 140 MPa and 750°C in air of new, commercial, centrifugally-cast heats of CF8C-Plus, with and without solution annealing heat treatments (HT). The CF8C-Plus cast stainless steel has longer rupture life and much more ductility than the standard CF8C steel, and clearly is better in the as-cast condition with no HT.

Communications/Visits/Travel

Detailed team communications between ORNL and Caterpillar occur regularly, at least once or twice a week. The new 3 year CRADA began on July 21, 2002, when the previous CRADA ended.

An invention disclosure and patent application on cast austenitic stainless alloys with improved performance were completed by Caterpillar and filed with the U.S. Patent Office in December, 2000. It is entitled "Heat and Corrosion Resistant Cast Stainless Steels With Improved High Temperature Strength and Ductility," by P.J. Maziasz (ORNL), T. McGreevy (U. of Bradley/CAT), M.J. Pollard (CAT), C.W. Siebenaler (CAT), and R.W. Swindeman (ORNL). Several quarters earlier, two separate new patent applications were developed and submitted to the U.S. Patent Office, one on the CF8C Plus steel and the other on the CN12 Plus steel.

Status of Milestones

Formal milestones were imbedded in the previous CRADA and in the new CRADA, which is part of the DOE/OFCVT Heavy Vehicle Propulsion Materials Program, but a task in the ORNL FWP. As before, all milestones have been successfully achieved on or significantly ahead of schedule.

Publications/Presentations/Awards

The new CF8C-Plus Cast Stainless Steel, which won a 2003 R&D 100 Award, has been highlighted as a significant accomplishment for both the Metals and Ceramics Division and the Oak Ridge National Laboratory in 2004.

Segregation of Tungsten to Interfaces in Lamellar TiAl

Luke L. Hsiung
Lawrence Livermore National Labs
and Clyde L. Briant
Brown University

Objective/Scope

There has been a great interest in recent years in lamellar TiAl, which is prepared by heat treating an alloy with a composition near Ti – (47-49) Al in the α-region (usually near 1400°C) and then cooling it to room temperature. During the cool down, γ-lamellae form along the basal planes of hcp-α. The γ-phase has the $L1_0$ structure and the stoichiometry of TiAl. The remaining α-phase becomes ordered Ti_3Al (α_2-DO19). The final microstructure consists of lamellae of these two phases. Two types of interfaces exist in this lamellar structure. One set is between Ti_3Al and TiAl (α_2/γ) and the other is between two lamellae of TiAl (γ/γ). The orientations of these interfaces have been determined that the former interfaces consist of 1/6<112> or 1/3<112> misfit dislocations while the latter, which are twin-related, contain $1/6[11\bar{2}]$ type twinning dislocations or geometrically necessary dislocations [1].

The engineering interest in this material stems from the fact that it is lightweight and also has good creep properties [2-5]. As a result of the promising results reported in the literature, efforts have been made to improve the creep resistance of the material and to understand the mechanism by which creep occurs. This research has focused on both structural refinement and stability and alloying additions to the material, and all of these have provided significant improvements [6-8]. One element that has received particular attention is tungsten [7,9-12]. This element has been found to increase creep resistance [7,9], oxidation resistance [13] and strength [14] and to also stabilize the lamellar structure during creep [9]. It has been proposed that one way in which tungsten provides this effect is through segregation to the interfaces between the lamellae, and Table I summarizes the segregation results that have been presented in the literature. This segregation could pin the dislocations whose motion allows creep to occur, and also affect the interfacial energy in such a way as to inhibit the coarsening of the lamellae.

In this note, we use a straightforward model to show that the segregation of tungsten observed experimentally is consistent to what would be expected for segregation of this solute to dislocations. This result lends credence to a model in which tungsten improves creep resistance by segregating to the core of interfacial dislocations and inhibiting their motion.

Technical Highlights

Models

In order to determine if segregation to dislocations is a plausible mechanism to explain the tungsten enrichment at interfaces in lamellar TiAl, two questions must be addressed. The first is whether or not there are any kinetic limitations to this segregation. The second is whether or not this type of segregation is consistent with the numbers reported in Table I.

Table I **Values for Tungsten Segregation in TiAl**			
Interface : Condition	Alloy Composition	Tungsten Composition at Interface	Reference
γ/α_2 : Crept 3 hours at 1073 K	Ti-46.5Al-2Cr-3Nb-0.2 W	0.5 +/- 0.1	11
γ/α_2 Ledge : Crept 3 hours at 1073 K	Ti-46.5Al-2Cr-3Nb-0.2 W	0.6 +/- 0.1	11
γ/α_2 : Crept at 1088 K	Ti – 47Al – 2Cr – 1Nb- 0.8Ta – 0.2W – 0.15B – 0.3Si	0.52	12
γ/α_2 Ledge : Crept at 1088 K	Ti – 47Al – 2Cr – 1Nb- 0.8Ta – 0.2W – 0.15B – 0.3Si	0.69	12
γ/α_2 Interface : Annealed at 1173K	Ti – 47Al – 2Cr – 1Nb- 0.8Ta – 0.2W – 0.15B – 0.3Si	0.35	12
γ/α_2 Ledge : Annealed at 1173K	Ti – 47Al – 2Cr – 1Nb- 0.8Ta – 0.2W – 0.15B – 0.3Si	0.30	12
γ/α_2 Interface : Annealed at 1173K	Ti-47Al – 2Cr – 1.8Nb – 0.15B – 0.2W	0.68+/-0.45 0.42 +/-0.25*	10
γ/γ Interface : Annealed at 1173K	Ti-47Al – 2Cr – 1.8Nb – 0.15B – 0.2W	0.38 +/- 0.13 0.33 +/- 0.15 0.33 +/- 0.15*	10

* Values obtained for different measurements in the same material

To determine if diffusion kinetics limited the amount of segregation that could during a test, we used the standard McLean model for interfacial segregation [15]. Although this model is usually applied to segregation to high angle grain boundaries, there is nothing in this model that limits its use to that type of interface. Rather the model simply gives the time required to reach a certain fraction of the equilibrium segregation at any interface.

The equation for this segregation is given by

$$\frac{C - C_0}{C_f - C_0} = 1 - ((\exp(4Dt/(\alpha\delta)^2) * erfc(2\sqrt{Dt}/\alpha\delta)) \qquad (1)$$

where C_0 is the initial concentration, C_f is the final concentration, α is the ratio of the initial to the final concentration, D is the diffusion coefficient, t is time and δ is the grain boundary width. Values used for these calculations are given in Table II.

The second type of calculation that is required is the segregation to the dislocation core. For this calculation we followed the model of Cottrell and Bilby [16] in which one first calculates the interaction energy E_I between a solute and an edge dislocation using the expression

$$E_I = 4(1+\nu)Gbr_a^3\Delta/(3(1-\nu)\ \sin\theta/r) \qquad (2)$$

and then determines the concentration as a function of distance [17] through the expression

$$C(r) = C_0 \exp\,[-E_I(r)/kT] \qquad (3)$$

In these expressions, r is the radial distance from the dislocation core, G is the shear modulus, r_a is the radius of the lattice site, ν is Poisson's ratio, Δ is the misfit parameter chosen so that the radius of the solute is $r_a\,(1 + \delta)$, b is the magnitude of the Burgers vector and $\sin\theta$ was taken to be 0.707 for these calculations, where θ is a polar coordinate. Table II lists the values used in these calculations.

It should be pointed out here that most considerations of interfacial segregation have dealt with segregation to high angle grain boundaries. It is generally assumed that the variety of sites afforded to the segregant, both in terms of size and coordination, provide a trap for the segregant and that as a result the local concentration of the segregant at the boundary increases [18,19]. It has also been shown that twin boundaries and other low angle boundaries, generally do not provide these types of sites and that segregation to these interfaces is much lower [19]. Thus the driving force for the observed segregation to these lamellar interfaces, which are either twin-related (γ/γ) or semi-coherent (γ/α_2), must primarily be a result of the presence of the dislocations on these grain boundaries which could provide local sites for segregation. It is for this reason that we have used the Cottrell-Bilby approach to model the segregation in these lamellar materials.

Kinetics of segregation

We first use McLean's equation to determine if segregation is kinetically limited. Figure 1 shows the results obtained for a temperature of 900°C.

Table II
Values of Parameters Used in Calculations

Parameter	Value
D	1.45×10^{-5} exp (-65380/RT)
α	3
δ	10 A
G	45 GPa
b	3A
Δ	0.05839
ν	0.33
r_a	1.45 A

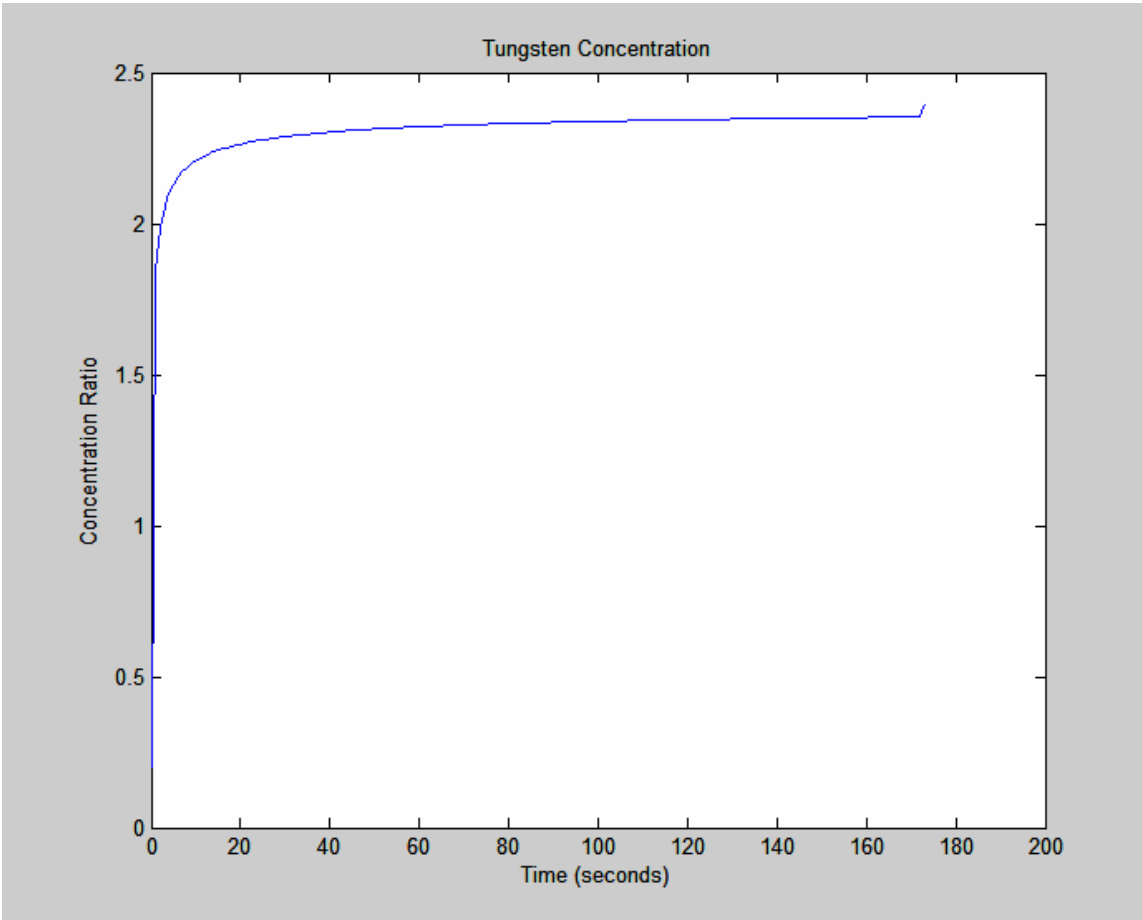

Figure 1 – The kinetics of segregation of W in lamellar TiAl at 900°C. Calculations made using equation 1.

Clearly the tungsten segregation approaches its equilibrium value in a matter of a few minutes. Even at 700°C we found that the segregation was complete in approximately 30 minutes. Thus it would appear that even during the creep tests, segregation to the interfaces could occur in times that were much shorter than the length of the test. Thus, we conclude that kinetics limitations are not of great importance in determining the measured values of the tungsten segregation reported in Table I.

Segregation to dislocations

We now use the Cottrell-Bilby approach to calculate segregation to dislocations. Figure 2 shows the segregation at 700°C plotted as a function of distance from the dislocation core. We see that at this temperature the maximum segregation is on the order of 0.6. Figure 3 shows the maximum segregation values calculated for temperatures ranging from 700 to 1400°C. This range was chosen because it is similar to the range used for annealing (between 900 and 1400°C) and creep testing (700-900°C). We see that there is a significant increase in the segregation as a result of decreasing temperature.

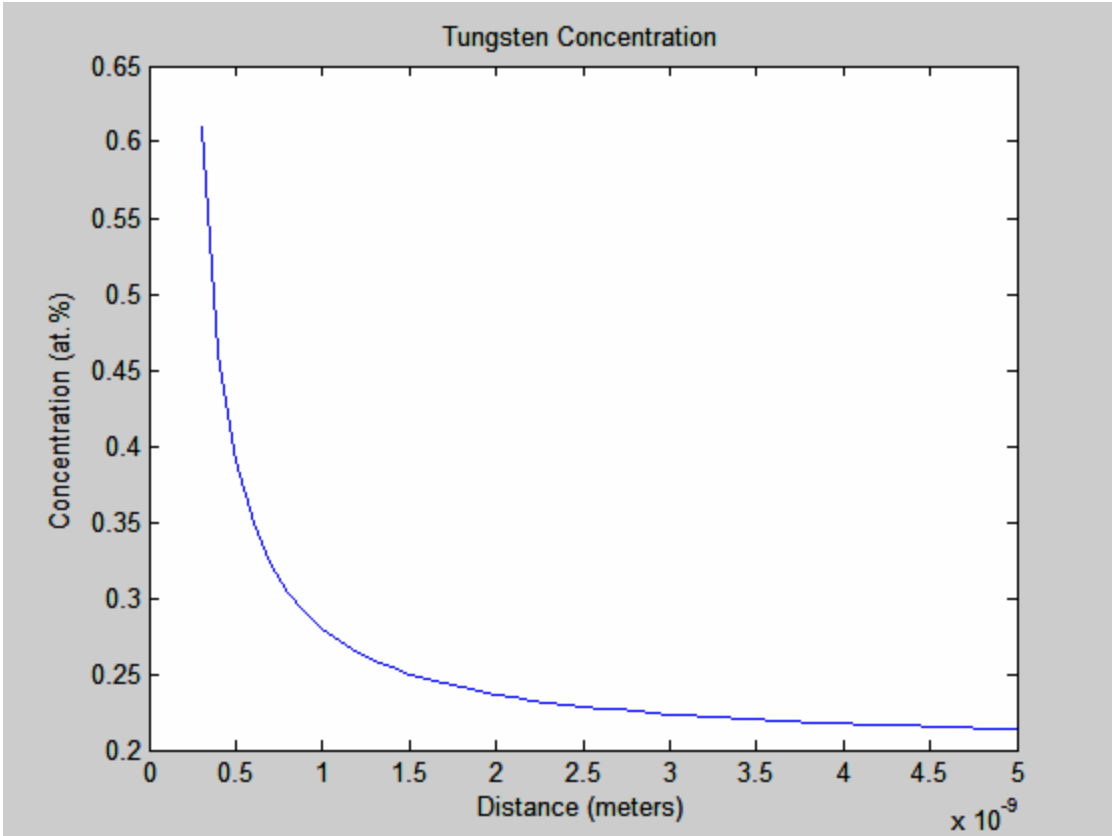

Figure 2 – Segregation of tungsten to a dislocation in lamellar TiAl. The amount of tungsten is plotted as a function of distance from the dislocation. Calculations made using equations 2 and 3. Values are for a temperature of 700°C.

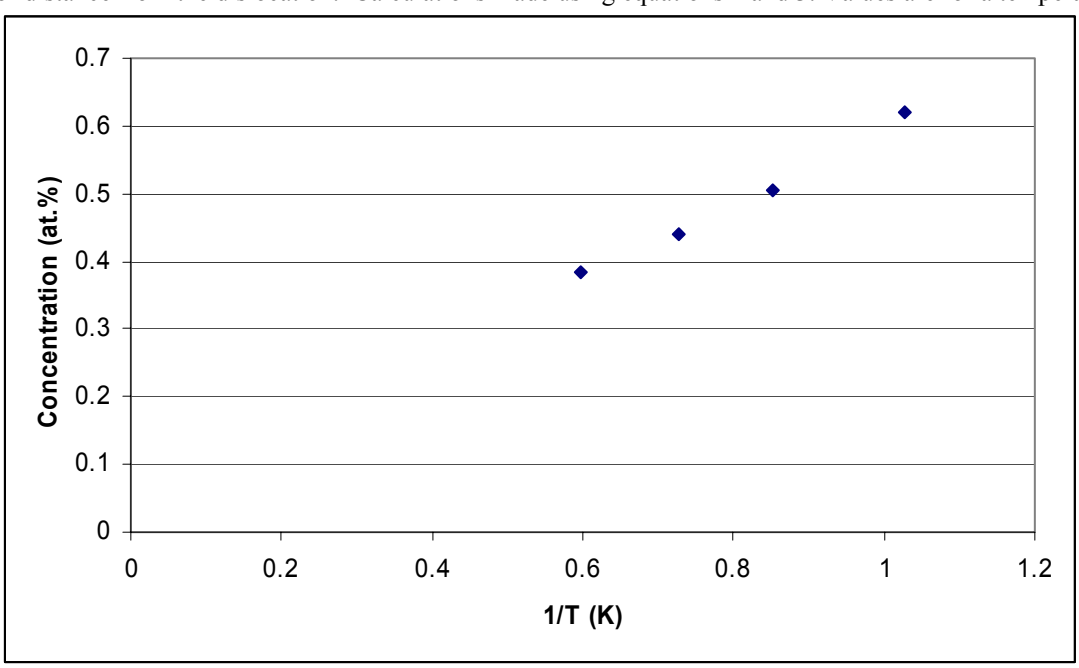

Figure 3 – The maximum concentration plotted of tungsten segregated to a dislocation in TiAl plotted as a function of the inverse of the temperature. Temperature values ranged between 700 and 1400°C. Calculations made using equations 2 and 3.

The values presented above are in good agreement with the measurements reported in the literature (Table I). The data reported were obtained by either atom probe field ion microscopy [10] or energy dispersive spectroscopy in a high resolution TEM [11,12]. To make an exact comparison one would have to include the number of dislocations that are present in the volume of material that is analyzed. However, the simple calculation performed here gives a first order estimate of the amount of segregation one should observe. Several additional points should be noted in making these comparisons. The first is that Larson *et al.* [10] reported that there was less segregation at the γ/γ interface than at the γ/α_2 interface. Our calculations would not distinguish between these two types of interfaces but if the dislocation density were higher along the γ/α_2 interface, then one would expect this difference. These authors also report that they measured different levels of segregation at different interfaces. This difference could be explained by the fact that there are different dislocation densities at different points along the interface. Another important point is that ledges were found to have more segregation than the interface, and this can be explained by the fact that dislocation can pile up at the ledges as the move along the interface [12]. Finally, it should be noted that none of the studies reported the type of cooling used after the heat treatments or creep tests. Since additional segregation could occur during a slow cool down, this part of the heat treatment could be important for creep performance.

Conclusions

We report calculations in which we have used the Cottrell-Bilby model to estimate tungsten segregation at the lamellar interfaces present in lamellar TiAl. The results show good agreement with measured segregation and also show that this segregation should not be kinetically limited at the temperatures of annealing or creep testing. Thus it would seem reasonable that tungsten enhances creep resistance by segregating to the dislocation cores and limiting their mobility, both in their glide along the interface and their climb at ledges. If this segregation does have this positive effect, creep resistance might be further enhanced by a low temperature aging, which would increase segregation to existing dislocations and make their motion even more difficult.

Status of FY 2004 Milestones

Milestone: Collaboration with Brown University (Professor Clyde Briant) on theoretical modeling of solute segregation at lamellar interfaces was completed.

Milestone: Continue creep tests to investigate the creep resistance and microstructural stability of the nanolaminate composites at elevated temperatures up to 850 $^{\circ}$C, which will be reported in next quarterly report.

Milestone: "Continue to collaborate with ORNL (Dr. C.T. Liu) to fabricate to fabricate and characterize the oxidation-resistant class of in-situ $TiAl/Ti_3Al$ nanolaminate composites with high Nb content (>10 at. %) using hot-extrusion processing techniques."

Publications

L.M. Hsiung and T.G. Nieh, "Microstructures and Properties of Powder Metallurgy TiAl Alloys," Mater. Sci. Eng., **A364**, 1 (2004).

L.M. Hsiung, A. J. Schwartz, and T.G. Nieh, "In Situ TEM Observations of Interface Sliding and Migration in a Refined Lamellar TiAl Alloy," *Intermetallics*, 2004, in press.

References

1. L.M. Hsiung, T.G. Nieh, Mater. Sci. Eng., **A239-240**, 438 (1997).
2. Y-W. Kim and D.M. Dimiduk, JOM, **43** (8), 40 (1991).
3. J. Beddoes, W. Wallance, L. Zhao , Internat. Metals Review, **40**, 197 (1995).
4. Y-W. Kim, Acta Metall. Mater., 40, 1121 (1992).
5. K. Hono, E. Abe, T. Kumagai, H. Harada, Scripta Mater., **35**, 495 (1996).
6. C.T. Liu, J.H. Schneibel, P.J. Maziasz, J.L. Wright, D.S. Easton, Intermetallics, **4**, 429 (1996).
7. P.L. Martin, M.G. Mendiratta, H.A. Lipsitt, Metall. Trans. A, **14A**, 2170 (1983).
8. Y-K. Kim, in Y-K. Kim, R. Wagner, M. Yamaguchi, eds., Gamma Titanium Aluminides, TMS, Warrendale, PA, 1995, p.3
9. P.J. Maziasz, R.V. Ramanujan, C.T. Liu, and J.L. Wright, Intermetallics, **5**, 83 (1997).
10. D.J. Larson, C.T. Liu, and M.K. Miller, Mater. Sci. Eng., **A239**, 220 (1997).
11. X.-W. Du, J. Zhu, X. Zhang, Z.Y. Cheng, and Y-W. Kim, Scripta Mater., **43**, 597 (2000).
12. L.M. Hsiung, Mat. Res. Soc. Symp., 740, 287 (2003).
13. G.E. Fuchs, Mat. Sci., Eng. A, **192/193**, 707 (1995).
14. D. McLean, *Grain Boundaries in Metals*, Oxford Univ. Press, London, (1957).
15. A.H. Cottrell and B.A. Bilby, Proc. Phys. Soc., **A62**, 49 (1949).
16. D. Hull and D.J. Bacon, Introduction to Dislocations, Butterworth-Heinemann, Oxford, 2001, p. 206.
17. C.L. Briant, Metall. Trans. A, **21A**, 2339 (1990).
18. T. Ogura, C.J. McMahon, Jr., H.C. Feng, and V. Vitek, Acta Metall., **26**, 1317 (1978).

Laser Surface Texturing Of Lubricated Ceramic Parts

Peter J. Blau
Oak Ridge National Laboratory

Objective/Scope

The objective of this effort is to evaluate the frictional benefits of laser dimpling patterns on the lubrication of ceramic surfaces. This project is being conducted jointly with Argonne National Laboratory to study the benefits of a laser surface texturing (LST) process that was developed by Prof. Itzhak Etsion, Surface Technologies, Ltd., Israel. That process uses a computer-controlled laser system to produce a pattern of shallow, rounded dimples on bearing surfaces. Based on calculations, preliminary tests, and limited field trials, the developer claims that LST enhances the ability of a lubricated surface to establish a load-bearing hydrodynamic film that decreases friction relative to a non-dimpled surface. The ORNL portion of this joint effort is focused on two aspects of LST: (1) conducting reciprocating tests on LST ceramic surfaces using lubricants with various viscosities, and (2) determining the microstructural changes associated with the LST process. These results will be placed into context with other methods for surface engineering, including the use of solid lubricants for friction reduction.

Technical Highlights

New fixtures and specimens. New, spring-loaded test fixtures are being installed to achieve better contact alignment of the dimpled (LST) parts against their flat counterfaces during friction tests. In addition, specimens of transformation-toughened zirconia and silicon nitride are being ground in preparation for the new series of experiments. The TTZ will be sent to Surface Technologies Ltd for treatment. In the mean time, remaining dimpled specimens of TTZ will be used to verify the alignment characteristics of the new fixtures.

Guest worker. A guest worker, Prof. Timothy Ovaert, Aerospace and Mechanical Engineering Department, University of Notre Dame, will be joining ORNL for a summer research collaboration in several tribology areas. He has won society-level research awards from the American Society for Mechanical Engineers and the Society of Automotive Engineers. His comprehensive background in modeling and experimentation will enable him to contribute to the current project on laser surface treatment as well as to related tribology efforts in scuffing, friction brake materials, and the improvement of engine component durability.

Future Plans

(1) Conduct friction experiments of laser-dimpled surfaces using the improved test fixtures.
(2) Work with guest researcher T. Ovaert to study effects of dimpling on friction reduction in ceramics.

Travel

None.

FY 2004 Milestones

1) Prepare a literature review of techniques uses to achieve changes in friction by surface patterning and compare these with laser dimpling. (January 2004 – completed)

2) Complete characterization of the effects of laser dimpling on the micro-mechanical properties and fine structure of TTZ and SiC ceramics (September 2004).

Presentations and Publications

None this period.

High Density Infrared Surface Treatment of Materials For Heavy-Duty Vehicles

T. N. Tiegs, D. C. Harper, F. C. Montgomery, and C. A. Blue
Oak Ridge National Laboratory

Objective/Scope

High Density Infrared (HDI) technology is relatively new to the materials processing area and is gradually being exploited in materials processing. For many applications in heavy-duty vehicles, superior properties, such as corrosion and wear resistance, are only required at the material surface. The project using HDI technology will be exploratory and will examine (1) application of wear-resistant coatings, and (2) modification of plasma-sprayed coatings.

Technical Highlights

Earlier work had shown that adherent coatings of hardmetal compositions could be applied to a variety of metal substrates. Cross-sections of the coatings and base alloys revealed some large porosity within the coatings and also at the interface with the underlying alloy. These bubbles are believed to be porosity that is trapped during the melting of the coating. To minimize the presence of the bubbles, the IR treatment procedure was modified to give a double exposure of the coating to produce a remelting of the coating. The idea was that this would allow the bubbles to escape during the second melting. A similar technique has been used before with silica refractories to reduce trapped porosity. The effects of the double exposure on the properties of the coating and underlying base metal were mixed.

Samples of WC-(Ni-Cr-Fe) on 4140 steel are shown in Figs. 1 and 2 for the one-step and two-step HDI processing. No reduction in the presence of the trapped porosity was observed. However, the level of trapped porosity was decreased by additional time during a one-step IR exposure as shown in Fig. 3. Evidently, the additional time during the liquid formation allowed the trapped gas to escape. Some cracks in the coating were observed with the additional exposure times.

In another sample, the double exposure resulted in a reduction of the trapped porosity as shown in Figs. 4 and 5. The additional exposure also appeared to increase the mixing between the coating and the underlying base metal. The effects on the hardness for the different exposure conditions will be determined.

Status of Milestones

On schedule.

Communications/Visits/Travel

None.

Problems Encountered

None.

Publications
None.

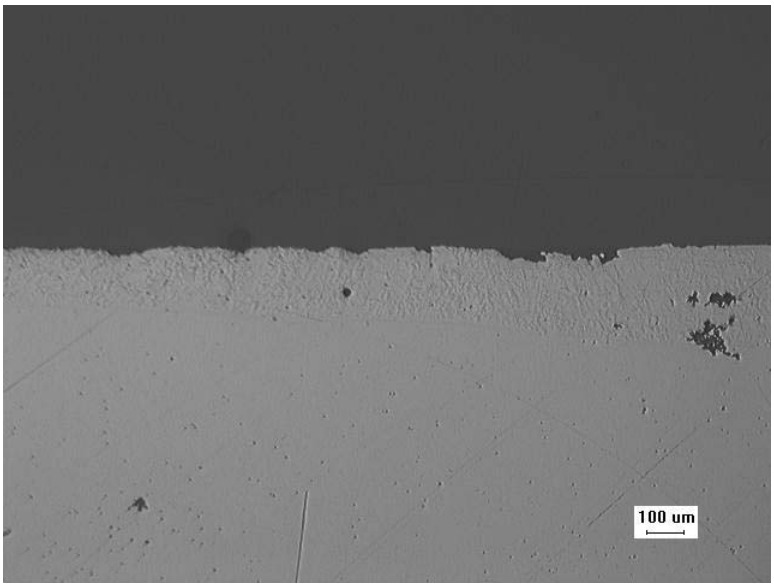

Fig. 1. Cross-section of WC-(Ni-Cr-Fe) coating on 4140 steel after one-step HDI processing. IR exposure consisted of a lamp power of 900 amps for 2 sec.

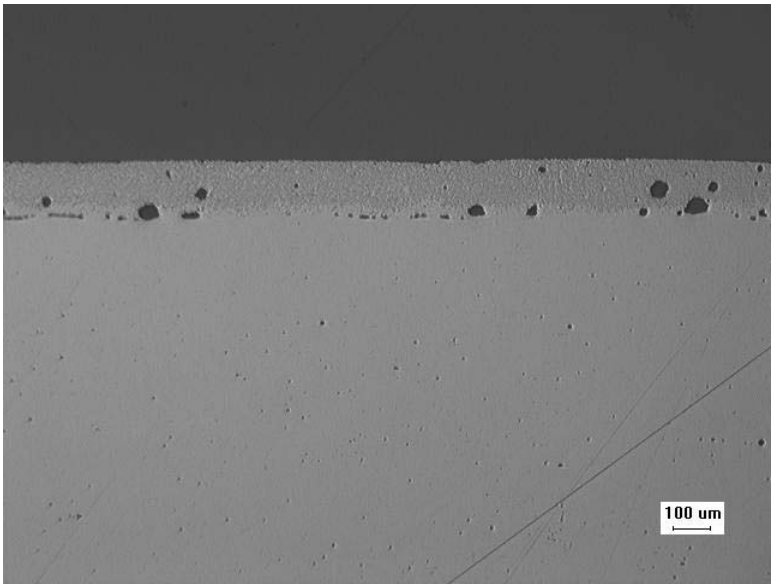

Fig. 2. Cross-section of WC-(Ni-Cr-Fe) coating on 4140 steel after two-step HDI processing. IR exposure consisted of a lamp power of 900 amps for 2 sec, 15 sec non-exposure, followed by 900 amps for 1 sec.

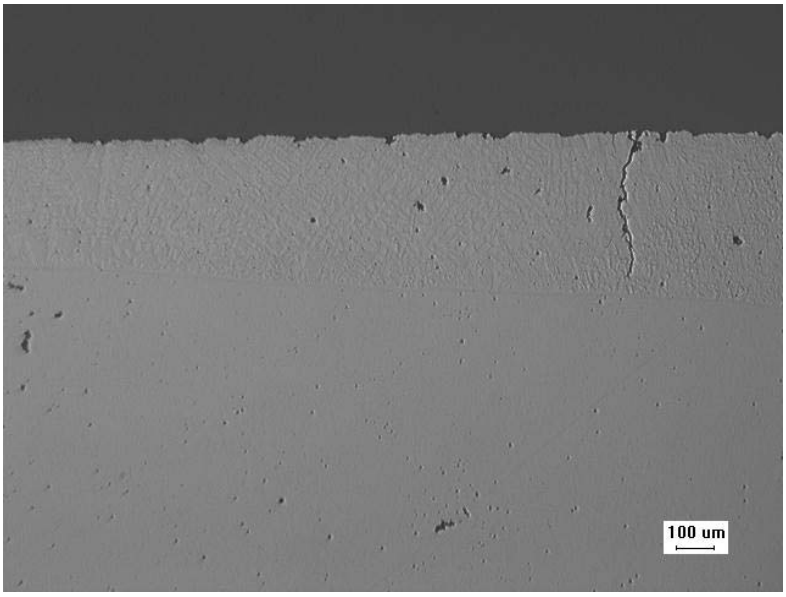

Fig. 3.Cross-section of WC-(Ni-Cr-Fe) coating on 4140 steel after one-step HDI processing. IR exposure consisted of a lamp power of 900 amps for 3 sec.

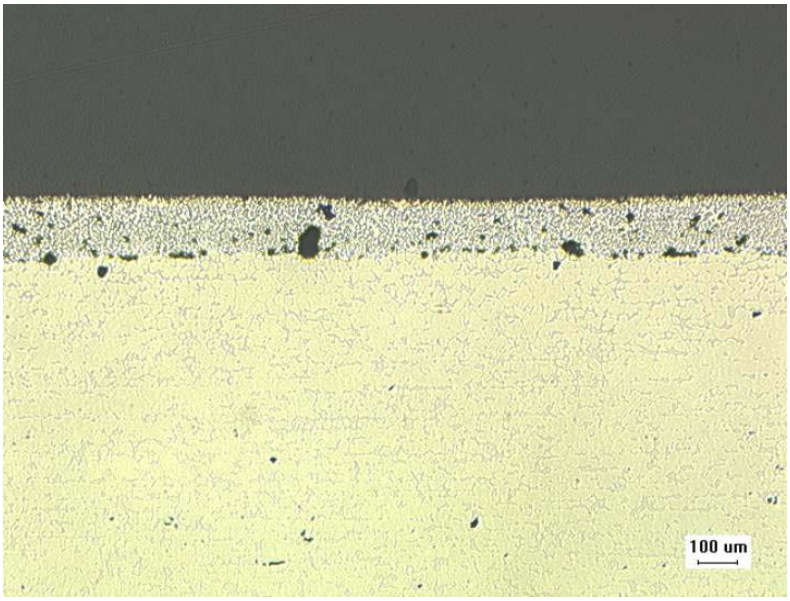

Fig. 4. Cross-section of WC-Ni_3Al coating on D2 tool steel after one-step HDI processing. IR exposure consisted of a lamp power of 900 amps for 2 sec.

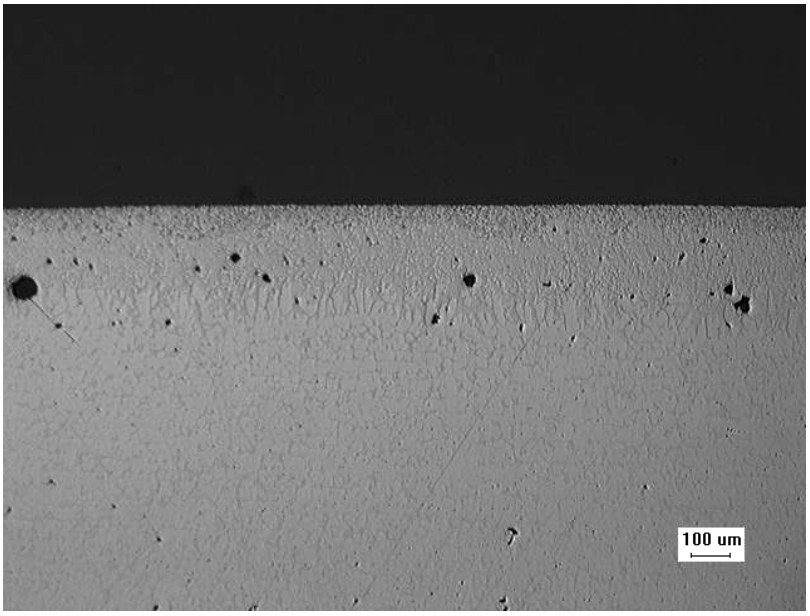

Fig. 5. Cross-section of a WC-Ni_3Al coating on D2 tool steel after a two-step HDI processing exposure. IR exposure consisted of a lamp power of 900 amps for 2 sec, 15 sec non-exposure, followed by 900 amps for 1 sec.

Titanium Alloys for Heavy-Duty Vehicles

Paul C. Becker
Oak Ridge National Laboratory

The replacement of cast iron by titanium in a heavy-duty diesel engine should be most attractive to the US military, at least in the near term. This is because Ti alloys are 40% lighter than cast iron and have mechanical properties four times greater than cast iron. This could lead to a lighter and more powerful engine than what is available today for the same engine size. These benefits could offset the additional cost associated with making the head and block from this high performance material.

The results of the FEA modeling on a production Cummins B-series engine rated at 305 hp (2400 psi peak cylinder pressure) was presented to the U.S. Army Tank Command (TACOM) in Warren, Michigan, for their review and comments.

Although, the analysis proved that the total engine weight could be reduced by between 14% and 17% without any design changes to the engine, TACOM was even more interested in determining if the use of a Ti alloy could allow the engine to be up-rated to as much as 600 hp.

Accordingly, the following work was proposed:

1. Model the same engine at 600 hp (3200 psi peak cylinder pressure) using Ti-6Al-4V for both the head and block.
2. In the head, the model should include the use of a reinforcing Al-Cu alloy insert in the valve bridges to better transport the heat away from the valve bridge regions. The use of an insert is not done in production, and if proved beneficial, would be the subject of an R & D project to ascertain how such an insert could be bonded to the Ti alloy head material.
3. In the model, modify the head design in the valve bridge area, to allow the coolant to contact directly the Al-Cu insert to better facilitate the transport of heat away from the valve bridge area.

Mechanical Behavior of Ceramic Materials for Heavy Duty Diesel Engines

A. A. Wereszczak and M. K. Ferber
Oak Ridge National Laboratory

Objective/Scope

The application of more ceramic components in engines and transportation systems would be enabled if they could be confidently manufactured and machined faster (i.e., more cost-effectively) and if mechanisms that limit their mechanical performance were understood, predictable, and controlled. This project quantifies "quasi-plasticity/fracture thresholds" in ceramics (e.g., cubic oxides and non-oxides, nanoceramics and nanocermets, piezoelectric ceramics, micaceous ceramics, and traditional structural ceramics) and examines the competing mechanisms that dictate when and how quasi-plasticity or fracture dominates the other during controlled and instrumented static and dynamic indentation and scratch testings. The thorough understanding of the competition of fracture and quasi-plasticity in ceramics will enable improved and faster means of ceramic component manufacturing and surface engineering (e.g., ductile regime machining) and maximize mechanical performance when surface condition (e.g., bending) or when surface-located events (e.g., wear, impact) are service-life-limiters in engine and transportation system components.

Technical Highlights

Conventional Vickers microhardness testing at 500 g was performed on numerous metallographically prepared materials (ceramics, cermets, intermetallic composites, and metals). Additional materials (not listed) will be tested as well. Each will be subjected to instrumented Hertzian indentation and scratch testings, and the measured performances will be modeled and their links to wear and machining will ultimately be sought.

Ce-TZP ZrO_2 (Coors)	4340 Steel Stage I
Ce-TZP ZrO_2 (Ferro)	4340 Steel Stage III
Mg-TTZ ZrO_2 (Coors)	Ti64
WC/6%Co	Al 15083
WC/10%Co	Al 7039
TiC-40%Ni_3Al	52100 Cr Steel
NBD 200 Si_3N_4 (Cerbec)	M-50 Tool Steel
SN 101C Si_3N_4 (Cerbec)	C1010/1020 C Steel
α-SiAlON (Kennametal)	316 SS
Toshiba bearing-grade Si_3N_4	440 SS
Ceralloy 147-31N Si_3N_4	Zr Bulk Amorphous Metal

Modeling (finite element analysis or FEA) was performed during the present reporting period to help with the interpretation of the indentation damage that results in ceramics. It has been observed that the microstructural damage that exists on the "sides" of the indents (spherical or even Vickers) generated in ceramics looks to be different than the damage that exists at the bottom of those very same indents. The radial surface stresses during spherical indentation

(Fig. 1) that exists just outside the contact area between indenter and material were modeled for a variety of indenter ball diameters.

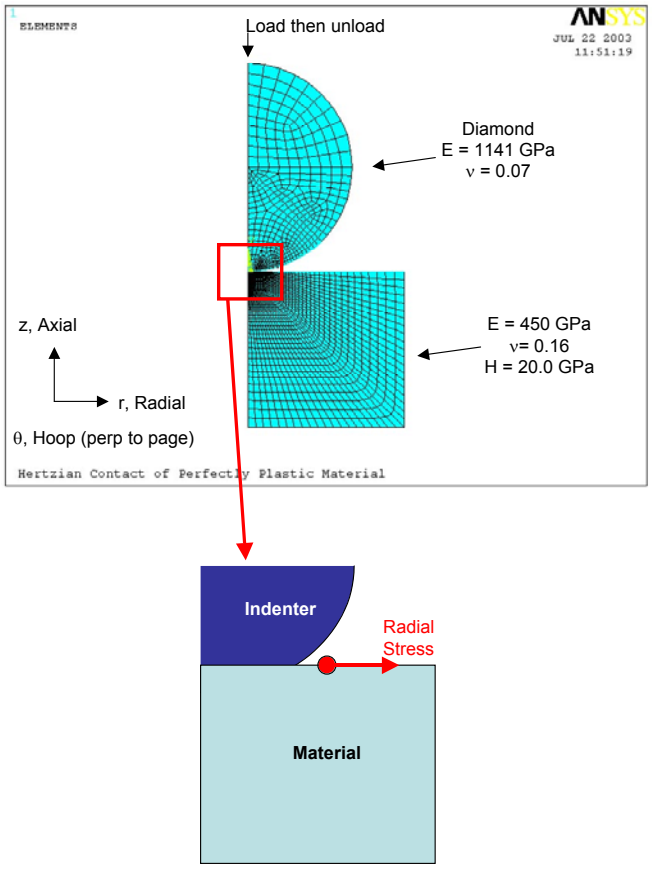

Figure 1. Surface radial stresses were modeled as a function of indentation load and indenter diameter.

The maximum surface radial stresses as a function of indentation load and ball diameter are shown in Fig. 2. If one assumes a "tensile strength" of 600 MPa for the material shown in Fig 2, then the results suggest that crack initiation could occur as low as 5N, 7N, 11N, and 17N when this material is indented with diamond sphere having a diameter of 1.0, 1.5, 2.0, and 2.5mm, respectively. This surface tensile stress field is highly localized at the surface - if crack initiation *were* to occur, then the compressive stress field just underneath it would likely arrest further propagation. For loads lower then these thresholds for those respective indenter diameters, there is an associated contact area covering a microstructure that was never subjected to tensile stresses sufficient to potentially cause crack initiation.

What could this mean? If that crack initiation were indeed induced at these low loads, then continued loading would increase the contact area and then subject an increasing sized annulus of microstructure to compression (that has previously been subjected to high tensile stresses at lower loads), see Fig 3. These series of event during loading (i.e., center contact area only being subjected to compressive stresses surrounded by an annulus of surface-located material that was

cycled between high tensile, then high compressive stresses) are consistent with the differences in microstructural damage within the indent. Acoustic emission detection during loading should potentially reinforce these FEA results, as well as carefully conducted scanning electron microscopy of the indents.

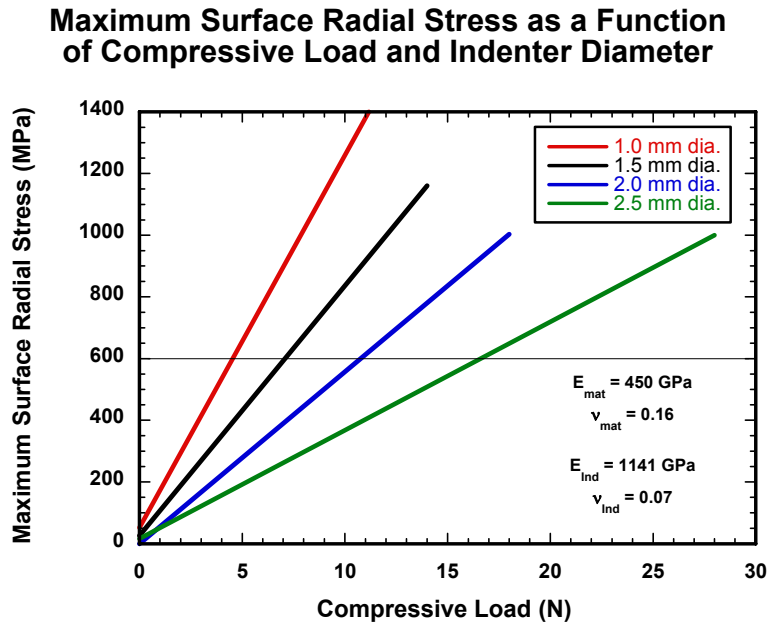

Figure 2. Maximum radial tensile stresses just outside the Hertzian contact area increase with increasing compressive load.

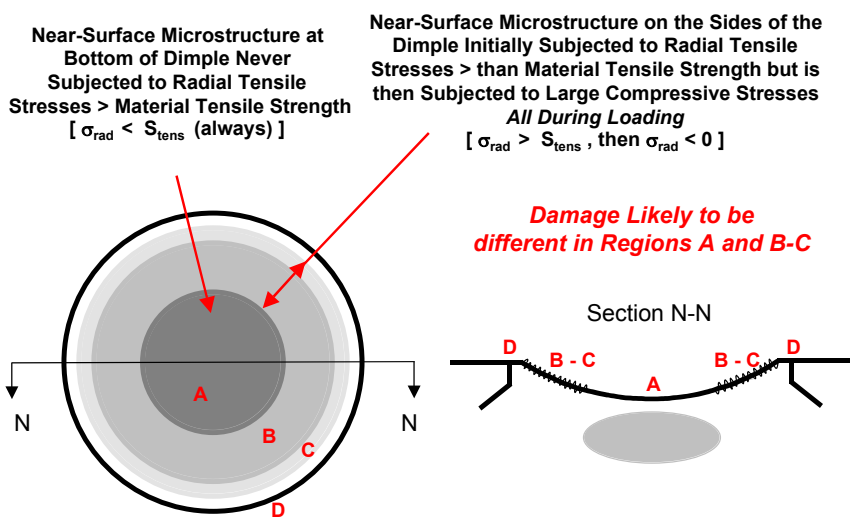

Figure 3. The finite element analysis results suggest that the surface microstructure damage should be different depending on where in the indent the microstructure is located.

The arrival of our instrumented (pendulum) scratch tester is anticipated in early Q3. The system underwent some final calibrations and aesthetic improvements so its receipt did not occur in Q2 as expected. The system will be used to characterize and interpret scratch-induced quasi-plasticity and fracture processes in ceramics. Linkages between its generated results and Grindability and other machining parameters will be sought.

A post-doctoral researcher, Hong Wang, will start working on this project early in Q3. Dr. Wang possesses a lot of experience with dynamic hardness and instrumented scratch testing, so his contributing efforts will benefit the program.

Numerous communications occurred with Prof. Ghatu Subhash of Michigan Technological University about instrumented dynamic indentation and instrumented scratch testing of ceramics. Formal interactions are planned between the PIs and Subhash whereby Subhash will assist in the establishment of the relationship between the subsurface damage in ceramics and its influence on the mechanical properties. The MITech group will perform coordinated experimental and theoretical studies that supplement in-house work at ORNL.

Status of FY 2004 Milestones

On schedule.

Communications/Visits/Travel

Wereszczak visited Ceradyne, Inc., Costa Mesa, CA on 26 February 2004 to discuss the present project and the testing of Ceradyne's Ceralloy 147-31N silicon nitride.

Wereszczak and Ferber visited DOE HQ on 02 March 2004 to meet with Sid Diamond and discuss the project's progress.

Publications

UT-Battelle requested authorization from the US Department of Energy to assert copyright of the *μ-FEA* software.

References

None.

Deformation Processes for the Next Generation Ceramics

Paul F. Becher
Oak Ridge National Laboratory

Objective/Scope

This project seeks to determine how to exploit the deformation response of ceramics to enhance mechanical properties and develop novel shape forming with particular emphasis on the impact of nano-scale microstructures.

Technical Highlights

A computer controlled mechanical test frame was modified to conduct both compressive creep and stress-strain (under controlled loading rates) studies at temperatures up to 1400°C in air. An additional frame will be upgraded later in the year. The system, which utilizes contact extensometers with displacement sensors based on changes in air gap capacitance, provides for high sensitivity and reproducibility in both load and displacement measurements. Analysis of the load-displacement data for sintered alpha SiC at 1200°C in air yielded elastic modulus consistent with that reported in the literature.

Next studies were initiated using a fully dense, high purity, 350 nm grain sized zirconia ceramic containing 2 mol % yttria was initiated. This data will serve as the baseline for understanding the behavior of < 100 nm grain sized zirconias being prepared in the processing studies at Pennsylvania State University. The 350 nm grain sized zirconia consists entirely of tetragonal phase with no evidence for the monoclinic or cubic phases. At room temperature, the material exhibits very high fracture strengths in four point flexure (1500 MPa) and a fracture toughness of ~7.5 MPa•m$^{1/2}$, as measured via the applied moment double cantilever beam method. The toughness is limited at room temperature by the very small grain size where it is known that at constant solute (e.g., yttria) levels the toughness due to the stress induced tetragonal to monoclinic phase transformation is inhibited as the grain size is reduced [1, 2]. However, the transformation can be enhanced by reducing the test temperature (Figure 1), which results in a transformed zone being generated ahead of and adjacent to the propagating crack tip.

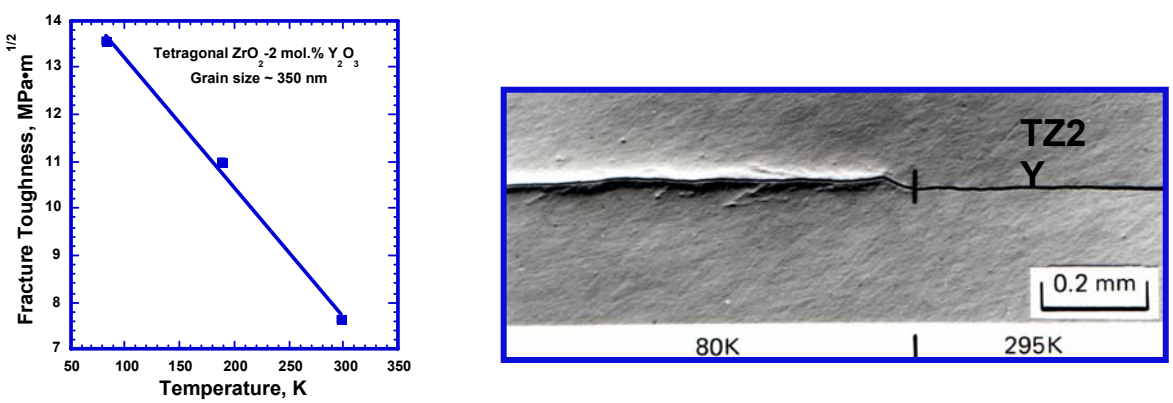

(a) (b)

Figure 1. Fracture toughness of TZ2Y increases with decrease in temperature (a) as the phase transformation associated with the crack propagation is enhanced (b)

Initial compressive creep data have been generated over the temperature range of 1100° to 1200°C and an applied stress range of 30 to 90 MPa. While these are preliminary data, the activation energies are consistent with those for creep limited by the diffusion of zirconium. The stress exponent of ~ 1.8 for temperatures ≥ 1150°C suggests a combination of grain boundary shear and diffusive creep. It has been suggested that grain boundary shear is only initiated above a temperature dependent threshold stress, which would imply change in the stress exponent with applied stress [3,4]. At 1100°C, the stress exponent is much lower suggesting creep is entirely diffusive in nature.

Additional experiments will be required to resolve these issues. In the meantime, experiments are underway to assess the stress-strain response of this material under fixed strain rates at elevated temperatures.

References

1. P. F. Becher and M. V. Swain, "Grain-Size-Dependent Transformation Behavior in Polycrystalline Tetragonal Zirconia," *J. Am. Ceram. Soc*., 75(3) 493-502 (1992).
2. A. Bravo-Leon, Y. Morikawa, M. Kawahara, and M. J. Mayo, "Fracture Toughness of Nanocrystalline Tetragonal Zirconia with Low Yttria Content," *Acta Mater*., 50: 4555-62 (2002).
3. M. Jimenez-Melendo, A. Dominguez-Rodriquez, and A. Bravo-Leon, "Superplastic Flow of Fine-Grained Yttria-Stabilized Zirconia Polycrystals: Constitutive Equation and Deformation Mechanisms," *J. Am. Ceram. Soc*. 81(11) 2761-76 (1998).
4. A. Dominguez-Rodriguez, f. Gutierrez-Mora, M. Jimenez-Melendo, J. L. Routbort, and R. Chaim, "Current Understanding of Superplastic Deformation of Y-TZP and Its Application to Joining," *Mater. Sci. & Eng'g*, A302: 154-61 (2001).

Status of Milestones

New project

Communication/Visits/Travel

Subcontract now in place to fund the optimization of the processing of nanocrystalline oxides at Pennsylvania State University under the direction of Dr. J. H. Adair.

Met with Prof. Hans Conrad at North Carolina State University on April 12, 2004 to discuss experimental studies of field effects on deformation behavior in oxides.

Publications

New project

Synthesis of Nanocrystalline Ceramics

James H. Adair
Pennsylvania State University

Objective

Advanced particle processing will be used to produce dense, bulk nanocrystalline oxide ceramics. Two routes to obtaining well-dispersed powders (i.e., comminution and colloidal processing) will be emphasized. The large surface areas of such powders lead to large quantities of adsorbates, which must be removed both to enhance particle packing and subsequent sintering. Both reactive atmosphere and microwave thermolysis have merit and will be evaluated to eliminate adsorbates at low temperatures. This project will scale-up the processes to be able to produce dense YSZ ceramics with grain sizes less than 100 nm having sample dimensions ≥ 25 mm in diameter by ≥3 mm in thickness to be delivered to ORNL for further testing. Additional effort will focus on fabrication of said samples with grain sizes < 50 nm for testing by ORNL staff.

Background

Particle processing has the potential to produce dense, bulk nanocrystalline materials with a variety of chemical compositions and architectures including composite materials. Outstanding challenges in particle processing to form bulk, dense nanograin sized materials include the dispersion of the nanosize particles and control of gas evolution from the very high surface area compacts during sintering. Typically, nanometer size particulates suffer from a high degree of agglomeration, which results in poor particle packing (green densities < 40% of theoretical) and inhibits sintering and promotes undesirable grain growth. Two routes to obtaining well-dispersed powders include comminution and colloidal processing. Recent advances in colloidal processing have obtained high green densities (> 50% of theoretical) with 8 nm YSZ particulates, which preliminary sintering efforts resulted in a translucent, fully dense 45 nm grain sized ceramic. Finally, gas evolution during sintering can occur due to the very high surface areas of nanoparticulate green bodies and disrupt sintering processes. While the thermodynamics and kinetics in the gas phase evolution reactions are reasonably well established, the fundamental science and engineering aspects must be addressed for each nanoparticulate system. Recent considerations indicate that innovative gas phase treatments (e.g., injection of reactive gases during the sintering cycle) can be used to overcome the undesirable effects of evolution gases from the nanoparticulate bodies during sintering.

Status

The Kimel and Adair approach has been used to prepare stable suspensions that will be used in preliminary pressure casting trials for pellet fabrication that can be sintered. The particle characteristics were similar to that of Kimel and Adair (in press, *J. Am. Ceram. Soc.*). The apparatus used for pressure casting in past studies is now set up with pressing trials to commence in late April. We have also begun exploring two critical features in the successful preparation of dense powder compacts suitable for sintering; organic removal and drying. Preliminary sintering trials have shown that sintering is somewhat inhibited if the organic additives (primarily oxalate used for dispersion) is not removed prior to the sintering process. We have found that ozone treatment is an effective tool in decomposing the oxalate to CO_2(g). An ozone generator has

been purchased that can be used as a bench top device to saturate the washing solvent with ozone prior to ejection of the pressure cast parts from the die. In addition, we are using solvent exchange to replace the water with a lower surface tension liquid (MEK-ethanol or MEK) during the ozone treatment process. This latter approach is to minimize the drying cracks often observed in pressure cast bodies that form because of the large capillary forces associated with water. It is anticipated that sintered materials for mechanical property evaluation will be sent to ORNL by the mid-May.

The focus of research during the past quarter has also been to increase zirconia yield from the reactant solution by increasing the concentration of zirconium in the starting stock solution. Using the procedure developed by Kimel and Adair, the final concentration of the stock zirconium solution, 0.5 M zirconium nitrate, after addition of the complexing agent, bicine, and pH adjustment with 2.43 M tetraethylammonium hydroxide (TEAOH) was about 0.2 M (about 25 g zirconia per liter). By doubling the concentration of zirconium nitrate, the final zirconium concentration was increased to about 0.3 M (about 37 g zirconia per liter), after the addition of bicine and pH adjustment. To increase concentration further, it was decided to adjust solution pH with a stronger base, namely 5 M potassium hydroxide; however, final zirconium concentration was only about 0.3 M, not significant enough an increase to warrant the addition of potassium to the material. Another organic base, tetramethylammonium hydroxide pentahydrate solid (TMAOH), was also considered for solution pH adjustment. A major concern with this material, however, was its already-high content of water in its solid form. It was calculated that the zirconium concentration limit would be about 2 M (about 250 g zirconia per liter) if TMAOH pentahydrate was used to adjust solution pH. In practice, however, zirconium concentration is limited by the solubility of the complexing agent, bicine. Using TMAOH penthydrate solid to adjust solution pH, zirconium concentration was increased to about 0.8 M (about 98 g zirconia per liter). The zirconia produces using this method had an average particle size (by BET surface area analysis) of 10-14 nm. Currently, efforts are being made to deagglomerate these concentrated suspensions using the oxalate displacement wash and dispersion.

Plans for Next Quarter

The emphasis over the next quarter will be to prepare small yield batches based on the Kimel and Adair approach. This approach only yields enough material for four to five pellets. However, it is our intent to produce enough sintered pellets to ORNL by May 15, 2004, to begin preliminary property evaluations. This slight advancement of this activity means that the activities to synthesize larger quantities at higher yields will be pushed back to 6/30/04.

Patents

None to report.

Publications/Presentations

None to report.

Milestone Status Table

ID Number	Task / Milestone Description	Planned Completion	Actual Completion	Comments
1	Particle Process for Nanoscale Zirconia	1/31/05		
1.1.1	Particle Preparation	3/30/04	3/30/04	
1.1.2	Particle Preparation Scale-up	3/30/04		New Date 6/30/04
1.1.3	Pressure Casting	4/30/04		New Date 5/15/04
1.1.4	Organic Removal	5/30/04		
1.2.1	Drying	8/15/04		
1.2.2	Sintering	10/15/04		
1.2.3	Characterization	12/15/99		
1.2.4	Shipment of Parts to ORNL for Evaluation	10/15/99		
1.3.5	Analyze Data	12/31/00		
1.4	Final Report	1/31/05		

Development of Titanium Alloys for Heavy-Duty Diesel Engines

Jesus Chapa-Cabrera and Mark J. Andrews
Caterpillar Inc.

Introduction

The present cost of producing titanium has significantly decreased, and the future forecast is for the decreasing trend to continue, making titanium alloys an attractive alternative to other strong, lightweight materials. Turbochargers on diesel engines play an integral role in meeting emission regulations and controlling fuel economy. Caterpillar Inc. has introduced the use of two turbocharger systems on some on-highway diesel engines in order to meet current and future emission regulations. The presence of two turbocharger systems challenges the already limited under the hood space for on-highway truck applications and so the development of an alternative turbocharger system that is smaller and lightweight is of great interest.

Project Objectives

The purpose of this program is to develop one or more heavy-duty diesel engine components using titanium alloys. The chosen engine components must demonstrate an improvement in fuel efficiency while reducing emissions. Caterpillar has selected the turbocharger wheel as an engine component to be fabricated from titanium aluminide (TiAl). In addition, Caterpillar has patented a new compact design for the turbocharger known as the HEAT™ (High Efficiency Air Turbo) that will utilize the TiAl turbo wheel. The HEAT™ consists of two compressor wheels and one turbocharger wheel attached to the same driveshaft. One compressor wheel is made from an aluminum alloy while the second compressor wheel is made of Ti-6V-4Al.

In order for the HEAT™ to meet the performance specifications of two turbocharger systems, a high strength, lightweight turbo wheel must be developed, which is the primary objective of this project. Thus lightweight titanium materials (e.g., TiAl) are the *enabling* technologies for the successful development of this new turbocharger design that will meet transient emission regulations while improving the engine's fuel efficiency.

Approach

An interdisciplinary team has been organized at Caterpillar to develop the TiAl turbowheel. Staff members from the Advanced Materials Technology (AMT) will lead and manage the project development efforts. Experts from the Large Engine Center (LEC) Air Systems division will work with Engine Research to design and bench test the turbo wheel. Manufacturing and Process engineers from the Mossville Engine Center (MEC) will work with machining experts at the Advanced Production Technologies to develop a cost competitive manufacturing implementation plan.

Summary

Two of the three subcontractors that were initially identified for the project have completed contract agreements with Caterpillar. The third subcontract is in the negotiation phase; alternative vendors have been preselected in the event that a contract is not completed with the third vendor.

A prototype HEAT™ Turbocharger has been built using an Inconel 713 turbo wheel, and it was tested on an internally designed Caterpillar gas stand as well as on an engine. The purpose of these prototype tests was to validate the compression capacity of the HEAT™ design, and to obtain baseline data for comparison with a HEAT™ turbo to be built using a TiAl turbo wheel. Steady and transient test results indicate that the HEAT™ likely has the potential to meet the performance and emission requirements of the engine. Data obtained from this test will be used as a basis for the redesign of the wheel.

Finite element modeling of the existing HEAT™ design has been completed using TiAl and Inconel 713 material properties. Temperatures and stresses resulting from critical transient conditions were obtained from the analyses. The results from the modeling indicate that total stresses on the wheel are reduced in approximately 50% by substituting the Inconel 713 with TiAl. Lower thermal and centrifugal stresses of TiAl are attributed to its higher thermal diffusivity and lower density relative to Inconel 713.

Modeling of the friction welding process was conducted using commercial simulation tools. Results from this simulation are being used to assist on the definition of the process parameters used for the welding trials.

The LEC Air Systems group ordered and received 14 TiAl turbo wheels and cast bars from a vendor that has interest in supplying TiAl wheels to Caterpillar. The wheels were essentially the result of casting trials and contained porous regions visible to the naked eye. Since the wheels did not meet print specification they were sold to Caterpillar at a significantly reduced price. Bars of the shaft material were also procured.

Test bars were machined from the TiAl and shaft material, and the surfaces of the TiAl wheels were conditioned for friction welding trials. The cross section area of the TiAl bars used for welding was equal to that of the wheels. Joints were produced between the TiAl and the shaft material using bar-to-bar and bar-to-wheel configurations. The friction welding process parameters were varied to produce the joints and the resulting bar-to-bar jointed specimens were tested to failure in bending. A combination of parameters was established that produced bar-to-bar joints with a strength higher than the TiAl base material. Using the same parameters for bar-to-wheel welds produced significantly weaker joints, indicating the high sensitivity of the process to changes in the thermal mass of the TiAl part being joined.

Future Plans

A redesign of the turbo wheel will commence once the aero analysis is completed. Welding trials with scrap TiAl wheels will continue in the next reporting period, producing at least 2 shafted wheels for gas stand testing. Procurement of the test samples is anticipated for completion in the next reporting period.

Surface Modification of Engineering Materials for Heavy Vehicle Applications

Stephen Hsu (primary contact), Xaiolei Wang, Yhun Chae, and Lewis K. Ives
National Institute of Standards and Technology

Objectives

- Organize an international cooperative research program on an integrated surface modification technology under the auspice of the International Energy Agency (IEA)
- Design and identify surface features and patterns that can achieve friction reduction and enhanced durability for heavy duty diesel engine components.
- Develop understanding and appropriate models to explain the texturing effects on frictional characteristics. Develop appropriate thin films and coatings to achieve synergistic and complementary relationship with texturing to enhance performance.
- Discover and develop surface chemistry for protecting the films and coatings which work in synergy with the textures.

Approach

- Review research activities in various countries on surface texturing, thin films, and lubricant chemistry.
- Design various surface textures and measure their effects on friction and wear.
- Explore economical ways to fabricate these surface textures on appropriate materials surfaces.
- Develop test methodology to measure the effects of these textures on friction and wear reduction.
- Concurrently, organize an international cooperative research program under the auspice of the International Energy Agency (IEA) to pool resources and share this energy conservation technology worldwide.
- Under IEA annex IV, seek approval from the IEA executive committee and organize a U.S. national working group centered at NIST to provide industrial inputs and exchange information with other national groups.

Technical Highlights

- Organized a special technical session on an integrated surface modifications technology during the STLE annual meeting in Toronto, Canada, on May 19, 2004.
- Received approval from IEA Executive Committee on March 4, 2004 to form the new annex IV on integrated surface modification technology. Will proceed to form the national working group and recruit companies this coming quarter.
- We have initiated a study to optimize the surface texturing technology under high speed low load conditions. Our main thrust, however, remains to explore new design principles in order to increase the loading capacity of surface textures.

The basic concept of this project is to use surface texturing features to artificially generate fluid lift force (hydrodynamic forces) to lower friction. Historically, such techniques work in high speed low load situations such as seals, journal bearings, and conformal contacts. In heavily loaded contacts, wear of the surface features makes such effects short-lived.

The surface textures were fabricated using two different techniques. A photolithography method employing a mask fabricated with features of the size, shape, and spacing for the desired texture pattern used to produce surface textures on specimens. A photoresist was applied to the polished ($R_a \approx 0.01$ μm) test surface and exposed to light through the mask. After development the specimen was electrolytically etched to produce texture features of the desired depth. The other technique used various mechanical means to achieve desired geometrical features such as nanoindentation, scribes, and others.

Optimization Of Geometric Size And Shape In Low Load, High Speed Regime

We have initiated a study to fully understand the effect of sizes and shapes of surface features in the low load, high speed regime. Based on the results obtained previously, we developed a study matrix of textural geometry, pitch, depth, and patterns to provide a design data base for friction reduction. Work is underway and we target Sept. 30 to conclude this study. This will provide a definitive design guideline for surface texturing in this regime.

New Design Principles For High Load Applications

High load experiments

Circular dimples were used to conducted high load experiments using stainless steel specimens. The load was raised up to 93 N on a smaller sample pin so the apparent contact pressure was approximately 15-20 MPa. To prevent wear of the dimples, a fully formulated synthetic lubricant was used. Baseline without dimples and dimpled specimens were compared. In each case, the dimples caused high friction.

We have confirmed that under high speed, low load conditions, surface texturing can reduce friction of metal-to-metal contacts. The fact that geometric shape and orientation direction made a different suggests that common fluid mechanics explanation (dimples increase hydrodynamic pressure) maybe insufficient to explain the results. Contact mechanics, edge stresses (sealing the features), leakage rates around the edges, and turbulence inside and around the features may provide additional insights. Under boundary lubrication conditions, the fluid flow is not continuous inside the contact, so a different model will need to be developed to guide the continual advances needed to develop this technology.

In order to raise the effectiveness of the surface texture, new design principles are needed. Towards this end, we are working first to understand the friction reduction mechanisms of surface textures by developing an in situ observation apparatus to identify the fluid flow patterns.

In Situ Observations

At relatively high sliding speeds, cavitation in the lubricant at surface pattern features having suitable size and geometry is considered to be one mechanism for friction reduction. Theoretical calculations[1] and experimental measurements[1, 2] appear to confirm this mechanism. The effect of cavitation is to produce a net increase in pressure in the lubricant film localized at the feature. The extent of cavitation will depend on the properties of the lubricant, sliding speed, applied load, as well as feature geometry, size and spacing. Direct observation would provide a useful means to assess the effect of these factors on cavitation and confirm that cavitation, and not some other mechanism, was responsible for the observed change in friction behavior. To implement direct observation, the currently used pin-on-disk tester was adapted as illustrated schematically

in Fig. 1. A new pin holder and weights were fabricated with drilled holes to allow observation of the contact surface through a transparent pin specimen. The transparent pin specimen was prepared by polishing flats on a 4.76 mm diameter sapphire ball. A dimple, shown in Fig. 2, with diameter of approximately 100 μm and depth of 8 μm was ground in the center of the contact flat.

A long working distance borescope with attached ccd camera and video monitor was used to observe the contact. In an initial test, some fluctuations in contrast were observed but the resolution was not sufficient to obtain detailed information. In future tests, a high-speed camera and improved optics will be employed to obtain improved images of the contact.

New Approaches To High Load Textures

Microplasto-hydrodynamic lubrication mechanism has been reported to effect lubrication under metal forming conditions. It utilizes surface textures, plastic deformation, and squeeze film concept to provide lubrication under very severe contact conditions. However, the theory in this practice is not developed and most practices are based on empirical trial and error.

Our approach is to combine microplasto-hydrodynamic lubrication with an artificial wedge plane concept. Various sizes of surface features will be fabricated with a build-in incline plane as the bottom of the surface features and uses plastic deformation to provide the squeeze action.

A four-ball wear tester with the configuration of ball-on-three-flat is used to get high contact pressure. The testing conditions are Ball: half inch diameter 52100 bearing steel ball sliding on brass or aluminum flats at 0.19 m/s – 1.9 m/s under 2, 5, 8 Kg of loads in Mobil 1 (15W40) Engine oil.

The surface texture was fabricated using both electrochemical etching and mechanical scribing actions to create an artificial wedge slope at the bottom of the features. Results are shown for an elliptical shape texture. Figures 4-6 illustrate the effect of such textures.

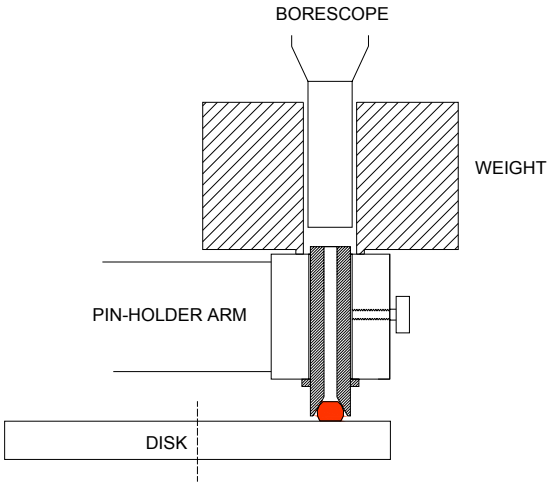

Fig. 1. Pin-on-disk tester adapted for observation of pin contact through transparent pin specimen.

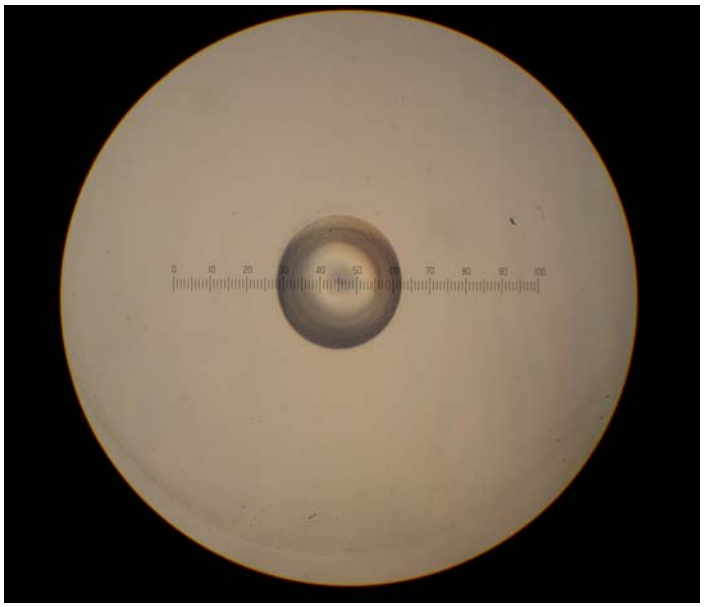

Fig. 2. Dimple, ~100 um diameter and ~8 um deep, ground at center of polished flat on sapphire ball.

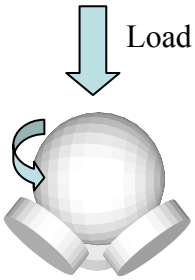

Fig. 3 Schematic diagram of the contacts of ball-on-three-flat

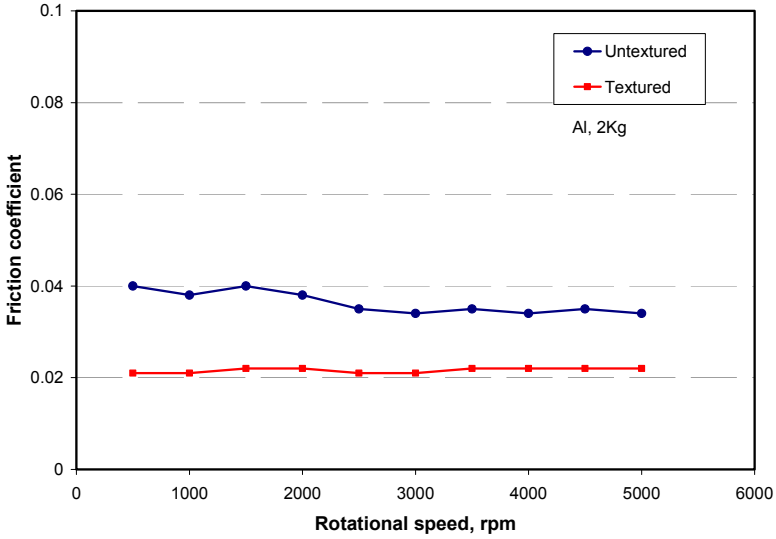

Fig. 4 Comparison of friction coefficient of the textured and untextured aluminum specimen at 2Kg

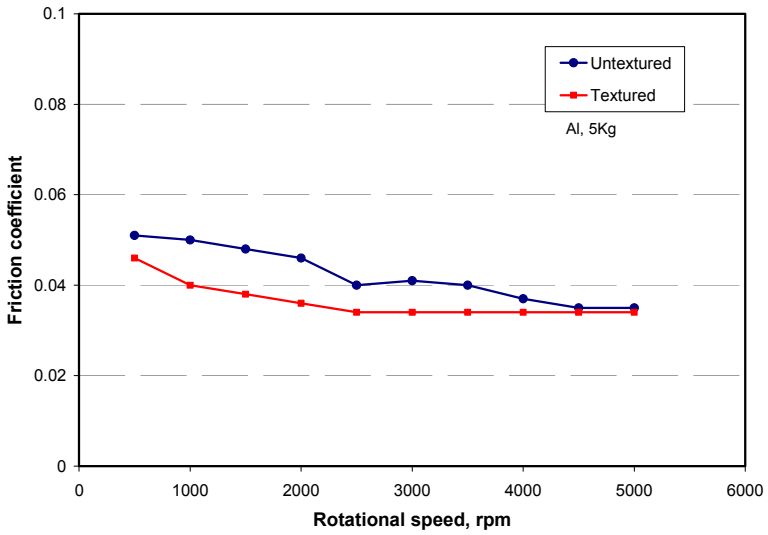

Fig.5 Comparison of friction coefficient of the textured and untextured aluminum specimen at 5Kg

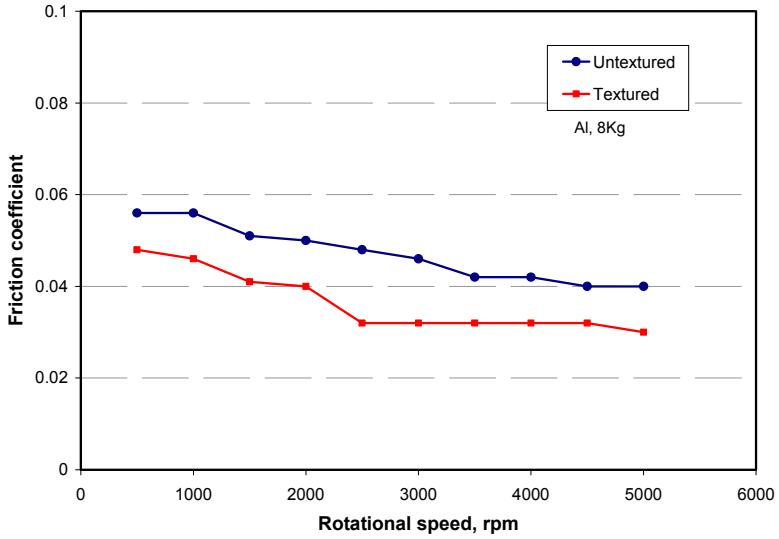

Fig.6 Comparison of friction coefficient of the textured and untextured aluminum specimen at 8Kg

The significance of this result is that the average contact pressure is well over the yield stress of the materials and in the GPa range. We believe this is the first time that surface texture of any kind has been shown to have a significant effect on friction on any materials. We have repeated the experiments several times and on brass. Similar and better results were achieved. This suggests that we have opened a new way to induce friction reductions.

Travel

1) Attended the IEA Executive Committee held on Oct. 22, 2003 in Oakland, CA and presented a detailed proposal on an integrated surface technology to the executive committee.

2) Attended ASME/STLE Joint Conference in Oct. 28, 2003 at Sawgrass Marriott Resort and Beach Club, Ponte Vedra Beach, Florida.

Status of FY 2004 Milestones

1.) Organize a symposium on contact reliability to compare testing procedures used in different countries (Oct. 2002).

–Done-- Completed a symposium among the participating countries on IEA activities on Oct. 29, 2002 during the ASME Tribology Conference in Cancun, Mexico.

2.) Propose to the IEA Executive Committee the formation of a new Subtask related to performance testing of nanostructured coatings for friction reduction (Jan. 2003).

Done. Received official approval from the IEA Executive Committee on March 4, 2004 to initiate a new project on surface modification.

References

1. I. Etsion, Y. Klingermen, and G. Halperin, Trib. Trans. Vol. 42, (1999) 511-516.
2. G. Ryk, Y. Kligerman, and I. Etsion, Trib. Trans. Vol. 45, (2002) 444-449.

Implementing Agreement For A Programme Of Research And Development On Advanced Materials For Transportation Applications

M. K. Ferber
Oak Ridge National Laboratory

Objective/Scope

The International Energy Agency (IEA) was formed via an international treaty of oil consuming countries in response to the energy crisis of the 1970s. A major objective of the IEA is to promote secure energy supplies on reasonable and equitable terms. The governing board of the IEA, which is composed of energy officials from each member country, regularly reviews the world energy situation. To facilitate this activity, each member country provides energy experts who serve temporary staff assignments at IEA headquarters. These staff or secretariat support the governing board by collecting and analyzing energy data, making projections in energy usage, and undertaking studies on specialized energy topics. The governing board is also assisted by several standing groups; one being the committee on energy research and technology (CERT), which encourages international cooperation on energy technology. Implementing agreements (IAs) are the legal instruments used to define the general scope of the collaborative projects. There are currently 40 active implementing agreements covering research topics such as advanced fuel cells, coal combustion science, district heating and cooling, enhanced oil recovery, fluidised bed conversion, fusion materials, solar heating and cooling, pulp and paper, hydropower, heat pumping technologies, hybrid and electric vehicles, high temperature super conductivity, wind turbines, and high temperature materials. A complete listing can be found at the IEA website, www.iea.org.

This progress report summarizes recent activities in the implementing agreement entitled, "Implementing Agreement For A Programme Of Research And Development On Advanced Materials For Transportation Applications" (IA-AMT). This implementing agreement currently consists of two active annexes: "Annex II: Co-Operative Program on Ceramics for Advanced Engines and Other Conservation Applications" and "Annex III: Co-operative Program on Contact Reliability of Advanced Engine Materials." The motivation for this IA is the development of new and improved ceramic materials, brittle material design methods, and life prediction methodology. The objective of Annex II is coordinated R&D on advanced ceramics leading to standardized methods for testing and characterization.

The Executive Committee for the IA on Advanced Materials is also exploring the possibility of adding a new effort focusing on light weighting of materials.

Technical Highlights

A strategic plan was prepared and distributed to executive committee members for comment. As stated in the plan, the current mission of the IA-AMT is to investigate promising new technologies for evaluating and ultimately improving the performance of materials for transportation systems. The primary motivation for this activity is the fact that new material technologies are required to increase efficiency and reduce harmful emissions in these systems. Examples of these technologies include (1) light weighting to improve fuel efficiency, (2) surface engineering to improve the resistance to wear and contact damage, (3) development of

durable coating systems for thermal, wear, and environmental management, and (4) development of revolutionary materials (structural ceramics and ceramic matrix composites) for operation at much higher temperatures and pressures [1]. The research activities within the IA-AMT focus specifically on (1) the identification of promising new technologies for improving materials performance and (2) the development of specialized characterization techniques for validating the applicability of these technologies to improve material properties while maintaining acceptable life-cycle costs.

In the case of performance improvement, the current emphasis is on integrated engineered surface technology or IEST and light weighting of materials. IEST encompasses the synthesis, processing, characterization, and application of technologies that enhance the functionality of surfaces in contact with the environment or with the surfaces of other solids. Two such technologies under consideration are Laser Shock Peening (LSP) and Micro-Dimpling. LSP has shown the potential to introduce an extensive zone of residual stress in certain metals. This residual stress tends to close surface cracks making the material less susceptible to stress-corrosion cracking and fatigue. Micro-dimpling involves the use of a laser to introduce periodic arrays of small dimples in the surface of a material. These dimples can be 2-20 microns in depth, 150-50 microns in diameter, and have a coverage ranging from 5 to 50%. The ability to control the surface texture and stress state is expected to have important implications on the integrity of coatings which are applied to promote thermal and wear resistance.

Activities on light weighting of materials focus on aluminum, high strength steels, magnesium, metal and polymer composites, titanium, intermetallic alloys and other advanced materials. The ultimate use materials in certain structural applications Current topics under consideration include (1) data on production and resource availability, (2) life cycle data on environmental impacts associated with production, processing and use of lightweight materials, (3) recycling information including regulatory frameworks, (4) data on crashworthiness, design and testing methodologies, (5) data on base material cost, (6) data on energy impacts of lightweight materials, and (7) shared information on research programs on lightweight materials.

In terms of performance evaluation, the primary focus is on techniques for (1) assessment of environmental degradation of structural (non-oxide) ceramics; (2) evaluating time-dependent degradation of mechanical performance of structural ceramics; (3) quantification of key properties of coatings for wear, thermal, and environmental protection of current transportation materials; and (4) the development of techniques for the measurement of key properties (topography, chemistry, subsurface damage) of engineered surfaces. Items 1 and 2 are motivated by the need to address key barriers to the use of this important class on material. For example, given the recent concern over environmental degradation of non-oxide ceramics in combustion environments [2-4], cost effective techniques are required to simulate these effects as well as to assess the effectiveness of environmental barrier coatings. The IA-AMT is currently evaluating a variety of techniques ranging from complex high-pressure burner rig tests to a simple cost-effective steam injection system.

Ceramic coatings hold considerable promise for (1) improving wear resistance, (2) providing thermal protection, and (3) reducing environmental degradation of for critical metallic components used in internal combustion engines. Unfortunately techniques for assessing key

properties particularly with respect the interface are unproven. Item 3 addresses this limitation. In a similar fashion, as surface modification technologies mature, proven characterization techniques will also be required to validate their performance (Item 4).

The annual report for 2003 for the IA-AMT was also prepared this reporting period. This report can be downloaded at the new web site for the IA-AMT: http://ia-amt.ornl.gov/index.html).

Status of Milestones

All milestones are on track.

Communications/Visits/Travel

The author visited Sid Diamond to discuss the strategic plan for the IA-AMT.

Publications

Implementing Agreement For A Programme Of Research And Development On Advanced Materials For Transportation Applications-Annual Report 2003.

Mechanical and Thermal Fatigue of Silicon Nitride within IEA Subtask 11, Final Report, February 2004.

References

None.

Mechanical Property Test Development

George Quinn
NIST

Objective/Scope

This task is to develop mechanical test method standards in support of the Propulsion Systems Materials Program. Test method development should meet the needs of the DOE engine community but should also consider the general USA structural ceramics community as well as foreign laboratories and companies. Draft recommendations for practices or procedures shall be developed based upon the needs identified above and circulated within the DOE engine community for review and modification. Round robins will be conducted as necessary. Procedures will be standardized by ASTM and/or ISO.

Technical Highlights.

1. General

Minor issues regarding several standards were cleared up this quarter. The error analysis for flexural strength testing of cylindrical rods is ongoing. A Guide to Practice for Fractography has been started. Investigations into diametral compression strength testing were resumed. Segmented cylinders were ordered for testing.

2. Fracture Toughness

A draft European standard for fracture toughness determination by the Single Edged V-notched beam was revised and comments sent to the European authors. This method, which is not yet in the ASTM standard C 1421, is a variant on the single-edged precracked beam and is becoming more popular with time. Instead of using a bridge precracker to pop in a through-crack in a common bend bar, a saw cut is made and then sharpened with a razor blade and diamond paste. A VAMAS round robin based on this method a few years ago had mixed, but generally successful results. In some cases, the sharpened notch gave good results (within 5 –10% of genuine sharp crack data), and in other instances overestimated the fracture toughness. Our approach in ASTM will be to monitor the European developments and then decide whether to incorporate this method into C 1421.

A set of notes were compiled on the limitations of the Vickers indentation crack length method for measuring fracture toughness.

3. Flexural Strength of Advanced Ceramics – Rectangular Specimens

Nearly all work on updating the ASTM standards and finishing the ISO standards is now complete. We believe that ASTM C-1161-02c is the definitive ASTM version. Andrew Wereczszack identified an editorial mistake and we asked ASTM to make the appropriate correction. A series of editorial corrections to the ISO version, ISO 14704 were also identified and the secretariat requested to make changes.

A Versailles Advanced Materials and Standards (VAMAS) round robin led by Dr. S.J. Cho of KRISS, Korea is nearing completion. This project is focusing on the effects of humidity on flexural strength. The current world standards suggest that if one suspects that slow crack growth is active, then faster than normal loading rates should be used or the testing should be done in an inert atmosphere. These steps are discretionary and the Koreans feel that more stringent requirements for testing should be required. We are not participating in this round robin, but we are monitoring the developments. Preliminary results were shown by Dr. Kristin Breder at the VAMAS Technical Working Area #3, Ceramics meeting in Cocoa Beach in January 2004.

4. Fractography

Work continued on a NIST user-friendly "Guide to Best Practice" for fractographic analysis.

5. Flexural Strength Testing of Cylindrical Ceramic Specimens

The error analysis of flexural strength testing of cylindrical rods is underway. Additional analysis of the "concentrated load" or wedging stress error problem has been done. We were fortunate to find a publication with an excellent finite element analysis of the problem done by Drs. Fok and Smart at the University of Manchester, England. Correspondence was exchanged with them

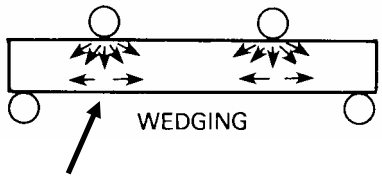

Tensile bending stresses may be disturbed here due to the concentrated loading on the opposite side.

Figure 1 Wedging stresses from concentrated loads.

6. Split cylinder flexural strength testing

We will resume flexural strength testing of split cylinder, or segmented cylinder rods. A new set of zirconia plunger pins was sent to a machining vender for preparation.

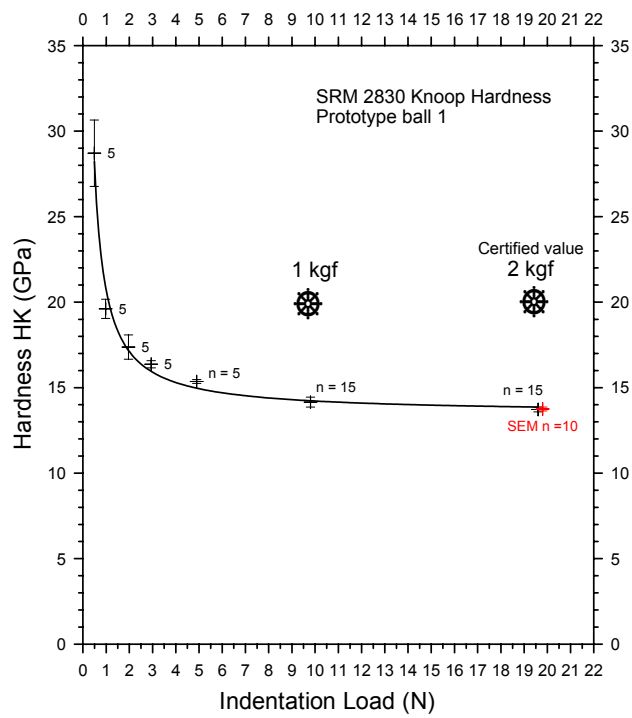

Figure 2. Knoop hardness versus indentation load for SRM 2830, silicon nitride. There is a slight hardness difference at 1 kgf compared to 2 kgf.

7. Hardness

Some work was done to remeasure the Knoop hardness of five NIST Standard Reference Material 2830 blocks that were originally measured and certified at 2 kgf. Some users have microindentation machines that can only go up to a 1 kgf maximum and they have some worries about using the SRM. There is a slight difference in hardness (0.40 to 0.65 GPa) at the two loads. Therefore, a new series of experiments were done with indentations at 1 kgf and 2 kgf in the five archival blocks. In addition, the complete hardness versus load curve (the Indentation Size Effect trend) was remeasured on one block as shown in **Figure 2.** Our goal is to get a simple adjustment or correction factor to enable users to make the 2 kgf to 1 kgf conversion if necessary. The NIST SRM Office was consulted on whether an amended SRM certificate may be prepared or whether a supplemental conversion flier may be added to the formal certificate.

During this period we learned that the United States Customs Service has adopted ASTM Standard C 1326 Knoop hardness for its testing program for certification and qualification of ceramic imports to the United States. The US Customs procedure is designated: USCL 69-nn, Procedure for Measuring the Hardness of Technical Ceramic Products.

8. Diametral Compression

We are planning on resuming investigations into the diametral compression strength test method, a convenient alternative to bend bar or direct tensile strength test methods. In March, Mr. Quinn met Professor Bryan Darvell of the University of Hong Kong at a conference and learned that Darvell had written a review paper on diametral compression in 1990. This came as a surprise since we had done a review of the literature and did not include this important reference. The paper was overlooked since its title was misleading ("Uniaxial Compression Strengths and the Validity of Indirect Tensile Strengths") and the key words and abstract made no mention of "Brazilian disk" or "diametral compression." Mr. Quinn had a long discussion with Prof. Darvell about the pros and cons of the test method. Darvell's paper was acquired and read in detail. Darvell does not believe that this method can produce reliable strength numbers and that many fractures actually are shear initiated. Mr. Quinn sent a long review of the paper to Prof. Darvell. Mr. Quinn also contacted Dr. Edgar Lara-Curzio at ORNL to pass the word about this important review paper.

Status of Milestones

412149	Prepare ballot-ready first ASTM draft of cylindrical rod flexure strength test	April 2002 **Overdue**
412151	Prepare review paper on flexural testing of cylindrical rods.	October 2002 **Overdue, Ongoing work on error analysis**

Communications/Visits/Travel

Andy Wereczszack informed G. Quinn about a typographical error in one of the drawings (Specimen C) in the ASTM C 1161 flexural strength standard. The cause of the error was tracked down and ASTM notified. Corrective action will be taken. A number of editorial errors in the ISO flexural strength standard ISO 14704 were also identified. These had occurred at ISO Headquarters in Geneva and had been brought to the Secretariat's attention previously, but no remedial action taken. We renewed our complaint and hopefully remedial action will be taken this time. Mr. Quinn attended the ASTMC-28 Advanced Ceramics and the VAMAS Technical Working Area #3 meetings in Cocoa Beach in January.

Publications and Presentations

None this quarter

Rolling Contact Fatigue

A. A. Wereszczak
Oak Ridge National Laboratory

Objective/Scope

The understanding and control of contact damage behavior of ceramics under rolling and sliding conditions are enablers to more widespread utilization of ceramics as cam followers, valves, valve seats, and other important transportation-related components. International interest exists to understand the fundamentals of rolling contact fatigue (RCF) of ceramics because greater control (or minimization) of RCF will result in longer life of such components. Rolling contact fatigue is internationally studied through a variety of test methods and analytical approaches; interest exists in the present project to link their measured performances. Toward that, RCF studies (primarily of Si_3N_4) involving both international and domestic interactions are being pursued as Annex III of the International Energy Agency (IEA) agreement.

Technical Highlights

Ceralloy 147-31N Si_3N_4 RCF and rotary bend strength (RBS) test specimens are being prepared - schematics respectively shown in Figs. 1-2. Both those specimen geometries are being machined three different ways (Tables I-II) with the intention to produce differing levels of sub-surface damage, and to ultimately examine how that sub-surface damage affects RCF performance. The RBS specimens will be tested in parallel to the RCF specimens because flexure tests are good at exploiting the effects of sub-surface damage (on strength in this case). The RBS specimen rotates during its monotonic loading to fracture, so its entire gage section is subjected to outer-fiber tensile stresses. To compare RBS results with static bending results, several of the RBS specimens are being axially sectioned (see Fig. 3) and will be strength-tested in four-point-flexure. Strength-size-scaling will be examined between those two strength specimens.

Instrumented static and dynamic indentation testing, and instrumented scratch testing of the Ceradyne 147-31N is starting and their performance dependencies on sub-surface damage will also be interrogated.

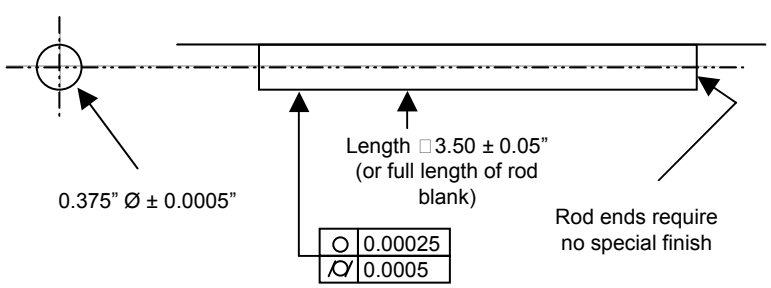

Figure 1. Rolling contact fatigue specimen.

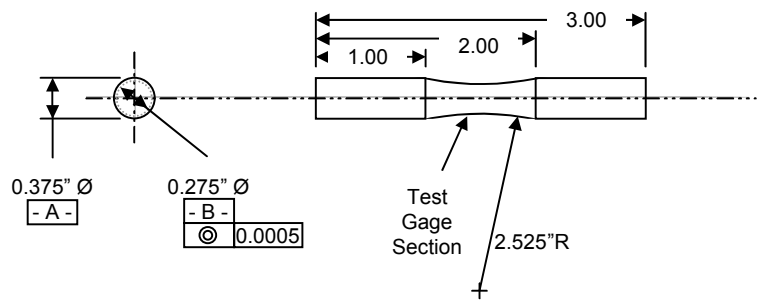

Figure 2. Rotary bend strength test specimen.

Table I. Rolling Contact Fatigue (RCF) and Rotary Bend Strength (RBS) Specimen Matrix.

Specimen Type	Finish Conditions (See Table II)	Quantities
RCF (Whole length)	Coarse Fine RCF Conventional	5 5 5
RBS (Gage section only, not shanks)	Coarse Fine RCF Conventional	20 (5 to be halved) 40 (10 to be halved) 20 (5 to be halved)

Table II. Grinding Conditions for RCF and RBS Test Coupons.

Finish	Step	Wheel	Removal	Removal per pass
Coarse	1 (roughing) 2 (induce damage) 3 (finishing)	accepted practice 100 grit 600 grit	 0.004" 0.0005"	0.001" 0.001" 0.0001"
Fine	1 (roughing) 2 (induce damage) 3 (finishing)	accepted practice 180 grit 600 grit	 0.004" 0.0005"	0.001" 0.001" 0.0001"
RCF-Conventional	Use the "accepted" practice for RCF test bar finishing			

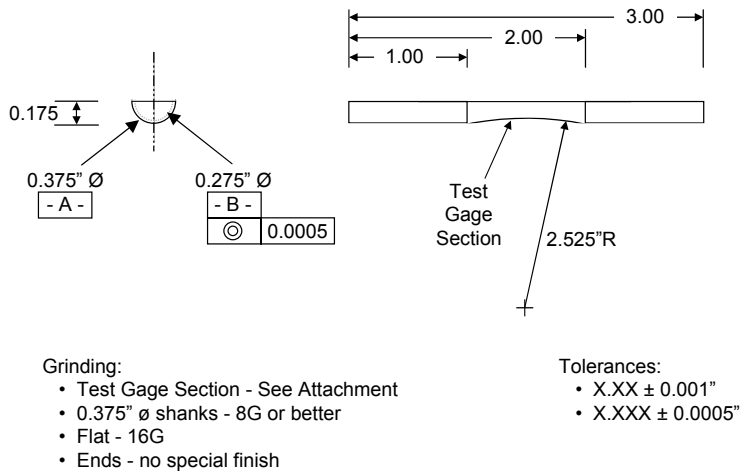

Figure 3. Half-rotary bend strength test specimen to be tested in (static) four-point flexure.

An International Energy Agency (IEA) Annex III Rolling Contact Fatigue (RCF) Working Group (WG) Meeting was held on 27 January 2004 at the Hilton Hotel in Cocoa Beach, FL. The WG Meeting was coincident with the 28th International Cocoa Beach Conference and Exposition on Advanced Ceramics and Composites (25-30 January 2004). The primary intent of the WG Meeting was for the attendees to become more acquainted with mutual RCF research efforts at the participating laboratories and to discuss future rolling contact fatigue characterization plans and interactions. The following individuals were in attendance: W. Kanematsu (AIST, Japan), M. Woydt (BAM, Germany), M. Mizuno (JFCC, Japan), M. Ferber (ORNL, USA), and A. Wereszczak (ORNL, USA). Annex III participant R. Morrell (NPL, UK) was unable to attend. A. Wereszczak (AW) was the WG Meeting organizer and facilitator.

The results from the ORNL-in-house RCF characterization study of Ceralloy 147-31N will guide the development of an international RCF study (Germany, Japan, UK, and US participation) to commence sometime in FY05 (01Oct04-30Sep05). The US will supply Ceralloy 147-31N billets or test coupons thereof and RCF performance measured by each country's test methods will be compared in a summary report written by ORNL.

Status of FY 2004 Milestones

On schedule.

Communications/Visits/Travel

An International Energy Agency (IEA) Annex III Rolling Contact Fatigue (RCF) Working Group (WG) Meeting was held on 27 January 2004 at the Hilton Hotel in Cocoa Beach, FL. The WG Meeting was coincident with the 28th International Cocoa Beach Conference and Exposition on Advanced Ceramics and Composites (25-30 January 2004). The following individuals were in attendance: W. Kanematsu (AIST, Japan), M. Woydt (BAM, Germany), M. Mizuno (JFCC, Japan), M. Ferber (ORNL, USA), and A. Wereszczak (ORNL, USA).

Wereszczak visited Ceradyne, Inc., Costa Mesa, CA on 26 February 2004 to discuss the present project and the testing of Ceradyne's Ceralloy 147-31N silicon nitride.

Wereszczak and Ferber visited DOE HQ on 02 March 2004 to meet with Sid Diamond and discuss the project's progress.

Numerous communications occurred with Prof. Mark Hadfield of Bournemouth University (UK) to initiate a formal collaboration starting in Q3 of FY04.

Publications
None.

References
None.